TECHNISCHE UNIVERSITÄT MÜNCHEN

Lehrstuhl für Technische Chemie II

Conversion of oxygen containing hydrocarbons via low temperature thermal and electrocatalysis

Yang Song

Statutory Declaration

I declare that I have authored this thesis on my own, that I have not used other that the declared (re)sources, and I have explicitly marked all material which has been cited either literally or by content from the used sources. At the end of each chapter, all collaborators are listed and their contributions are explained. Published content of this thesis is clearly marked at the end of each chapter and the publishing agreement of the publisher is stated in the associated content of each chapter.

December 2016, Munich   _____

To draw a nice period of my student life, to inspire my brand new future…

"Living without an aim is like sailing without a compass."

John Ruskin (1819 – 1900)

Acknowledgements

This doctoral thesis has come to a successful completion with the help of many people during the research. My thanksgiving goes to all the members from the Chair of Technical Chemistry II at Technische Unviersität München.

First and foremost, I am deeply grateful to Professor Dr. Johannes A. Lercher for giving me a challenging topic and his trust to me to accomplish it, and of course his patient guidance and unconditional support. During my stay here, I experienced his rigorous attitude to work, his hunger to science and his humor and wisdom during conversations. It has been a terrific experience and great pleasure to do my Ph. D. thesis under his supervision and to learn from his research expertise.

Second, I would like to give my great gratitude to my supervisor, Dr. Oliver Y. Gutiérrez, who is a very brilliant scientist, always mentoring and inspiring me in an efficient and pleasant way. That is an important reason why I can finish the doctoral thesis successfully and timely. Besides work, he is also a nice and important friend to me. I will never forget the knowledge, wisdom, morality that I learned from you, as well as those happy times I shared with you and your family.

As my topic is exploratory and challenging, I will not be able to make it without the help of Prof. Dr. Gasteiger from TU Munich, Prof. Dr. Gascon from TU Delft, for the faithful discussions and generous assistance for helping me to set this project up at the beginning. Thus I want to special thank these professors.

My partners and students, Dr. Udishnu Sanyal, Shaohua Chia, Jinyu Liu, Dhananjai Pangotra, Michealla Wübser, Chloe Freeman, Eduardo Lagunes, Guanhua Cheng. I would like to thank you all for your struggling and accompanies in our projects and I regard them as our firm friendship.

The technical and administrative staffs of TCII have been very kind and helpful, I would like to thank Xaver Hecht for BET and hydrogen chemisorption measurements and for solving technical problems of my devices whenever I approach him. Martin Neukamm, who has helped with AAS and SEM measurements, and extended his support in the order of chemicals and lab wares,

also for attending my wedding in China with your nice wife. I also thank Andreas Marx, for his efforts with all the electronic devices. I am grateful to our nice secretaries, Stefanie Maier, Bettina Federmann, Ulrike Sanwald, Helen Lemmermöhle and Karen Schulz, for their great assistance with all the miscellaneous administrative matters.

Furthermore, I would like to express my gratitude to our privileged research partners from Pacific Northwest National Laboratory (United States). I am indebted to Dr. Nirala Singh, Dr. Donald M. Camaioni for the discussion and nice cooperation.

I am very grateful to the members of TC II group, Dr. Yue Liu, Manuel Wagenhofer, Guoju Yang, Marco Peroni, Yuanshuai Liu, Sebastian Foraita, Peter Hintermeier, Sebastian Eckstein, Martina Braun, , Moritz Schreiber, for all the insightful discussions; as well as the present and former colleagues of TCII: Dr. Prof. Adreas Jentys, Dr. Erika Ember, Dr. Maricruz Sanchez-Sanchez, Dr. Ezter Baráth, Yu Lou, Ruixue Zhao, Kai Sanwald, Dr. Lei Zhong, Dr. Wenhao Luo, Dr. Bo Peng, Dr. Maximilian Hahn, Takaaki Ikuno, Jennifer Hein, Claudia Himmelsbach, Dr. Robin Kolvenbach, Wanqiu Luo, Yang Zhang, Xi Chen, as well as other members whose names are not mentioned here, for their friendship and all of the great times that we have shared.

Last but not least, I would like to present my greatest gratitude to my family for their infinated love and sacrifices. My parents have offered me unconditional understanding and best support in every single corner during my growth till now, holding their faith in me and standing by my side years by years. Special thanks to my wife, Jin yinhua, thanks for choosing to go with me in the rest of life, and you will always be the best thing in my life.

<div style="text-align:right">

Many thanks to all of you, Yang

November. 2015

</div>

Abbreviations

Å	Angstrom
AAS	Atomic absorption spectroscopy
ACF	Active carbon felt
BET	Brunauer-Emmett-Teller
BPE	Benzyl phenyl ether
cm^2	Squre centimeter
DPE	Diphenyl ether
$E^{\ominus}$	Standard electrode potential
E	Applying electrode potential
Ea	Activation energy
ECH	Electrocatalytic hydrogenation
EE	Electric efficiency
F	Faraday constant
FE	Faradic efficiency
g	Gram
$\Delta G^{\ominus}$	Standard free gibbs energy
GC	Gas chromatography
h	Hour
H_{ads}	Adsorbed hydrogen
HDO	Hydrodeoxygenation
HER	Hydrogen evolution reaction
K	Kelvin
(k)J	(Kilo) joule
(k)Pa	(Kilo) pascals
kV	Kilovolt
mA	Milli ampere
(m)L	(Milli) liter
Mm	Millimeter

(m)mol	(Milli) mole
min	Minute
(m)V	(Milli) volt
nm	Nanometer
NMR	Nuclear magnetic resonance
NP(s)	Nanoparticle(s)
pH	Numeric scale of acidity
pKa	Acid dissociation constant
PTE	*P*-tolyl ether
RVC	Reticulated vitreous carbon
SEM	Scanning electron microscopy
T	Absolute temperature
TCH	Thermal catalytic hydrogenation
TCD	Thermal conductivity detector
TEM	Transmission electron microscopy
TOF	Turn over frenquency
µmol	Micromole
wt.%	Weight percent
XRD	X-ray diffraction

Abstract

Oxygenated hydrocarbons were reduced in aqueous media at mild conditions on carbon supported noble metals. The reactions proceed either by H_2 provided or by hydrogen generated from H^+ at the cathode. The cleavage of ether bonds and hydrogenation of carbonyl groups and phenyl groups occurs without C-C cleavage. The H_2 chemical potential is controlled by the electrical potential. The rates are additionally influenced by the nature of the metal and solvent.

Kurzzusammenfassung

Sauerstoffhaltige Kohlenwasserstoffe wurden in wässriger Phase unter milden Bedingungen auf Kohlenstoff-geträgerten Edelmetallen reduziert. Die Reaktionen vollziehen sich entweder durch bereitgestelltes H_2 oder durch Wasserstoff, der aus H^+ an der Kathode generiert wird. Die Spaltung von Etherbindungen und die Hydrierung von Carbonyl- und Phenylgruppen laufen ohne C-C Spaltung ab. Das chemische Potential von H_2 wird durch das elektrische Potential kontrolliert. Die Reaktionsraten sind zusätzlich durch die Art des Metalls und des Lösungsmittels beeinflusst.

Table of contents

Chapter 3. Integrated electrocatalytic conversion of substituted phenols and diaryl ethers ..……………………………..……………71

Chapter 4. Hydrogenation of benzaldehyde via electrocatalysis and thermal catalysis on carbon-supported metal catalysts…120

Chapter 1

Introduction

1.1. General background

Fossil fuels, such as oil, coal and natural gas represent the prime energy sources in the world nowadays. However, due to the growth of global population, an increasing consumption will cause exhaustment of traditional fuels within the next 40-50 years as shown in Figure 1.1. Besides, concerns of environmental damages such as global warming, acid rain, urban smog due to the emissions from the fossil fuels are forcing governments to develop new alternative energy sources, which are environmentally friendly and sustainable [1-5].
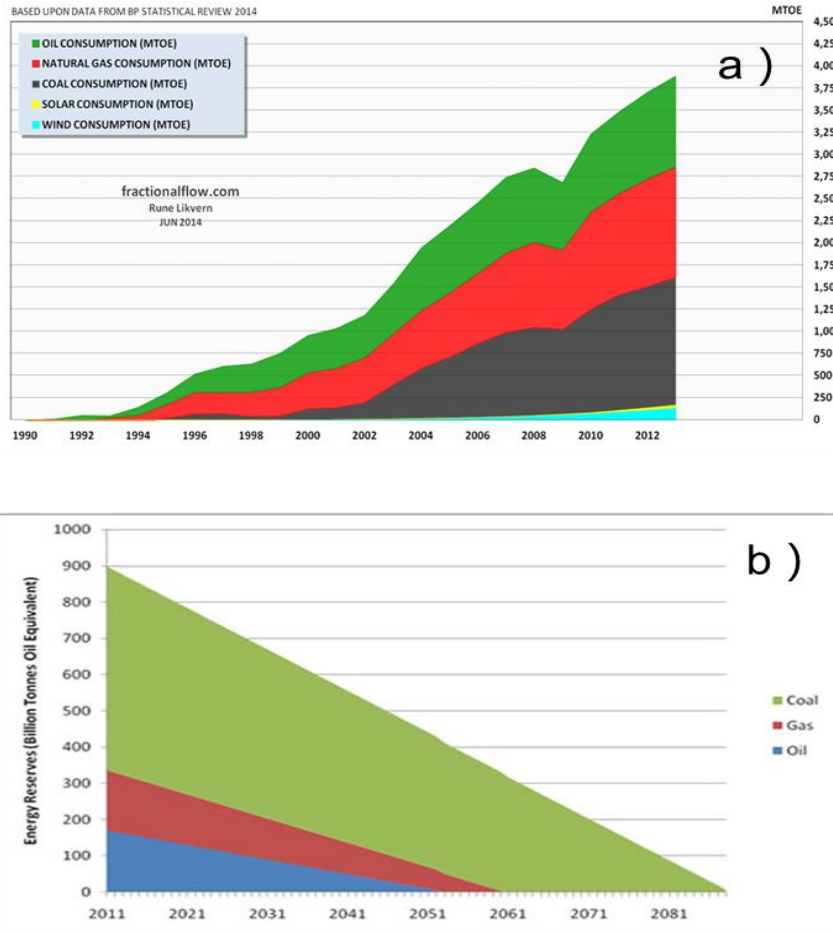
Figure 1.1. a) World energy consumption of fossil fuels and renewable energy since 1990 [5] and b) world energy reserves [3].

Biomass, as a renewable feedstock, is playing an increasingly important role in substituting of traditional fossil fuels, owing to its neutral carbon footprint and abundance [6-8]. Thus, biomass production for energy grows rapidly worldwide in recent decades, making biomass to rank as the fourth source of energy in the world, representing around 14% of global final energy consumption. For example, in the United States, biomass sources provide approximately 5% of all energy consumptions, and it supplies about 50% of all consumed renewable energy in recent years, which is much more than other renewable energies in combination, as shown in Figure 1.2 [9, 10]. In addition to the utilization in the U.S., biomass is

contributing in a noticeable amount in other countries as well, as shown in Table 1.1.
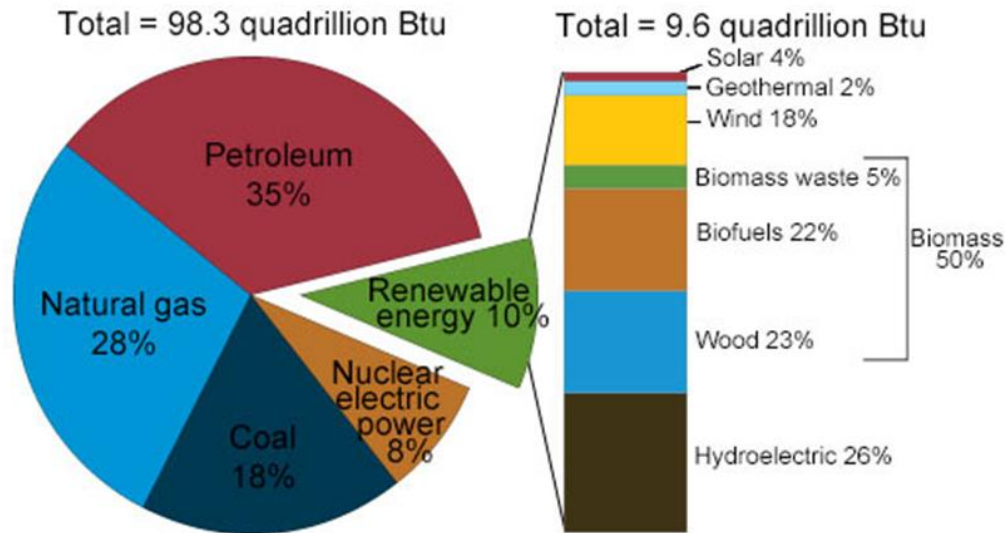
Figure 1.2. Energy consumption and construction in the United States in 2014 [9].

Table 1.1. The share of biomass in different regions in the world [11].

Region	Share of biomass in final energy consumption (%)
Africa	60.0
South Asia	56.3
East Asia	25.1
China	23.5
Latin America	18.2
Europe	3.5
North America	2.7
Middle East	0.3

Biomass is the name given to any organic matter which is derived from living, or recently living organisms. It mainly comes from the plants, which could be materials such as wood, crops, seaweed, wastes from agriculture and forestry processes. In detail, biomass will be classified into three generations based on the

feed stocks used for biofuel production[12-15]. Lignocellulosic bio-mass dominates in production volume and has low cost. Lignocellulosic materials can be converted to liquid bio-fuels via three primary processes. Gasification and pyrolysis are routes to produce upgraded bio-oil and syngas, respectively. Hydrolysis is the other route to break lignocellulose into constituent units and produce monosaccharides (eg. glucose), and further convert to biofuels, bioethanol or biodiesel. A list of classification of biomass feedstocks is shown in Table 1.2 [12].

Concerns about bioethanol and biodiesels, first generation feedstocks are that biodiesels are mainly obtained from transesterification process while bioethanol is primarily produced from edible biomass sources. Drawbacks of these low-quality diesels are fuel freezing in cold weather, reduced energy density, degradation of fuel under prolonged storage, and corrosive nature [16, 17]. Therefore, the study of the production of high energy-density biofuels via upgrading is essential. It will also be interesting and worth to decrease the severity of the operating conditions in industrial scale of biomass upgrading, which normally requires temperature over 300 °C and high pressure of hydrogen over 40 bar during hydrogenation and deoxygenation[18, 19].

Electricity produced via renewable sources such as photo voltaic, wind power, geothermal, and hydro power represents approximately 50% of all renewable energies as shown in Figure 1.2. However, limitations such as low reliability of the supply, high cost of storage and unbalanced power distributions are obstacles for its further usage and sometimes inefficiency during overproduction periods [20-22].

Table. 1.2. Classification of feedstocks for biofuel production [12].

Feedstock	Classification	Sources

1st generation	1. Food (energy) crops	1. Rapeseed, soybeans, sunflower seeds, canola, camelina, palm fruits, babassu kemel, coconut kernel, cotton seeds, wheat, barley, sugarcane, cassava, com/maize.
	2. Animal fats	2. Lard, animal intestines, animal parts.
2nd generation	1. Agricultural residues	1. Lignocellulosic materials such as straw, grass, leaves, prunings, miscanthus, willow, com stover, rice husks, palm empty fruit bunches, etc.
	2. Forest residues	2. Lignocellulosic materials like wood chippings, branches, foliage, roots, etc.
	3. Animal and oil wastes	3. Animal manure, tallow, chicken fat, fish oils, waste cooking oil
	4. Nonfood (energy) crops	4. Jatropha seeds, soap nut seeds, mahua seeds (*Madhuca indica*), indian beech/pongame seeds (*Pongamia pinnata*), karanj seeds, castor beans, Hemp, etc.
	5. Biowastes streams	5. Municipal solid wastes (*e.g.*, kitchen/household wastes, construction wood wastes, packaging wastes, etc.), sewage sludge, industrial liquid wastes.
3rd generation (green,	1. Microalgae	1. Botryococcus, Chlamydomonas, chlorella, spirulina, etc.

brown and red algae)	2. Macroalgae (macrophytes or seaweeds)	2. Cladophora, Spirogyra, Hydrodictyon, *Batracho spermum,* Halimeda, Maiden's Hair, Caulerpa, etc.

Using overproduced electricity from renewable products, to upgrade lignin biomass via electrocatalysis becomes an important topic owning to several benefits from electrocatalysis methods, such as high pressure is not needed since hydrogen can be produced in-situ via the electro reduction of protons in the electrolyte. Reactions can proceed at room temperature, since a required energy from heat can be replaced by electrical potential [23, 24]. Thus, in this thesis, conversion of biomass under mild conditions via electrocatalysis is performed by studying the different properties of electrocatalysts, reaction conditions and reactants, to maximize the reactivity. Kinetic results, reaction mechanisms and activities are thoroughly compared to thermal catalysis to obtain a better understanding of the low temperature transformations.

1.2. Lignocellulose derived feedstocks

1.2.1. The components and structures of lignocellulose

Wood-based biomass is available in large abundance and low cost, consisting of three major components: cellulose, hemicelluloses, and lignin. Cellulose (about 40-50% of lignocellulose) are linear polysaccharides in the cell wall of wood fibers, consisting of d-glucose molecules bound together by 1,4-glycoside linkages. Hemicellulose is an amorphous and heterogeneous group of branched polysaccharides (copolymer of any of the monomers glucose, galactose, mannose, xylose, arabinose, and glucuronic acid); hemicellulose (about 20-40%) surrounds the cellulose fibers and is a linkage between cellulose and lignin. Lignin is a mixture of highly complex three-dimensional polymers of different phenyl propane units

bound together by ether and carbon-carbon bonds. Lignin is concentrated between the outer layers of the fibers, leading to structural rigidity and holding the fibers of polysaccharides together (about 18-35%). Besides, lignin has the highest energy contents among the lignocellulose materials, due to the fact that the carbons in lignin structures are the most reduced ones, compared to its accompanied polysaccharides. Further, beyond providing mechanical rigidity to a plant, lignin enables water transport owning to its relatively hydrophobic property from the aromatic structures [25, 26], thus causing more interest to be chosen as model compounds to study biomass conversion. The structures of cellulose, hemicellulose and lignin are shown in Figure 1.3. Besides, small amount of extraneous organic compounds is also found in lignocellulosic materials (about 1-4%) [27, 28].
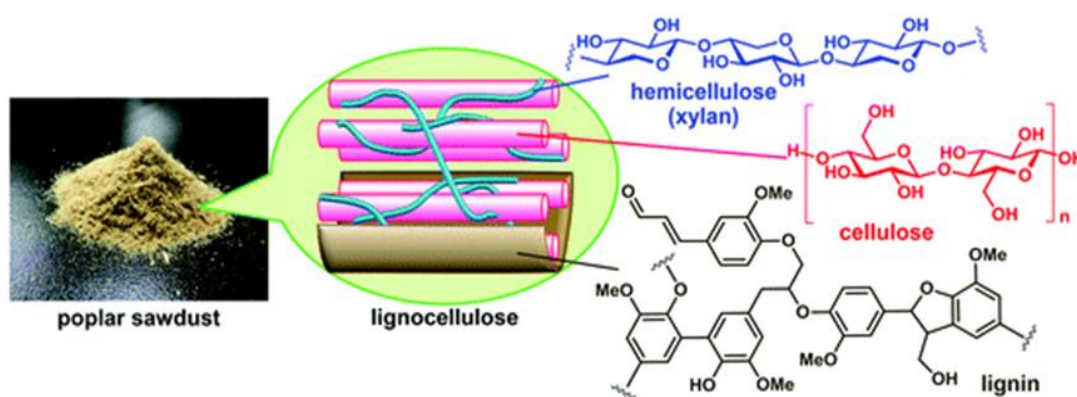
Figure 1.3. Components and structures of lignocellulosic biomass [28].

1.2.2. Conventional technologies for lignocellulose conversion

In general, lignocellulosic biomass conversion into liquid fuels proceeds through a range of pathways. In the case of ligniocellulosic biomass, depolymerization step to produce smaller molecules is initially needed. There are three main approaches that should be considered which are shown in Figure 1.4 [29]. Firstly, lignocellulose can be gasified via gasification to produce syngas ($CO+H_2$), to remove impurities by certain treatments and could be further

converted to hydrocarbons via Fischer-Tropsch synthesis. Alcohols conversion could be achieved using anaerobic bacteria during the syngas treatment. Additional hydrogen from the water and carbon monoxide present could be produced via water-gas shift catalysis, which could be used in a variety of refinery and chemical processes.
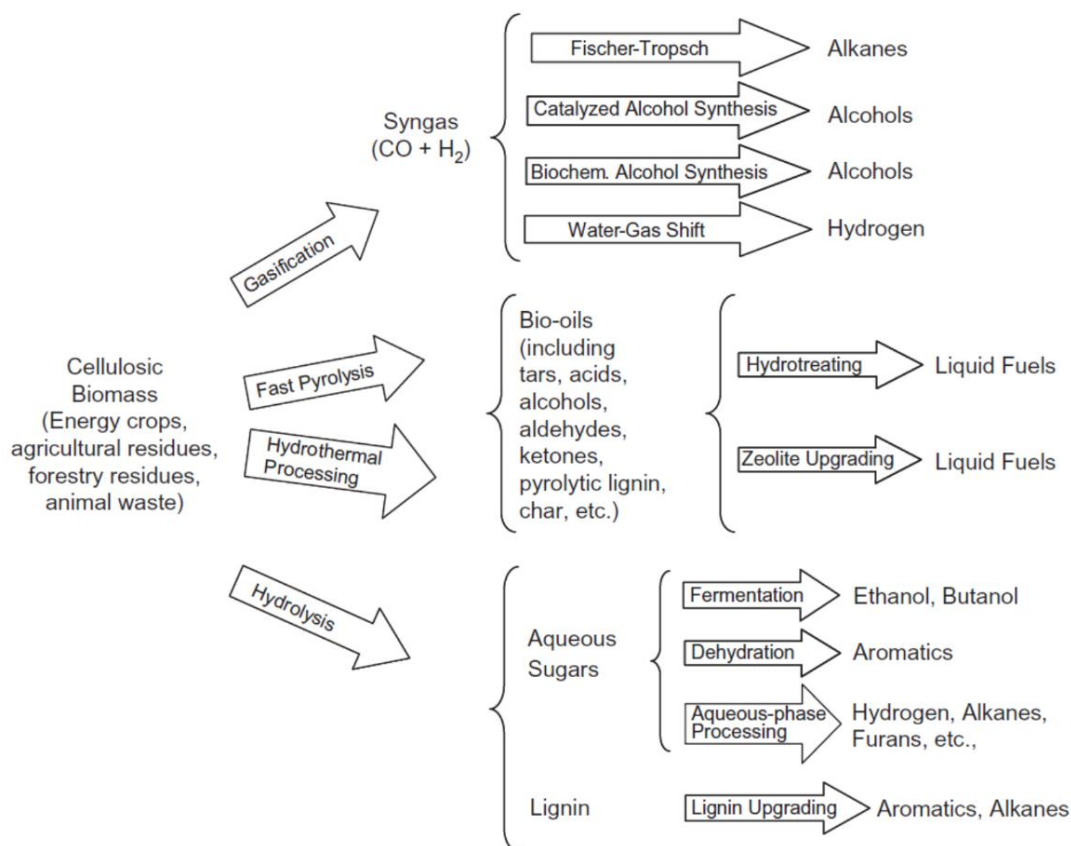
Figure 1.4. Summary of pathways for lignocellulosic biomass conversion to liquid fuels [29].

The second approach involves direct use of thermochemical conversion processes including fast pyrolysis and hydrothermal processing, during which biomass is heated without air to produce crude bio-oil. Fast pyrolysis a treatment at high temperatures (around 500 °C) and short residence time (less than 3 seconds) to produce liquid products [30]. Solvolysis is one of the biomass hydrothermal upgrading processes, which using water as solvent. Biomass is treated for 5 to 20 minutes under subcritical conditions (300-350 °C, 10-18 MPa) [31]. Another hydrothermal option is high-pressure liquefaction, where catalyst, high

temperatures (300-400 °C), and hydrogen pressures up to 20 MPa are needed[32]. A limitation of these crude bio-oils produced from these direct conversion processes is that they are not able to be used as transportation fuels without further upgrading due to their high oxygen content (up to 40 wt.% on a dry basis) and water content (up to 25 wt.%).

The third approach to lignocellulosic biomass conversion to liquid fuels involves the utilization of enzymes or acid- or base- catalyzed hydrolysis to decompose sugar polymers into their constituent monomers, the sugars can be further fermented into alcohols, dehydrated to aromatics or produced to variety of fuel products such as furans, alkanes and hydrogen [33-35]. Lignin can be converted to aromatics and alkanes through catalytic conversion or hydro treating [36, 37].

1.2.3. Bio-oil upgrading

As mentioned from the above section, bio-oil is crude oil and cannot be directly used as transportation fuels, mainly owning to its low heating value, high oxygen content and corrosiveness. Bio-oil upgrading is essential to practical usage. Hydrodeoxygenation (HDO) is considered as an effective method for it, as it can reduce the oxygen content and reactive functionalities. The conventional hydrodeoxygenation process is carried out in the presence of high H_2 pressure (80 bar - 200 bar) and at high temperatures (250 °C – 450 °C) in the presence of a catalysts [38]. The HDO reaction is closely related to hydrodesulphurization (HDS) process, used in the elimination of sulphur from organic compounds[39,40]. HDO also use hydrogen for the exclusion of the heteroatom (oxygen), forming H_2O and saturated hydrocarbons. Potential catalysts are of great interest to decrease the severity of reaction conditions.

Raney Ni with Nafion/SiO_2 catalyst was chosen as heterogeneous catalyst for the research on a simple, green, low cost and efficient route for converting phenolic components in bio-oil to hydrocarbons[41]. As shown in Table 1.3, hydrodeoxygenation of 4-n-propylphenol was performed in aqueous phase at 200 °C, with different Pd and Ni catalysts at 40 bar of H_2. 4-n-Propyphenol could be efficiently converted with cycloalkane selectivity of 98% to 99%. over low cost

Raney Ni catalysts combining solid acids such as zeolite and Nafion. These observations indicate that using non-noble Ni catalyst with suitable solid acid is able to act as efficiently as Pd/C, to be a potential one in future industrial application.

Table 1.3. Aqueous-phase hydrodeoxygenation of 4-n-propylphenol using Pd and/or Ni based catalysts and acids at 473 K [41].

Catalyst	Acid	Conv. (%)	Cycloalkane selectivity [C%]
Pd/C	H_3PO_4	100	84
Pd/C	CH_3COOH	100	74
Pd/C	Zeolite (H-Beta)	100	1.5
Pd/C	Zeolite (H-Y)	100	5.2
Pd/C	Nafion solution	100	98
Pd/C	Nafion/SiO_2	100	98
Ni/SiO_2	Nafion/SiO_2	9	43
Ni/ASA	Nafion/SiO_2	37	50
RANEY Ni®2400	Nafion/SiO_2	51	36
RANEY Ni®4200	Nafion/SiO_2	96	64
RANEY® Ni	Nafion/SiO_2	100	99
RANEY® Ni	Nafionsolution	100	98
RANEY® Ni	H_3PO_4	0	—
RANEY® Ni	CH_3COOH	0	—

Other works from this group studied the mechanisms of selective cleavage of C-O bonds in di-aryl ethers in aqueous phase by using Ni/SiO2 catlayst at relatively mild conditions (120 °C, 6 bar)[42]. The C-O bond of di-aryl ethers (diphenyl ether, p-tolyl ether and 4.4'-dihydroxydiphenyl ether) was cleaved by parallel hydrogenolysis and hydrolysis on Ni. The rates as a function of H2 pressure from 0 to 10 MPa indicated that the rate-determining step is the C-O bond cleavage on Ni surface. TOFs of the di-aryl ethers conversion followed the order dihydroxydiphenyl ether (69 h^{-1}) > dipheyl ether (26 h^{-1}) > p-tolyl ether (1.3 h^{-1}). The C-O bond cleavage mechanisms are shown in Scheme 1.1. Most of the di-

aryl ethers were converted via hydrogenolysis and hydrolysis (C-C cleavage with HO· addition), and then further hydrogenated to saturated hydrocarbons. In all, it was encouraging that C-O bond cleavage of ethers was achieved under mild operation conditions (393 K, 0.6 MPa H_2) at which maximum rates were observed, indicating that H_2 competes with the hydrocarbon for adsorption sites. Besides, compared to C-O bond cleavage from phenol, the C-O bonds energies from mentioned ethers are weaker[43], and this is also a reason that the C-O bond cleaved at such mild conditions.
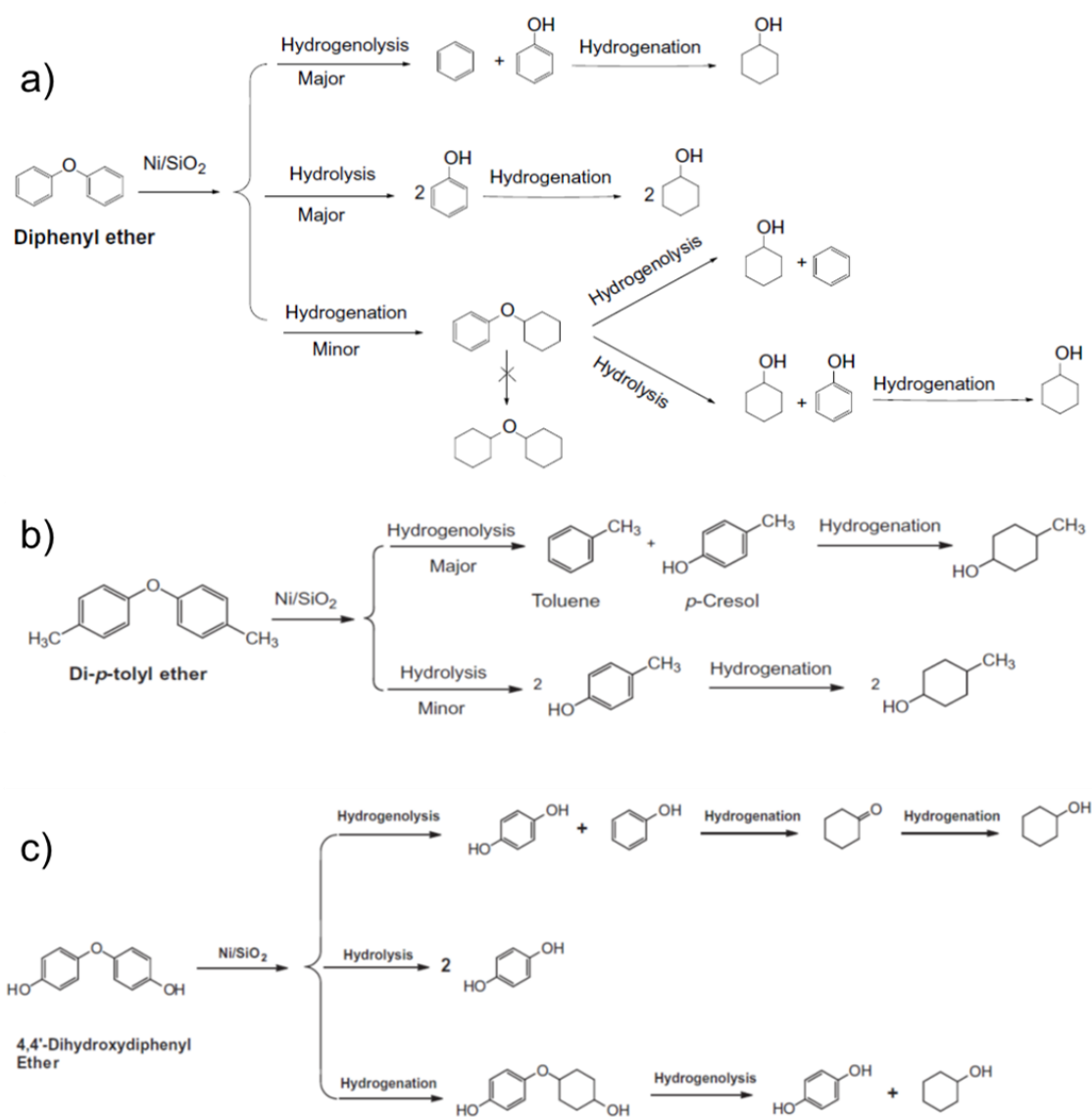
Scheme 1.1. Reaction pathways on a) diphenyl ether, b) di-p-tolyl ether and c) 4,4'-dihydroxydiphenyl ether conversion on Ni/SiO$_2$ in aqueous phase [42, 43].

1.3. Electrocatalysis

1.3.1. General aspects of electrocatalysis

Electrochemistry is a branch of physical chemistry that studies the relationship between electricity and identifiable chemical changes, with either electricity considered an outcome of a particular chemical reaction or vice versa. These reactions involve electric charges moving between electrodes and an electrolyte (or ionic species in a solution). Thus electrochemistry deals with the interaction between electrical energy and chemical change. When a chemical reaction is caused by an externally supplied current, as in electrolysis, or if an electric current is produced by a spontaneous chemical reaction as in a battery, it is called an electrochemical reaction. Chemical reactions, where electrons are transferred directly between molecules and/or atoms are called oxidation-reduction or (redox) reactions [44].

Electrocatalysis, an important branch of electrochemistry, is a type of catalysis, which studies catalysts on the surface of an electrode, or as an electrode, that results in the modification of the rate of an electrochemical reaction occurring on the electrode surface. Subjects of electrocatalysis are reaction rates depending on electrical potential, electrode materials, electrolyte, temperature etc. [45]. An electrochemical reaction is normally performed in an electrochemical cell, which is a reactor containing cathode (the electrode to produce a reduction reaction), anode (the electrode where oxidation reaction takes place), and reference electrode. The latter is an electrode, which has a stable and well-established electrode potential by employing a redox reaction with constant concentrations of each participant, thus can be used as a reference to reaction potential calculation. Electrodes can

be made from a variety of conductive materials, including metals, semiconductors, conductive polymers and graphites. Electrolyte is needed to support an electrochemical reaction, as ions in the electrolyte can move freely to promise the electrical conductivity. Typical electrochemical cells are shown in Figure 1.5. The figure in (a) is a typical single compartment three-electrode electrochemical cell, and the Figure in (b) is a two compartment cell, cathodic chamber and anodic chamber is separated by a proton exchange membrane (normally Nafion membrane).
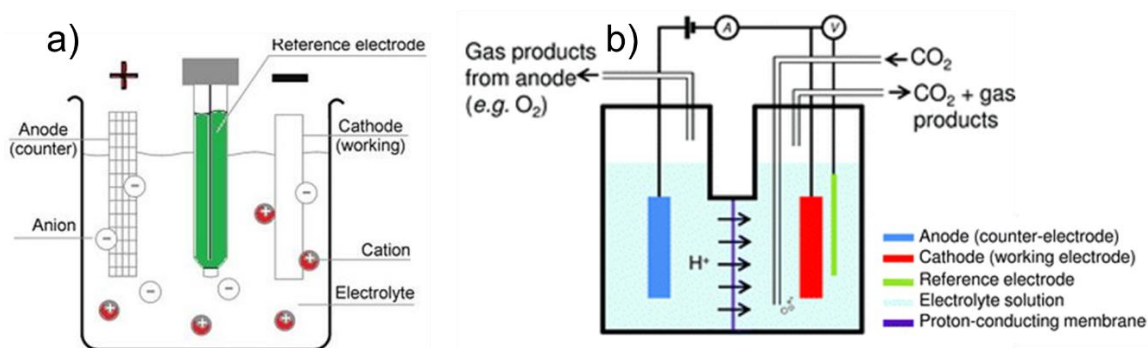
Figure 1.5. Schematic representation of a three electrode a). single-compartment electrochemical cell [46]; and b) two-compartment electrochemical cell [47].

1.3.2. Water electrolysis and Nernst equation

Electrolysis of water [48-50] is the decomposition of water into oxygen gas (O_2, on the anode) and hydrogen gas (H_2, on the cathode) through the application of external electrical potential. The general reaction proceeds as shown in the following equations:

Cathode: $2 H_2O$ (l) $+ 2 e^- \rightarrow 2 H_2$ (g) $+ 2 OH^-$ (aq)

Anode: $2 H_2O$ (l) $\rightarrow O_2$ (g) $+ 4 H^+$ (aq) $+4 e^-$

Overall: $2 H_2O$ (l) $\rightarrow 2 H_2$ (g) $+ O_2$ (g)
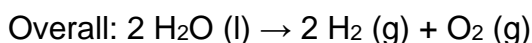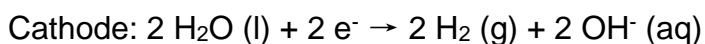
The reduction reaction takes place on the cathode which is negatively charged, electrons are passed from the cathode to hydrogen cations to form hydrogen gas.

13

While on the anode, electrons are taken by the anode from hydroxide anions to form oxygen gas via oxidation reaction. The hydrogen cations produced on the anode will move to cathode to be reduced to hydrogen gas. Decomposition of pure water into hydrogen and oxygen at standard temperature and pressure is not favorable in thermodynamic terms, as Gibbs free energy for electrolysis of water is 474.4 kJ, an external potential (-1.23 V) is needed based on the calculation via the Nernst equation below:

$\Delta G^{\ominus} = - nFE^{\ominus}$

Where $\Delta G^{\ominus}$ is the standard free Gibbs energy, n is the number of electrons transferred, F is the Faraday constant, and $E^{\ominus}$ is the standard potential. The reaction is affected by pH according to the Nernst equation. In acid conditions (pH = 0), the equation of water electrolysis follows:

Cathode: $4 H^+ + 4 e^- \rightarrow 2 H_2$ $\hspace{4cm}$ $E^{\ominus} = 0.0$ V

Anode: $2 H_2O \rightarrow O_2 + 4H^+ + 4e^-$ $\hspace{3cm}$ $E^{\ominus} = +1.229$ V

And in alkaline conditions (pH = 14), the half reactions occur as:

Cathode: $4 H_2O + 4 e^- \rightarrow 2 H_2 + 4 OH^-$ $\hspace{2.5cm}$ $E^{\ominus} = - 0.828$ V

Anode: $4 OH^- \rightarrow O_2 + 2 H_2O + 4 e^-$ $\hspace{2.8cm}$ $E^{\ominus} = + 0.401$ V

The onset potential of hydrogen evolution reaction (HER) is affected by the pH of electrolyte, according to the calculations from the Nernst equation:

$$E_{red} = E_{red}^{\ominus} + \frac{RT}{zF} \ln \frac{a_{Ox}}{a_{Red}}$$

$$E_{cell} = E_{cell}^{\ominus} - \frac{RT}{zF} \ln Q_r$$

Where, E_{red} is the half-cell reduction potential at the temperature of interest; $E_{red}^{\ominus}$ is the standard half-cell reduction potential; E_{cell} is the cell potential at the temperatue of interest; $E_{cell}^{\ominus}$ is the standard cell potential; R is the universal gas

constant, which is 8.314 JK^{-1}mol^{-1}; T is the temperature in K; a_{Ox} is the activity of the oxidizing agent; a_{Red} is the activity of the reducing agent; Q_r is the reaction quotient; F is the Faraday constant, which is 96485 C mol^{-1}; z is the number of moles of electrons transferred in the cell reaction or half reaction.

At room temperature (25 °C), the Nernst equation is expressed in terms like:

$$E = E^{\Theta} + \frac{0.05916}{z} log_{10} \frac{a_{Ox}}{a_{Red}}$$

Thus, the equation of water reduction reaction (HER) can be simplified to:
$$E = E^{\Theta} - 0.059 \times pH$$

1.3.3. Applications of electrocatalysis

Applications and studies on electrocatalysis are a classic research discipline. An important specific issue is the study on hydrogen evolution (HER) via electrocatalysis because H$_2$ is a promising energy carrier that can efficiently be used to produce electricity from its stored chemical energy. It is a potential power source for vehicular and stationary applications, solving the twin problems of depletion of fossil fuel reserves and CO$_2$ emissions [51-53]. Besides, water electrolysis for hydrogen production has many advantages such as high purity, simple process, no pollution and plenty of water sources. The problems or disadvantages of renewable primary energy are regionalism, intermittence and unstorability, which will result in instability of power source. Hydrogen produced by water electrolysis is considered as the best energy carrier to adjust the balance between the generation of power source by renewable primary energy and energy demand for end-use. It provides an inspiring opportunity to develop water electrolysis technology. Figure 1.6 depicts a promising roadmap of sustainable energy. The majority of renewable energy provides power source for end-use, and excess electricity is used to electrolyze water to produce storable hydrogen and oxygen. Then, hydrogen is transported to the regions where renewable energy is

lacked, and serves to industry, traffic, electric station and household. The sustainable energy route is feasible and convenient.

One of the challenges in water electrolysis is to reduce energy consumption of water electrolysis for large-scale application in the future. Cell voltage (U), an important criterion of energy consumption, consists of theoretical decomposition voltage (U^θ), ohmic voltage drop ($i \times \Sigma R$) and reaction overpotential (η). Impacts on kinetics such as overpotential, ohmic drop, bubble coverage on the electrode are widely studied to optimize water electrolysis reaction. Besides, low-cost and high performance alternative catalysts for HER are also of great interest in industrial scale, as noble metal catalysts are not suitable for big scale process [53, 54]. For this needed development, HER onset potential and activity of the catalysts should be considered.
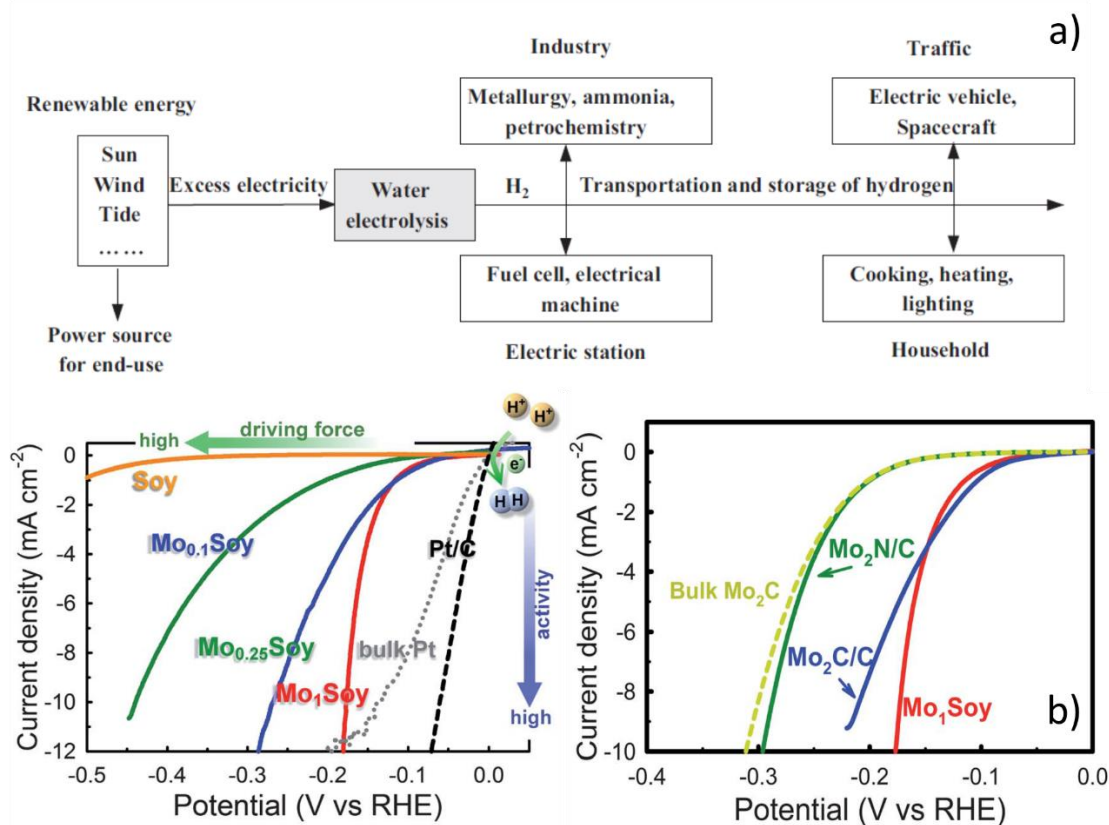
Figure 1.6 a). Sustainable production and application of energy [53]. b) Water electrocatalysis performances of promising earth-abundant catalysts compared with Pt [54].

Another emerging study is electrocatalytic reduction of carbon dioxide. The development of modern energy economy and chemical industry are still heavily dependent on fossil resources. Thus sustainable alternatives need to be developed to secure long-term economic growth while mitigating socio-environmental problems potentially associated with increasing anthropogenic emissions of CO_2. One potential solution to alleviate this concern while simultaneously addressing rising concentrations of atmospheric CO_2 is its electrochemical reduction to carbon-based energy carriers [55]. Recent reports showed that CO_2 could be effectively reduced to low-carbon fuels, including CO, $HCOOH/HCOO^-$, CH_2O, CH_4, $H_2C_2O_4/HC_2O_4^-$, C_2H_4, CH_3OH, CH_3CH_2OH and others. The electrocatalysts are classified into several categories, including metals, metal alloys, metal oxides, metal complexes, polymers/clusters, enzymes and organic molecules. Electro reduction of CO_2 has several advantages such as: 1) the reduction process is under control by adjusting reduction potential and reaction temperature; 2) the electrolyte can be fully recycled to minimize the chemical consumption; 3) electricity used to derive the reduction can come from renewable power source without further CO_2 generation, as mentioned above. However, challenges such as the slow kinetics of CO_2 electro-reduction, high requirement of reduction potentials, low energy efficiency and high energy consumption of the process have to be considered [56]. In study, electrochemical reduction of CO_2 is found to proceed via 2-, 4-, 6-, and 8-electron reduction pathways in gaseous, aqueous and non-aqueous phases, typical thermodynamic electrochemical half-cell reduction standard potentials are listed in Table 1.5.

1.3.4. Electrocatalysis study on biomass

Conventional catalytic conversion of biomass to fuels and chemicals has attracted great attention as one of the future technologies for mitigating global warming and for building a carbon-neutral energy cycle [4, 40]. Thermal catalytic hydrogenation (TCH) has been shown to be a good method for bio-oil stabilization, converting most aldehydes, ketones, phenols and sugars to saturated alcohols and polyols[58, 59]. However, such hydrogenation process is normally run at high temperatures and high pressure of hydrogen gas. Instead, electrocatalytic hydrogenation (ECH) process is always performed at less than 80 °C and ambient pressure. Such mild operating conditions promise a minimization of both polymerization of the organic reactant, and catalyst deactivation by coke. Besides, there is no need to feed external hydrogen gas to the ECH, since during the ECH, atomic hydrogen (H_{ads}) is in-situ formed on the catalytic electrode surface via the reduction of the protons from the electrolyte. In short, ECH is a promising strategy, which simplifies the hydrogenation processing and avoids the external requirement of fossil-based hydrogen gas and associated equipments. The electricity could come from carbon-free sources such as wind, solar and nuclear power as we mentioned above. Thus, ECH will represent a green, carbon-retentive pathway for stabilization and further upgrading of biomass-derived bio-oil to produce fuels and chemicals [60].

Table 1.5. Selected standard potentials of CO_2 in aqueous solutions (V vs. SHE) at 1.0 atm and 25 1C, calculated according to the standard Gibbs energies of the reactants in reactions [57].

Half-electrochemical thermodynamic reactions	Electrode potentials (V vs. SHE) under standard conditions
$CO_2(g) + 4H^+ + 4e^- = C(s) + 2H_2O(l)$	0.210
$CO_2(g) + 2H_2O(l) + 4e^- = C(s) + 4OH^-$	-0.627
$CO_2(g) + 2H^+ + 2e^- = HCOOH(l)$	-0.250
$CO_2(g) + 2H_2O(l) + 2e^- = HCOO^-(aq) + OH^-$	-1.078
$CO_2(g) + 2H^+ + 2e^- = CO(g) + 2H_2O(l)$	-0.106
$CO_2(g) + 2H_2O(l) + 2e^- = CO(g) + 2OH^-$	-0.934
$CO_2(g) + 4H^+ + 4e^- = CH_2O(l) + H_2O(l)$	-0.070
$CO_2(g) + 3H_2O(l) + 4e^- = CH_2O(l) + 4OH^-$	-0.898
$CO_2(g) + 6H^+ + 6e^- = CH_3OH(l) + H_2O(l)$	0.016
$CO_2(g) + 5H_2O(l) + 6e^- = CH_3OH(l) + 6OH^-$	-0.812
$CO_2(g) + 8H^+ + 8e^- = CH_4(g) + 2H_2O(l)$	0.169
$CO_2(g) + 6H_2O(l) + 8e^- = CH_4(g) + 8OH^-$	-0.659
$2CO_2(g) + 2e^- = C_2O_4^{2-}(aq)$	-0.590
$2CO_2(g) + 2H^+ + 2e^- = C_2H_4O_4(aq)$	-0.500
$2CO_2(g) + 12H^+ + 12e^- = CH_2CH_2(g) + 4H_2O(l)$	0.064
$2CO_2(g) + 8H_2O(l) + 12e^- = CH_2CH_2(g) + 12OH^-$	-0.764
$2CO_2(g) + 12H^+ + 12e^- = CH_3CH_2OH(l) + 3H_2O(l)$	0.084
$2CO_2(g) + 9H_2O(l) + 12e^- = CH_3CH_2OH(l) + 12OH^-$	0.744

Recently, Koper and his team have studied electocatalytic hydrogenation on variety of biomass based model compounds including glucose, and 5-hydroxymethylfurfural [61-63]. Glucose is converted to sorbitol or 2-deoxysorbitol on multiple solid metal electrodes in neutral media. Tested metal catalysts are divided into three groups based on the reaction products from glucose reduction: (a) metals forming sorbitol, (Fe, Co, Ni, Cu, Pd, Au, Ag, and Al); (b) metals forming solely H_2 (Ti, V, Cr, Mn, Zr, Nb, Mo, Hf, Ta, We, Re, Ru, Rh, Ir, and Pt), and (c)

metals forming sorbitol and 2-deoxysorbitol, with very little hydrogen (Zn, Cd, In, Sn, Sb, Pb, and Bi), as shown in Figure 1.8 a), b) and c) respectively. In comparison, Ni shows the lowest overpotential for the onset of sorbitol formation (-0.25 V) whereas Pb generates sorbitol with the highest yield (< 0.7 mM cm^{-2}). Different to smooth Pt electrode, a largesurface-area Pt/C electrode hydrogenates glucose to sorbitol from -0.21 V with relatively low current. This emphasizes the importance of the active sites and the surface area of the catalyst. The mechanism to form 2-deoxysorbitol from glucose and/or fructose is discussed according to the observed reaction products. The yield and selectivity of hydrogenated products are highly sensitive to the chemical nature and state of the catalyst surface.
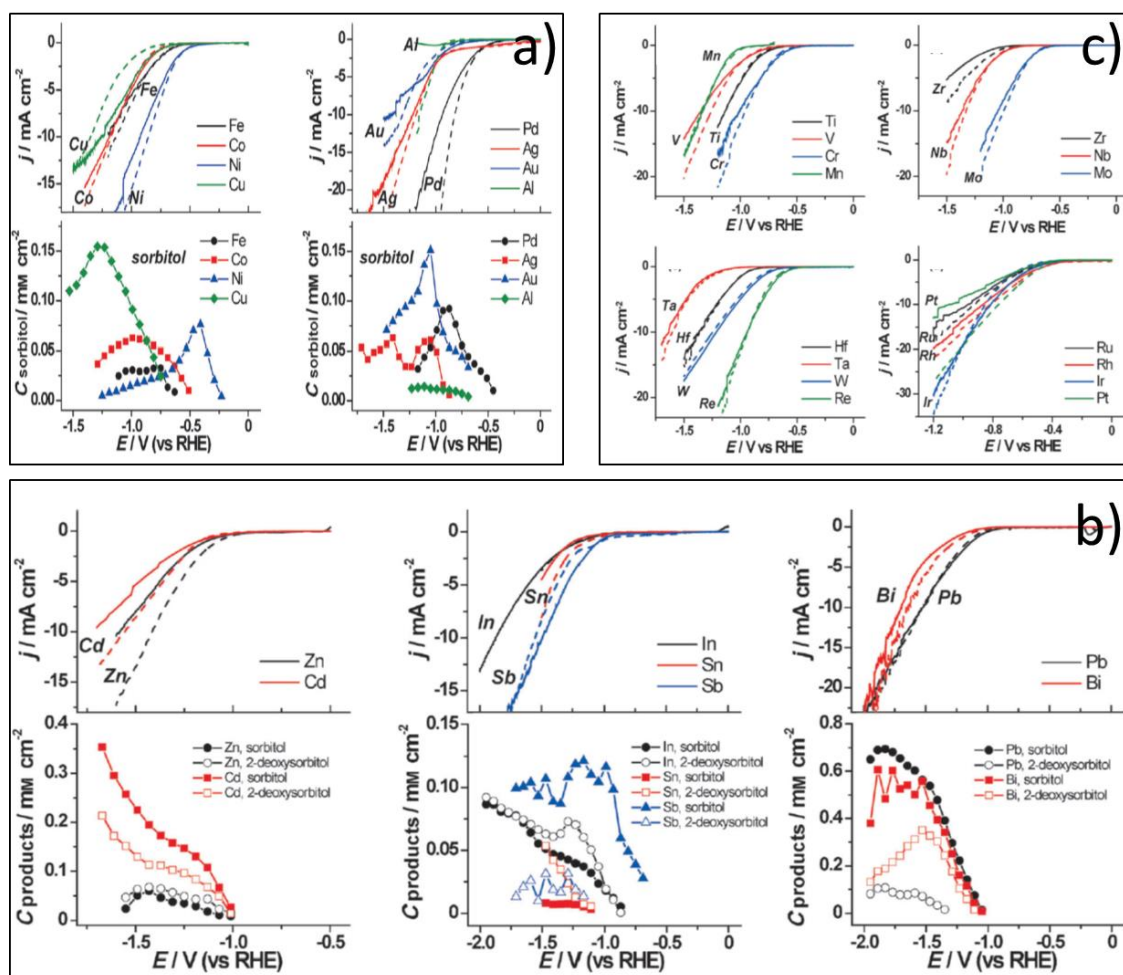
Figure 1.8. Electrocatalytic glucose reduction and current density profiles with and without glucose in the solution to a). only sorbitol, b). sorbitol and 2-deoxysorbitol and c). only hydrogen (H_2) [61].

Another interesting topic to study is the ECH of 5-hyroxymethyl (HMF) furfural on different solid metal electrodes in acidic solution. Three soluble products from HMF hydrogenation were distinguished: 2,5-dihydroxymethylfuran (DHMF), 2,5-dihydroxymethyltetrahydrofuran (DHMTHF), and 2,5-dimethyl-2,3-dihydrofuran (DMDHF). Based on the dominant reaction products, the metal catalysts were divided into three groups: (1) metals mainly forming DHMF (Fe, Ni, Cu, and Pb), (2) metalsforming DHMF and DMDHF depending on the applied potentials (Co, Ag, Au, Cd, Sb, and Bi), and (3) metals forming mainly DMDHF (Pd, Pt, Al, Zn, In, and Sb). Nickel and antimony are the most active catalysts for DHMF (0.95 mm cm^{-2} at ca. -0.35 V_{RHE} and -20 mA cm^{-2}) and DMDHF (0.7 mm cm^{-2} at -0.6 V_{RHE} and -5mA cm^{-2}), respectively. The pH of the solution plays an important role in the hydrogenation of HMF. Acidic conditions lower the activation energy for HMF hydrogenation and hydrogenates the furan ring further to tetrahydrofuran. The reaction network is shown in Scheme 1.2.
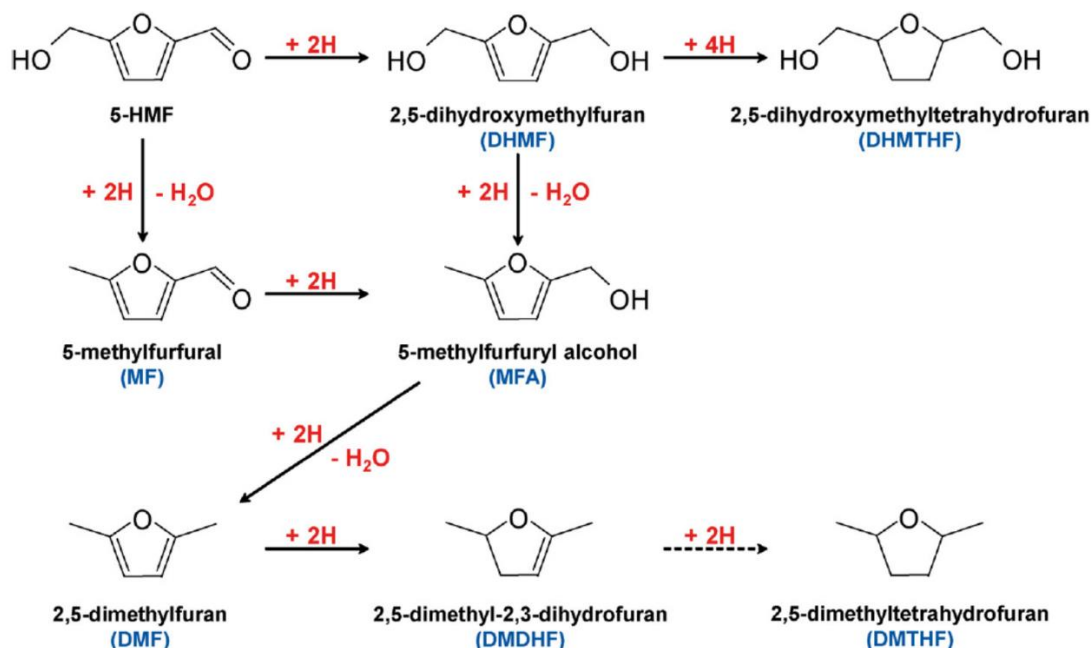
Scheme 1.2. Schematic of HMF electrocatalytic hydrogenation pathways in acidic condition[62].

Ménard et al. have studied electrocatalytic hydrogenation of phenol on Pd catalysts focusing on kinetics, the impact of support of the catalyst, and pH value of the solution [64-66]. In their study, ECH was highly dependent on the physicochemical and conducting properties of the matrix. Tin dioxide was chosen as oxide matrix owning to its changeable conductivity by doping with fluorine. Comparison of non-conductive and conductive catalysts for ECH of phenol showed that conductive F-doped SnO_2 increased the rate of electro hydrogenation. During ECH, phenol converts via 2 consecutive steps of hydrogenation, producing cyclohexanone as intermediate, and cyclohexanol as final product, as shown in scheme 1.3.
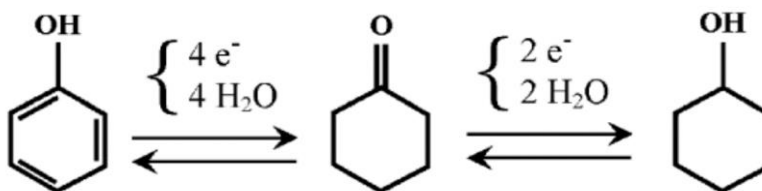
Scheme 1.3. Schematic of phenol electrocatalytic hydrogenation pathways.

Hydrogenation of cyclohexanone via thermal catalytic hydrogenation (TCH) and electrocatalytic hydrogenation (ECH) on Pd catalysts was studied and compared. ECH provided an alternative way to hydrogenate organic molecules under mild conditions, and the success of this method was related to the electrochemical generation of hydrogen and the catalytic hydrogenation. The main difference between TCH and ECH processes lies in the method of generating atomic hydrogen. The TCH process involves an external source of gas [Eq. (1)], whereas in the ECH process, electro reduction of hydronium ions leads to in-situ generated atomic hydrogen [Eq. (2)]. This species reacts with organic unsaturated molecules [Eq. (6)] adsorbed on the catalyst surface [Eq. (5)]. The hydrogenation step [Eq. (6)] is in competition with the electrochemical production and desorption

[Eqs. (3) and (4), respectively] of H_2. The last step in the ECH and CH process is the regeneration of the adsorption sites by desorption of the hydrogenated compound [Eq. (7)].

$$H_2 + 2\ M \leftrightarrow 2\ MH_{ads} \tag{1}$$

$$H^+ + e^- + M \leftrightarrow MH_{ads} + H_2O\ \text{(Volmer reaction)} \tag{2}$$

$$H^+ + MH_{ads} + e^- \leftrightarrow M + H_2 + H_2O\ \text{(Heyrovsky reaction)} \tag{3}$$

$$2\ MH_{ads} \leftrightarrow 2\ M + H_2\ \text{(Tafel reaction)} \tag{4}$$

$$Y{=}Z + M \leftrightarrow (Y{=}Z)_{ads}A \tag{5}$$

$$(Y{=}Z)_{ads}A + 2\ MH_{ads} \leftrightarrow (YH{-}ZH)_{ads}A + 2\ M \tag{6}$$

$$(YH{-}ZH)_{ads}A \leftrightarrow YH{-}ZH + M \tag{7}$$
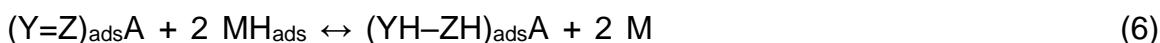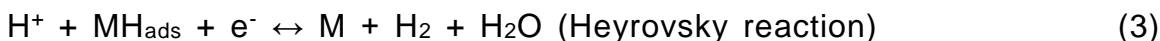
Where, M represents the metallic sites (Pd), where atomic hydrogen is formed (MH_{ads}), $Y{=}Z$ describes the organic unsaturated molecule (cyclohexanone), $(Y{=}Z)_{ads}A$ is the adsorbed organic unsaturated molecule (cyclohexanone), and $YH{-}ZH$ represents the organic saturated molecule (cyclohexanol). The target molecule is adsorbed on the adsorption sites (A) located on the catalyst matrix (alumina). Increasing the density of the target molecule in the immediate vicinity of the adsorbed hydrogen facilitates the overall hydrogenation process [64].

This work shows that organic compounds containing C=O functional groups can be efficiently hydrogenated by using Pd/alumina catalyst [64]. The Pd/alumina catalyst in the presence of phosphoric acid as the supporting electrolyte is ineffective in electrocatalytic and catalytic hydrogenation but becomes very efficient in the electrocatalytic process when used in acetic acid solution at slightly acidic pH, as shown in Figure 1.9. Compared to the activity of CH, ECH is a much more active alternative method. Further, pH of the electrolyte affects the ECH activity. Once the pH value increases (still pH < 7), the activity of ECH conversion increases as well. Higher activities were observed at pH 5-6 in acetic acid is because that the dissociation degree of acetic acid is higher, thus unprotonated form of acetic acid is better adsorbed on the alumina surface thus to modify the surface by a better coverage of organic phase. This affects the adsorption and the

diffusion of cyclohexanone across the interface. In pH 5-6, the modified surface is stable in and the adsorption is enhanced, thus to increase the ECH efficiency.
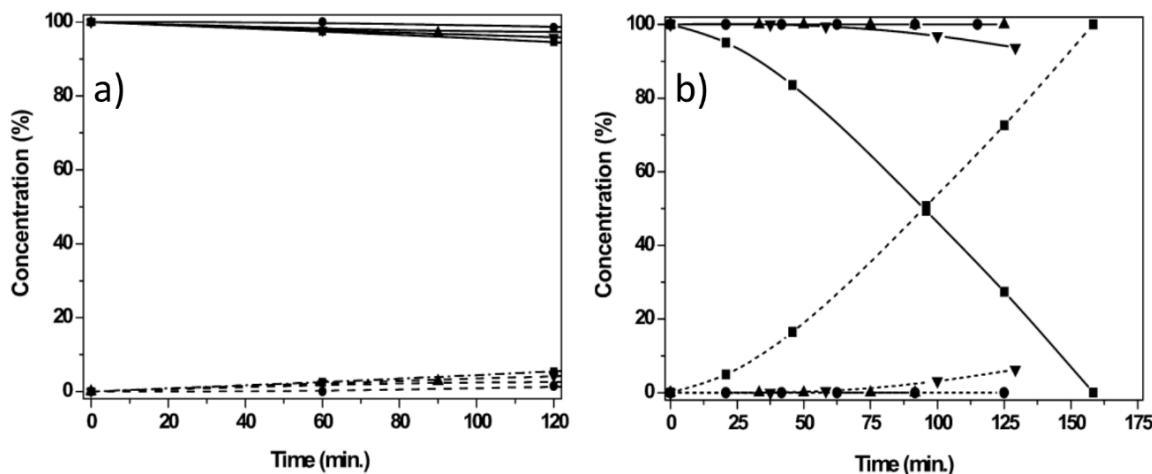
Figure. 1.9. Cyclohexanone (solid line) depletion to cyclohexanol (dash line) in a). CH and b) ECH process: (■) 10% Pd/alumina + acetic acid; (▼) 10% Pd/alumina + phosphoric acid; (▲) finely divided Pd + acetic acid; (●) finely divided Pd + phosphoric acid [64].

1.4. Scope of this thesis

Electrocatalysis of biomass-derived hydrocarbons has become increasingly attractive as shown by abundant reports since 2000 [65-70]. However, detailed kinetic studies that define reaction rates, turnover frequencies (TOFs), energy of the activation (Ea), faradic efficiency (FE), and reaction mechanisms (differentiating pathways such as hydrogenation, hydrogenolysis and hydrolysis) are still scarce. This hinders further application of the technology.

Thus, the main purpose of this thesis is to make a detailed study on the transformation of a series of O-containing compounds via electrocatalysis. All aspects of the research are covered such as designing and improving of electrocatalysis reactors, effects of the nature of the metal catalysts and operating

conditions, and reaction mechanisms. The objective of the research was to identify the parameters that will allow to maximize the activity and efficiency of electrocatalytic processes.

In the first part of the work, described in the second chapter, phenol was chosen as a model compound for lignin bio-oil and its hydrogenation via electrocatalytic hydrogenation ECH was studied for initial screening of operation conditions and catalysts. Catalysts studied include Pt, Rh and Pd supported on activated carbon. The impacts of temperature, electrolytes, pH values of the electrolyte, and electric current were investigated in order to optimize reaction conditions for ECH. In parallel, thermal catalytic hydrogenation (TCH) under operating conditions similar to ECH was performed and compared with ECH to understand the reaction mechanisms during the ECH process. The results showed that Rh/C is much more active in phenol hydrogenation via both ECH and TCH than on Pt/C and Pd/C under mild conditions. Besides ECH rates and faradic efficiency, selectivity is very sensitive to the variations of reaction conditions, such as the electrolyte, pH of the electrolyte, temperature. Similarities of reaction orders in phenol and activation energies between ECH and TCH indicated that phenol hydrogenation proceeds in the same pathway via ECH and TCH, the difference is the source of adsorbed hydrogen, which is provided by H_2 dissociation in TCH, and electroreduction of H^+ in ECH.

The second step of this research, described in the third chapter, was to explore the effects of molecular structure on the rates and reaction pathways for the conversion of phenolic compounds and aryl ethers. The optimum reaction conditions found in the previous work package were applied and further optimized, e.g., the geometry of the electrolysis reactor was improved. The conversion of phenol, phenolic substitutes as cresols and methyl phenols, and diaryl ethers via TCH and ECH. The impact of potential on ECH activity was studied showing that the reaction rates increase with increasingly cathodic potentials. This is related to the coverage of adsorbed hydrogen. ECH rates may exceed TCH rates under similar conditions of temperature pressure and solution composition. This is an encouraging signal of the potential of ECH application in the future. Furthermore,

it was interesting to observe that more reaction pathways and production of oxygen-free hydrocarbons were observed with increasing the complexity of the reactant structure. C-O bond cleavage in ethers is achieved via hydrolysis or hydrogenolysis. Besides, the surface chemical potential of hydrogen can be increased also by generating a H_2 atmosphere above the reaction media, supporting the conclusion that thermal and electrochemical routes share the same reaction pathways on these reactions.

The final findings of this thesis, reported in the fourth chapter, concern the study on ECH and TCH of benzaldehyde on Pt, Rh, Pd and Ni. Benzaldehyde is hydrogenated to benzyl alcohol via hydrogenation only on the carbonyl group, instead of a hydrogenation on benzene ring. Different reaction orders in ECH were observed on different metals. The observations indicate that benzaldehyde hydrogenation proceeds differently on ECH and TCH in function of the metal surface. Remarkably, Pd is found to be very selective for ECH of benzaldehyde, keeping a very good activity.

The results of this thesis shed better understanding of the conversion of oxygenated hydrocarbons at mild conditions while stablishing routes towards the application of electrocatalytic processes to obtain fuels. These results also advance the understanding of the metal function in condense phases and the associated reaction mechanisms.

References

[1] M. Koh, W. Hoi, Biomass. Bioenerg. 25 (2003) 517-529.

[2] N. Sasaki, W. Knorr, D. Foster, H. Etoh, H. Ninomiya, S. Chay, Appl. Energy. 86 (2009) 140-150.

[3] CIA World Factbook.

[4] G. Huber, S. Iborra, A. Corma, Chem. Rev. 106 (2006) 106 4044-4098.

[5] BP Statistical Review of World Energy 2014-BP Global http://www.bp.com/content/dam/bp-country/de_de/PDFs/brochures/BP-statistical-review-of-world-energy-2014-full-report.pdf

[6]   AIE   Australian   institute   of   energy.   Fact   sheet   8:   biomass. http://aie.org.au/Content/NavigationMenu/Resources/SchoolProjects/FS8 BIOMASS.

     pdf; 2010 [accessed 20.03.10].

[7] T. Abbasi, S. Abbasi, Renew. Sustain. Energy. Rev. 14 (2010) 919–937.

[8] TNP. The need project: biomass. http://www.need.org/needpdf/infobook activities/SecInfo/BiomassS.pdf; 2010 [accessed 25.12.09].

[9] U.S. Energy Information Administration, Monthly Energy Review. 2015

[10] Oregon.Biomass.energy. http://www.oregon.gov/ENERGY/RENEW/Biomass/ BiomassHome.shtml; 2010 [accessed 05.01.10].

[11] A. Demirbas, Progress. Energy. Combus. Sci. 30 (2005) 171-192.

[12] K. Lee, C. Boateng, Sustainability of biofuel production from oil palm biomass, Springer 2013.

[13] M. Stöcker, Angew. Chem. Int. Ed. 47 (2008) 9200-9211.

[14] N. Mosier, C. Wyman. B. Dale, R. Elander, Y. Lee, M. Holtzapple, M. Ladisch, Bioresour. Technol. 96 (2005) 673-686.

[15] M. Himmel, S. Ding, D. Johnson, W. Adney, M. Nimlos, J. Brady, T. Foust, Science 35 (2007) 804-807.

[16] K. Bozbas, Renew. Sustain. Energy. Rev. 12 (2008) 542–552.

[17] J. Hill, E. Nelson, D. Tilman, S. Polasky, D. Tiffany, PNAS. 103 (2006) 11206-11210.

[18] E. Kunkes, D. Simonetti, R. West, J. Ruiz, C. Gärtner, J. Dumesic, Science, 322 (2008) 417-421.

[19] A. Demirbas, Energ. Convers. Manage. 42 (2001) 1357-1378.

[20] P. Menanteau, D. Finon, M. Lamy, Energy. Policy. 31 (2003) 799-812.

[21] W. Kempton, J. Tomić, J. Power. Sources. 144 (2005) 280-294.

[22] J. Carrasco, L. Franquelo, J. Bialasiewicz, E. Galvan, R. Guisado, M. Prats, J. Leon, N. Alfonso, IEEE. T. Ind. Electron. 53 (2006) 1002-1016.

[23] G. Mul, C. Schacht, W. Swaaij, J. Moulijn, Chem. Eng. Process. 51 (2012) 137-149.

[24] Y. Kwon, K. Schouten, J. Waal, E. Jong, M. Koper, ACS Catal. 6 (2016) 6704-6717.

[25] W. Boerjan, J. Ralph, M. Baucher, Annu. Rev. Plant. Biol, 54 (2003) 519-546.

[26] P. Kenrick, P. Crane, Nature, 389 (1997) 33-39.

[27] N. Sun, H. Rodríguez, M. Rahman, R. Rogers, Chem. Commun. 47 (2011) 1405-1421.

[28] H. Kobayashi, A. Fukuoka, Green. Chem. 15 (2013) 1740-1763.

[29] G. Huber, J. Dumesic, Catal. Today. 111 (2006) 119-132.

[30] A. Bridgwater, Chem. Eng. J. 91 (2003) 87-102.

[31] Z. Srokol, A. Bouche, A. Estrik, R. Strik, T. Maschmeyer, J. Peters, Crab. Res. 339 (2004) 1717-1726.

[32] F. Behrendt, Y. Neubauer, M. Oevermann, B. Wilmes, N. Zobel, Chem. Eng. Technol. 31 (2008) 667-677.

[33] T. Carlson, T. Vispute, G. Huber, ChemSusChem. 1 (2008) 397-400.

[34] J. Chheda, G. Huber, J. Dumesic, Angew. Chem. Int. 46 (2007) 7164-7183.

[35] R. West, E. Kunkes, D. Simonetti, J. Dumesic, Catal. Today. 147 (2009) 115-125.

[36] M. Crocker, R. Andrews, Thermochemical Conversion of Biomass to Liquid Fuels and Chemicals, (2010) 1-25.

[37] J. Lange, Biofuels. Bioprod. Bioref. 1 (2007) 39-48.

[38] P. Mortensen, J. Grunwaldt, P. Jensen, K. Knudsen, A. Jensen, Appl. Catal. A-Gen. 407 (2011) 1-19.

[39] A. Bridgwater, Catal. Today 29 (1996) 285–295.

[40] A. Corma, G. Huber, Angew. Chem. Int. Ed. 46 (2007) 7184–7201.

[41] C. Zhao, Y. Kou, A. Lemonidou, X. Li, J. Lercher, Chem. Commun. 46 (2010) 412-414.

[42] J. He, C. Zhao, D. Mei, J. Lercher, J. Catal. 309 (2014) 280-290.

[43] J. He, C. Zhao, J. Lercher, J. Am. Chem. Soc. 134 (2012) 20768-20775.

[44] A. Bard, L. Faulkner, Electrochemical Methods: Fundamentals and Applications, John Wiley & Sons, Inc., 2001.

[45] S. Sun, S. Chen, Electrocatalysis, Chemical industry press, 2013.

[46] T. Mehmood, A. Mukhtar, B. Khan, K. Wu, Am. J. Chem. Eng. 4 (2016) 57-61.

[47] E. Kondratenko, G. Mul, J. Baltrusaitis, G. Larrazábal, J. Ramírez, Energy. Environ. Sci. 6 (2013) 3112-3135.

[48] K. Zeng, D. Zhang, Prog. Energy. Combust. Sci. 36 (2010) 307-326.

[49] C. Hamann, A. Hamnett, W. Vielstich, Electrochemistry (2nd) Wiley-VCH, 2007.

[50] F. Schafer, G. Buettner, Free. Radical. Bio. Med. 30 (2001) 1191-1212.

[51] J. Turner, Science. 305 (2004) 972-974.

[52] Hydrogen production road map: Technology pathways to the future, FreedomCAR & Fuel partnership. Hydrogen Production Technical Team, 2009.

[53] M. Wang, Z. Wang, X. Gong, Z. Guo, Renew. Sust. Energ. Rev. 29 (2014) 573-588.

[54] W. Chen, S. Iyer, S. Iyer, K. Sasaki, C. Wang, Y. Zhu, J. Muckerman, E. Fujita, Energy. Environ. Sci. 6 (2013) 1818-1826.

[55] N. Lewis, D. Nocera, Proc. Natl. Acad. Sci. U.S.A. 103 (2006) 15729-15735.

[56] J. Qiao, Y. Liu, F. Hong, J. Zhang, Chem. Soc. Rev. 43 (2014) 631-675.

[57] A. Bard, R. Parsons, J. Jordan, Standard potentials in aqueous solutions, CRC press, 1985.

[58] T. Vispute, G. Huber, Green. Chem. 11 (2009) 1433-1445.

[59] F. Mahfud, S. Bussemaker, B. Kooi, H. Heeres, J. Mol. Catal. A: Chem. 264 (2007) 227-236.

[60] Z. Li, M. Garedew, C. Lam, J. Jackson, D. Miller, C. Saffron, Green. Chem. 14 (2012) 2540-2549.

[61] Y. Kwon, M. Koper, ChemSusChem. 6 (2013) 455-462.

[62] Y. Kwon, Y. Bordja, S. Raoufmoghaddam, M. Kopper, ChemSusChem. 8 (2015) 1745-1751.

[63] Y. Kwon, E. Jong, S. Raoufmoghaddam, M. Kopper, ChemSusChem. 6 (2013) 1659-1667.

[64] C. Cirtiu, A. Wittmeyer, H. Ménard, J. Catal. 245 (2007) 191-197.

[65] D. Tountian, A. Wittmeyer, P. Nkeng, G. Poillerat, H. Ménard, J. Appl. Electrochem. 39 (2009) 411-419.

[66] A. Bannari, P. Proulx, H. Ménard, C. Cirtiu, Appl. Catal. A: Gen, 345 (2008) 28-42.

[67] J. Roylance, K. Choi, Gree. Chem. 18 (2016) 2956-2960.

[68] N. Itoh, W. Xu, S. Hara, K. Sakaki, Catal. Today. 56 (2000) 307-314.

[69] K. Carroll, T. Burger, L. Langenegger, S. Chavez, S. Hunt, Y. Leshkov, F. Brushett, ChemSusChem. 9 (2016) 1-8.

[70] L. Xin, Z. Zhang, J. Qi, D. Chadderdon, Y. Qiu, K. Warsko, W. Li, ChemSusChem. 6 (2013) 674-686.

Chapter 2

Aqueous phase electrocatalysis and thermal catalysis for the hydrogenation of phenol at mild conditions

The electrocatalytic hydrogenation (ECH) of phenol on Pt/C, Rh/C, and Pd/C was explored in an H-type two-compartment cell with respect to the impact of electrolyte, pH, current, and catalyst concentration. In all cases, the electric efficiencies increased with increasing phenol conversions. Rh/C exhibited the highest hydrogenation rate normalized to the concentration of accessible metal (TOF) followed by Pt/C in terms of mass of metal and intrinsic activities. Therefore, the effect of temperature on ECH and of mild thermal hydrogenation (TH) of phenol was explored on these catalysts. The activation energies for ECH were ca. 23 kJ·mol^{-1} and 29 kJ·mol^{-1} on Rh/C, and Pt/C, respectively. TH is much faster than ECH, although both pathways have the same activation energy. Cyclic voltammetry of bulk Pt and Pt/C in the presence of phenol indicated that phenol is adsorbed on the metal and reacted with hydrogen radicals. Hence, ECH was concluded to proceed via a Langmuir-type mechanism where the surface hydrogen is produced by reduction of protons (which occurs when the catalyst contacts the electrode) instead of H2 dissociation as in TH. Although competitive reactions

evolve H2 during ECH, the involvement of this H2 in phenol hydrogenation was minor. Thus, ECH and TH are independent processes and do not exhibit any synergy. In both pathways, the reaction path is phenol → cyclohexanone → cyclohexanol. C-O bond cleavage was not observed.

2.1. Introduction

Reductive biomass conversion and electricity generation from renewable sources (e.g., photovoltaics, wind power, and hydropower) are essential to secure a sustainable supply of energy, fuels, and chemicals [1-4]. Most of the techniques that are emerging for producing biofuels from biomass-derived feedstocks require H_2 to remove oxygen from the biogenic material [5-7]. Whereas H_2 may not be available in the decentralized locations, excess electricity generated from renewable resources may be stored supplying the reduction equivalents. Thus, coupling electrochemical water reduction with the reduction of biomass-derived feedstocks would help to improve the utilization of wind and solar energy by storing energy via reduction of the locally available feedstock.

The electrocatalytic hydrogenation (ECH) of biomass is beginning to emerge as a conceptually attractive alternative for thermal upgrading bio-oil at mild conditions using reduction equivalents generated by electricity [8, 9]. During ECH, H· is formed on the surface of the catalyst *via* reduction of protons supplied by the electrolyte, hydrogenating organic substrates. The conversions are ideally achieved at mild conditions and the overpotential required for ECH can be minimized by adapting the electrocatalyst [10].

Lignocellulosic biomass deconstructed *via* thermal or chemical methods is easily available at a local level, stimulating substantial efforts in the catalytic reduction of complex mixtures to fuels and chemicals [11, 12]. Exploring the conversion of compounds, representative of deconstructed biomass, on well-defined materials is critical to elucidate structure-activity correlations needed for the development of better catalysts, which must be stable in the presence of

substantial concentrations of water associated with the treatment of bio-oils [13]. Estimulating efforts on the conversion of representative compounds in aqueous phase have been reported in literature [14, 15]. However, classical electrochemical mechanisms have been given for granted and the involvement of thermal pathways is a question that is not addressed. Conversions routes accessed by thermal catalysis might be relevant at mild conditions over the metals that offer the highest activity and stability in electrochemical processes performed in aqueous solutions. Comparing thermal catalysis and electrocatalysis is of prime importance as H_2 produced from water electrolysis can be used as external H_2 supply to maximize hydrogenation efficiency.

Thus, the present work investigates the performance of a series of C-supported noble metal catalysts (Pt, Pd, and Rh) integrated in an electrolytic cell for the cathodic transformation of phenol in aqueous phase. The effects of electrolyte, current, pH and temperature on selectivity, intrinsic activity (TOF) and electrical efficiency of the catalysts are described. ECH is compared to thermal catalysis at the same mild conditions in order to understand the reaction mechanisms.

2.2. Experimental

2.2.1. Chemicals and catalytic materials

All chemicals were obtained from Sigma Aldrich and used as received, i.e., phenol (≥99.0%), acetate buffer solution (pH 4.6), phosphoric acid (≥99.9%), acetic acid (≥99.0%), sulfuric acid (≥99.9%), toluene (≥99.9%, HPLC), ethyl acetate (≥99.9%, HPLC), NaOH (≥99.9%, HPLC), and KCl (≥99.0%). High purity water, obtained with a Milli-Q water purification system with a resistivity of 18.2 MΩ·cm, was used for all experiments. The supported noble metal catalysts used in this study were purchased from Sigma Aldrich: Pt/C, Pd/C, and Rh/C. All these materials had a metal content of 5 wt. %.

2.2.2. Catalyst characterization

The surface areas and pore diameters of the catalysts were determined by N_2 adsorption at 77 K on a PMI automated BET sorptometer. The samples were outgassed before measurements at 523 K for 20h. The surface areas and pore distributions were calculated according to BET and BJH models.

The dispersion of the metal phase was determined by H_2 chemisorption. Prior to the measurements, the materials were treated in vacuum at 588 K for 1h and then cooled to 313 K. Hydrogen adsorption isotherms were measured at 1 to 40 kPa H_2. Afterwards equilibration with H_2, the samples were outgassed at 313 K for 1h and a second set of isotherms was measured. The concentrations of chemisorbed H_2 on the metal were determined by extrapolating the difference isotherms to zero hydrogen pressure. The dispersion of the supported metals was estimated from the concentration of chemisorbed H_2 assuming a stoichiometry of 1:1 metal to hydrogen atoms.

The dispersion of the metal was also explored by transmission electron microscopy (TEM). Samples of the catalysts were ground, and ultrasonically dispersed in ethanol. Drops of the suspensions were applied on a copper-carbon grid and the measurements were carried out in a JEOL JEM-2011 electron microscope with an accelerating voltage of 120 keV. Statistical treatment of the metal particle size was done by counting at least 200 particles detected in several places of the grid.

2.2.3. Electrocatalytic hydrogenation (ECH)

Electrolysis was carried out at atmospheric pressure in an H-type two-compartment electrochemical cell with a jacket for temperature control. Typically, the temperature was kept at 296 K (room temperature), except during a series of experiments performed at temperatures up to 353 K. The two compartments of the

cell were separated by a Nafion 117 proton exchange membrane (Ion Power, Inc.), which was treated in sulfuric acid (2 M) before use. A piece of reticulated vitreous carbon (RVC, ERG Aerospace Corp., 100 pores per inch) shaped into a 20 mm × 20 mm × 12 mm cuboid, and connected to a graphite rod (Sigma Aldrich), was used as working electrode in the cathode compartment. A Pt wire (Alfa Aesar, 99.9 %) was used as counter electrode in the anodic compartment. The reference electrode was a home-made Ag/AgCl electrode with a double junction. The cathode compartment was filled with 58 mL of electrolyte solutions at defined pH (adjusted by adding small amounts of aqueous NaOH or the corresponding acid). A chosen amount of catalyst was added into liquid at the cathode compartment as powder, stirring the slurry at 500 rpm. Prior to ECH, polarization of the catalyst was performed under a constant current of -40 mA for 30 min. After polarization, 2 mL of phenol solution was added into the cathode compartment to obtain a final concentration of 17.7 mmol/L. ECH was then performed at galvanostatic (-40 mA) or potentiostatic (-0.72 V on Pt/C and -0.65 V on Rh/C) conditions, while a flow of N_2 was maintained through the cell. During all these described procedures, the anode compartment was filled with 40 mL of solution containing the corresponding electrolyte. All electrochemical procedures were performed with an electrochemical workstation (VSP-300, Bio Logic). Before each ECH test (and before the voltammetric experiments described below), the cell compartments and other materials were cleaned with concentrated H_2SO_4 and immersed in boiling water for 2 h several times. Prior to the reactions, the electrodes were alternatively immersed in H_2SO_4 (5 M) and KOH (5 M) for 15 min. After each immersion, the materials were thoroughly cleaned (Pt electrodes were further ultrasonically treated) in ultrapure water for 15 min.

2.2.4. Catalytic hydrogenation (CH) and additional electrochemical measurements

Catalytic hydrogenation (i.e., thermal, with and without the presence of any electric potential) was carried out at atmospheric pressure of H_2 at constant temperature. This was achieved by flowing 20 mL/h of H_2 through the solution in the cathode compartment. The concentration of phenol was kept at 17.7 mmol/L, whereas different amounts of catalyst was used (to control the reaction rates) suspended in the solution and magnetically stirred at constant rate. Electrocatalytic hydrogenation in the presence of H_2 (20 mL/h) was performed following the procedure for the ECH process mentioned above.

Selected cyclic voltammetric experiments were performed using Pt wires as cathode and anode. An Ag/AgCl electrode was used as reference electrode, whereas the electrolyte was an aqueous solution of acetic acid at pH of 5. The potential window from -0.5 V to 0.9 V was applied with a scan rate of 20 mV/s. CVs were performed using a RVC cathode with a potential window from -1.4 V to 0.2 V and a scan rate of 20 mV/s.

2.2.5. Product analysis

The course of the ECH and CH experiments was followed by periodically withdrawing aliquots of 1 mL from the cathode compartment. The products were extracted with 3mL of ethyl acetate. The organic phase (ethyl acetate) was separated from the aqueous phase by decantation and dried on Na_2SO_4. 1 mL of the dry organic phase was mixed with 0.5 mL of a solution containing toluene as standard. Quantitative analyses of those samples were performed by gas chromatography coupled with mass spectrometry (Shimadzu GCMS-QP2010), equipped with a plot Q capillary column (30m x 250 µm) and a thermal conductivity detector (TCD).

2.3. Results and discussion

2.3.1. Physicochemical properties of catalysts

The textural properties of the catalytic materials are compiled in Table 2.1. All materials exhibit comparably high specific surface areas and pore volumes. Microporosity, also comparable for all materials, is the major contribution to the overall pore volume. The average particle size, as determined by H_2 chemisorption was 2.7, 2.1, and 3.4 nm, for Pt/C, Pd/C, and Rh/C respectively. These particle sizes were in reasonable agreement with the sizes estimated from TEM images (Figure 2.1). That is 3.3 nm for Pt/C, and Pd/C, and 3.9 nm for Rh/C. The particle sizes determined by TEM are larger than those determined by H_2 likely because some small particles escaped from detection in microscopy.

Table 2.1. Textural properties and metal particle size of carbon-supported metal catalysts.

	BET surface area (m^2g^{-1})	Mesopores surface area (m^2g^{-1})	Micropore volume (cm^3g^{-1})	Total pore volume (cm^3g^{-1})
Pt/C	957	301	0.34	0.709
Pd/C	744	233	0.3	0.662
Rh/C	921	288	0.26	0.729
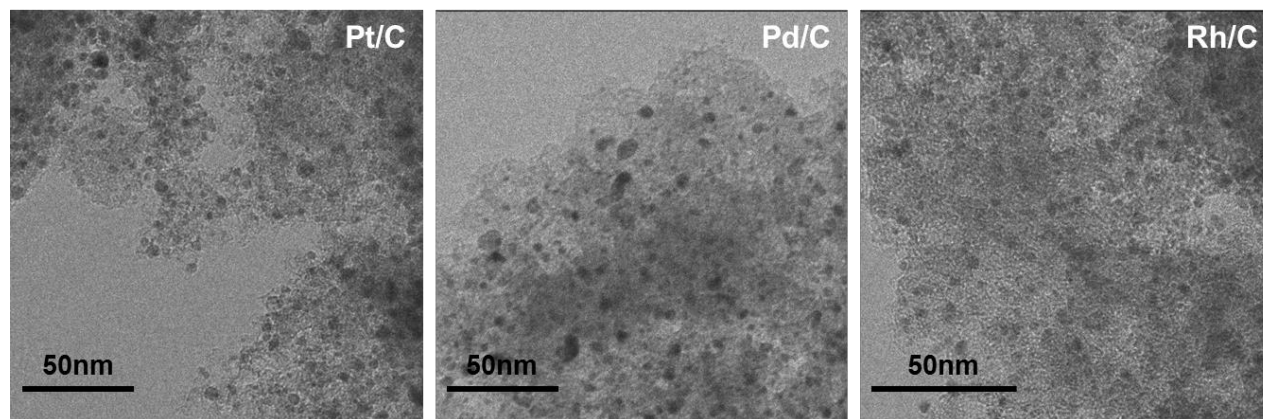
Figure 2.1. Representative TEM micrographs of Pt/C, Pd/C, and Rh/C.

Reticulated vitreous carbon (RVC) of 100 pores per inch (100 ppi, surface area of 66 cm^2 per cm^3) was selected as working electrode. This material has been widely applied in electrochemistry due to its high surface area, high conductivity, and good mechanical strength [16, 17]. The microscopic morphology of RVC was characterized by HR-SEM. Figure 2.2 presents the typical carbon network that characterizes the morphology of RVC. The images in the Figure were taken from materials tested in ECH experiments. Therefore, particles of catalyst (Pt/C), of around 1 to 10 μm, could also be visualized as granular material. Light spots on the granules are identified as domains with abundant concentrations of Pt particles.
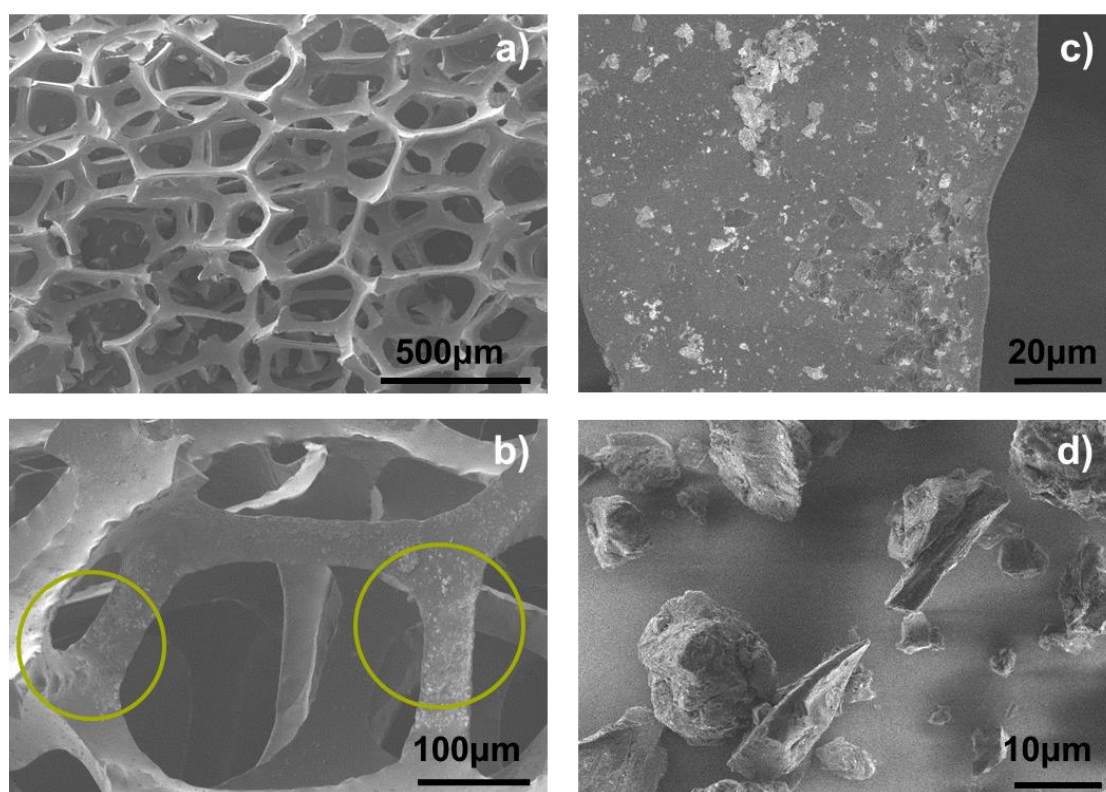
Figure 2.2. SEM images of selected materials after ECH reactions: bare RVC (100ppi) (a); SEM images of RVC covered with Pt/C (b) and (c); SEM image of Pt/C particles (d).

2.3.2. Impact of reaction parameters on the electrocatalytic hydrogenation of phenol

The activities of the catalysts were tested in the electrocatalytic hydrogenation (ECH) of phenol in the presence of three different electrolytes at pH 5 with a current of -40 mA. The amount of catalysts, added as slurry to the cathode compartment with the RVC electrode, was 50 mg in all experiments. As shown in Figure 3, the trend in activity of the catalysts did hardly depend on the electrolyte. Namely, Rh/C was the most active material followed by Pt/C, whereas Pd/C showed very low activities.

The use of acetic acid as electrolyte leads to the highest activities for Rh/C and Pt/C, followed by phosphoric acid, whereas the use of sulfuric acid leads to the lowest conversions. The beneficial effect of acetic acid on the hydrogenation of phenol over alumina-supported Pd catalysts has been attributed to the adsorption of the acid on the support, which eases the adsorption of phenol via electrostatic forces [18-20]. However, on the catalysts explored, acetic acid reduced the rate of phenol hydrogenation, likely due to competitive adsorption on the metal surface. Therefore, we hypothesize that phosphate and sulfate ions adsorb on the metal surface stronger than acetic acid, which leads to lower rates in the presence of the former two electrolytes. The performance of Pd/C, poor compared to Rh/C and Pt/C, was not affected by the nature of the electrolyte to a significant extent.
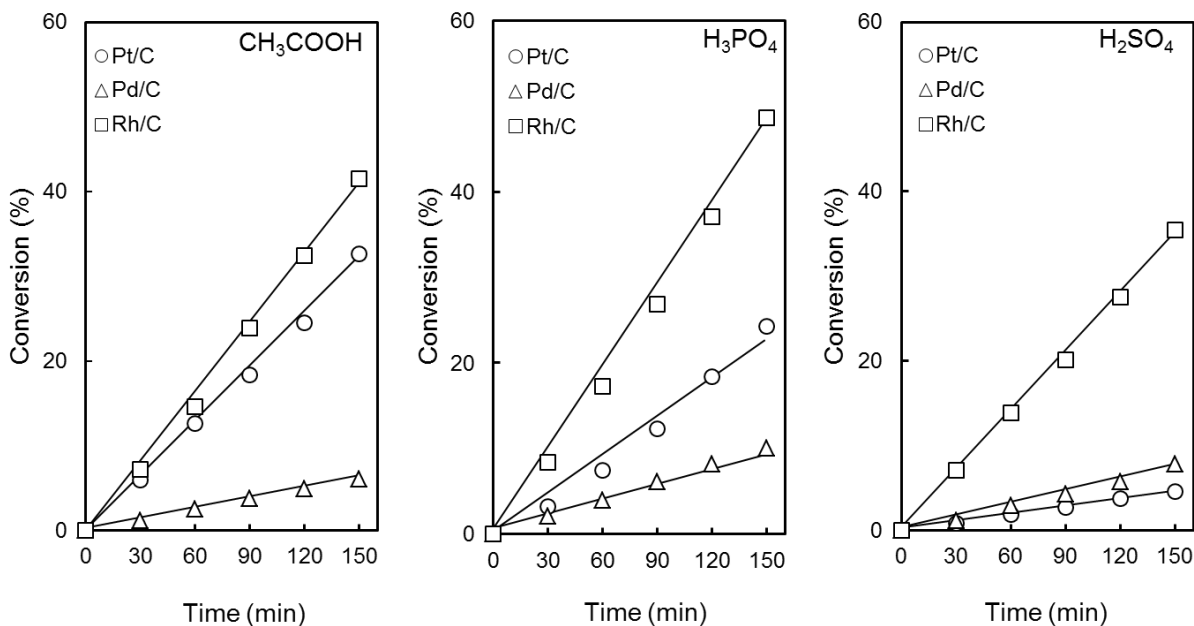
Figure 2.3. Conversion of phenol on different catalysts, and in the presence of selected electrolytes. All reactions were performed at -40 mA, room temperature, pH 5, and with 50 mg of catalyst.

ECH rates, turnover frequencies (TOFs) and electrical efficiencies (EE) calculated from the experiments reported in Figure 2.3 are shown in Table 2.2. As expected, the ECH rates follow the same trends described for phenol conversion. Rh/C converts 1.6×10^{-5} - 2.1×10^{-5} mol of phenol per second and gram of metal, Pt/C slightly less than that, i.e., 1.1×10^{-5} – 1.5×10^{-5} mol/s·g_{metal} (in the presence of sulfuric acid, the ECH rate on Pt/C decreases by one order of magnitude). The conversion rates on Pd/C are in the range of 2.2×10^{-6} - 4.1×10^{-6} mol/s·g_{metal}. In terms of TOF, the differences are more evident, Rh/C is an outstanding catalyst with TOF values from 30 to 38 h^{-1}. The intrinsic activity of Pt/C depends stronger on the electrolyte exhibiting TOFs from 6.7 to 28 h^{-1}. The intrinsic activity of Pd/C was also low, i.e., in the range of 4 to 6.5 h^{-1}. Interestingly, the electrical efficiency (EE) of the catalysts (the percentage of electrons used to hydrogenate phenol, see

the supporting information), is proportional to the conversion rates of phenol. That is, Rh/C leads to the highest EE (between 50 % and 66 %), followed by Pt/C (between 5.8 % and 41 %). Evidently, Pt/C and Rh/C are the most active catalysts and acetic acid is a suitable electrolyte to perform the reaction on both catalysts. Therefore, the following experiments focus on ECH of phenol on Pt/C and Rh/C in the presence of acetic acid.

Table 2.2. ECH rate (mol/s·g_{metal}), TOF (h^{-1}), and EE (%) under different electrolyte and catalyst

	Acetic acid			Phosphoric acid			Sulfuric acid		
	Rate[a]	TOF[b]	EE[c]	Rate	TOFs	EE	Rate	TOF	EE
Pt/C	$1.5×10^{-5}$	28.8	41	$1.1×10^{-5}$	19.7	30.5	$3.5×10^{-6}$	6.7	5.8
Pd/C	$2.9×10^{-6}$	6.5	7.6	$4.1×10^{-6}$	7.4	12.5	$2.2×10^{-6}$	3.9	10
Rh/C	$1.8×10^{-5}$	33.7	52.2	$2.1×10^{-5}$	38.7	66.5	$1.6×10^{-5}$	30.2	58.8

[a] reaction rate calculated as shown in the supporting information

[b] turnover frequency calculated with the dispersion obtained by H_2 chemisorption

[c] electrical efficiency calculated as shown in the supporting information

ECH of phenol was performed on Pt/C and Rh/C under galvanostatic conditions at -20 mA, -40 mA and -60 mA. The conversion of phenol is shown in Figure 2.4. The higher the current input, the higher the conversion of phenol. This is not surprising as increasing the input of electrons should accelerate the conversion of phenol (at least as long as the phenol concentration at the metal surface is not the limiting reactant). At all conditions, the conversion of phenol on Rh/C is faster than on Pt/C, e.g., $3.5×10^{-5}$ mol/s·g_{metal} on Rh/C, compared to $2.6×10^{-5}$ mol/s·g_{metal} on Pt/C at -60 mA. Note that the increase in phenol conversion is not linearly proportional to the current increase. Varying the current from -20 mA to -40 mA, and -60 mA, which corresponds to current increases by two and three,

respectively, leads to increases of ECH rates and TOFs of nearly 7 and 13 times (Table 3). This is attributed to the low potentials generated at -20 mA, which are -0.55 V (vs Ag/AgCl) on Pt/C and -0.53 V (vs Ag/AgCl) on Rh/C. These potentials are close to the theoretical potential of hydrogen evolution reaction (HER) of -0.523 V as calculated for the conditions of the experiments (the calculation is shown in the supporting information). In contrast, at -40 mA, and -60 mA, the potentials generated are < -0.65 V, and < -0.75 V, respectively. This leads to higher overpotentials to drive the ECH.
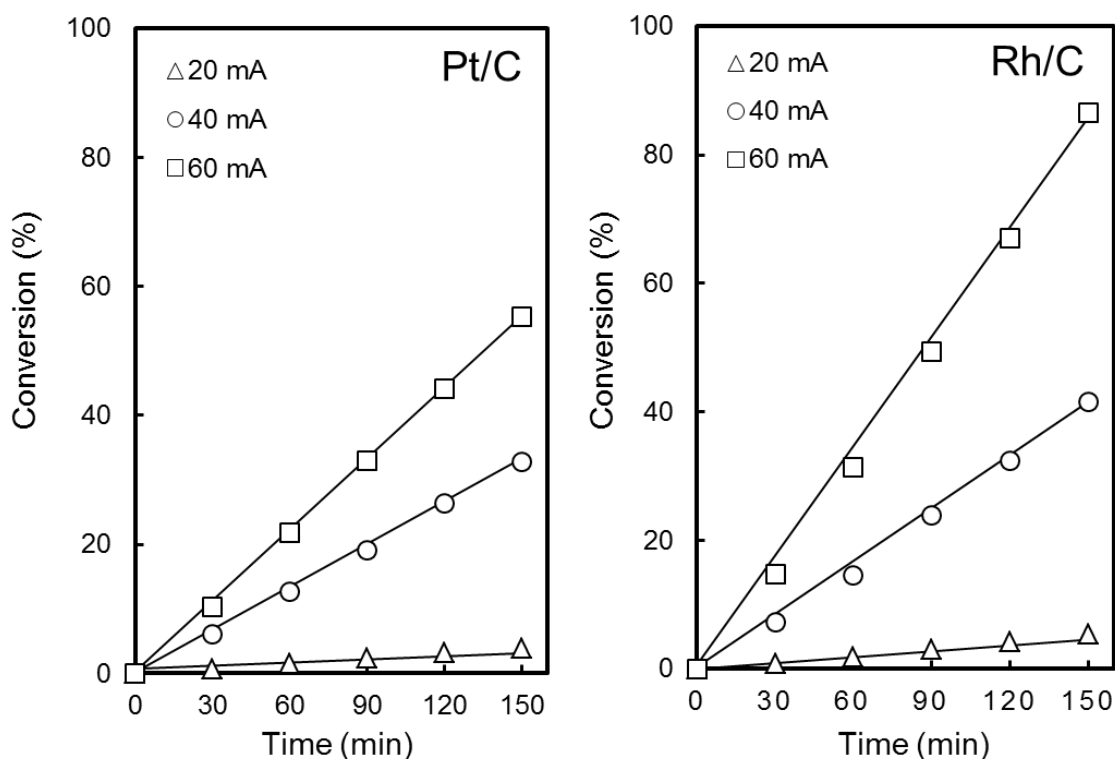
Figure 2.4. Conversion of phenol under different currents on Pt/C (left) and Rh/C (right). The reactions were performed at room temperature, pH 5, in acetic acid, with 50mg of catalyst.

Varying amounts of catalysts (20 mg, 50 mg and 200 mg) were used in ECH of phenol on Pt/C and Rh/C. The observed dependences of conversion on time and amount of catalysts are shown in Figure 2.5. The use of 50 mg leads to substantial

increases of phenol conversion, compared to using only 20 mg. However, increasing the amount of catalyst to 200 mg does not increase the conversion rates further. This implies that, under the experimental conditions, the rate of electron transfer does not vary when stirring 50 mg or 200 mg of powder catalyst.
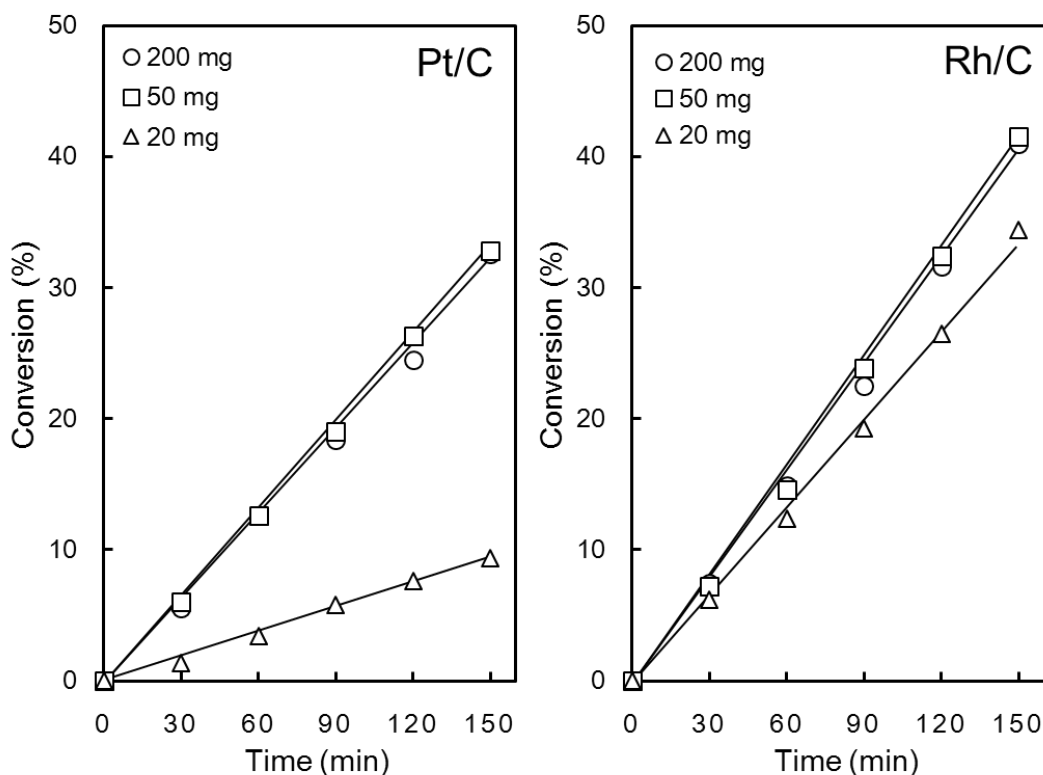
Figure 2.5. Conversion of phenol with varying amount of catalyst, Pt/C (left) and Rh/C (right). The reactions were performed at room temperature, -40 mA, pH 5, in acetic acid.

It is reported that the pH of the solution plays an important role on the conversion rates of biomass-derived compounds conversions via ECH [21-24]. ECH of phenol with Pt/C and Rh/C at initial pH values of 3, 5, and 10 was carried out in the presence of acetic acid. The catalytic performance is reported in Figure 2.6. Interestingly, the dependences on pH are different on both catalysts. The conversion rate on Pt/C is 1.3×10^{-5} mol/s·g_{metal} at pH 3, 1.5×10^{-5} mol/s·g_{metal} at pH

5, and decreases to 8.2×10^{-6} mol/s·g_{metal} at pH 10. In contrast, the conversion rate on Rh/C increases with increasing pH, i.e., 1.6×10^{-5} mol/s·g_{metal} at pH 3, 1.8×10^{-5} mol/s·g_{metal} at pH 5, and 2.5×10^{-5} mol/s·g_{metal} at pH 10. There is not a straightforward explanation for these different trends. The complication arises from the fact that the distribution of species in solution changes dramatically in the range of pH explored. Besides the decreasing concentration of protons in solutions with increasing pH, acetic acid (electrolyte) and phenol are present in neutral forms at pH 3. At pH 5 acetic acid (pKa=4.75) is present as acetic ion, whereas at pH 10, phenol (pKa=9.95) will produce phenolate anions. The concentration of chemical species on the surface of the solids has to be influenced by those changes in solution, and it may also be affected by the charge of the solid surface at different pH values (point of zero charge of the carbon). We hypothesize that the factor determining the rates of ECH at varying pH is the adsorption of phenol on the metal particles as the slowest ECH rates are observed at pH 3 (the condition with the highest concentration of protons in solution among the explored conditions). Further analysis will be addressed in ongoing studies.
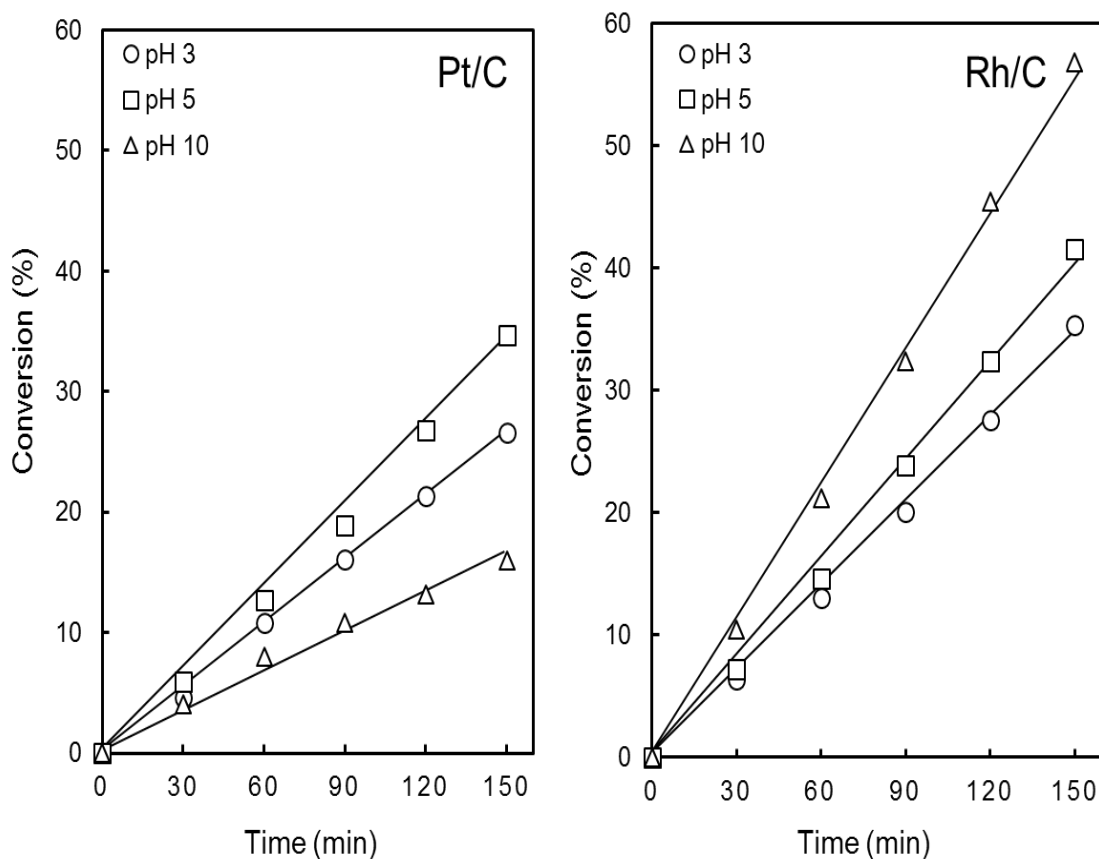
Figure 2.6. Conversion of phenol in solutions of acetic acid at varying pH on Pt/C (right) and Rh/C (left).

Table 2.3 summarizes the rates, TOF, and EE values determined for the ECH of phenol on Pt/C, and Rh/C under varying currents amount of catalyst and pH. Under all conditions, Rh/C exhibited higher weight specific (per gram of catalyst) and intrinsic (TOF) activity than Pt/C. Interestingly, the higher the activities (conversion rates and TOF), the higher the associated electric efficiencies. This is very relevant as it implies that improving the performance of the catalyst would also improve the energy utilization associated to the process.

We would like to highlight the fact that the potential observed at pH 10 was -1.25 V and -1.05 V, for Pt/C and Rh/C (last entry in Table 3). This is significantly more negative than the potentials observed at lower pH values. It suggests that the identity of the hydrocarbon species being hydrogenated at the metal changes by increasing the pH to 10. Furthermore, the activity of Pt is severely affected by the change reflected with this potential as its activity for ECH drops at pH 10. Another outstanding result is the extremely high EE (95 %) obtained on Rh/C at pH 10. This high efficiency reflects the fact that phenol was almost quantitatively converted to cyclohexanol, which consumes 6 electrons per molecule of phenol converted.

Table 2.3. Potential, reaction rate (mol/s·g_{metal}), TOF (h^{-1}), and EE (%), observed in the ECH of phenol on Pt/C and Rh/C under several conditions.

		Pt/C				Rh/C			
		Potential[a]	Rate[b]	TOF[c]	EE[d]	Potential[a]	Rate[b]	TOF[c]	EE[d]
Current	-20	-0.55	1.8×10^{-6}	3.4	9.6	-0.53	2.5×10^{-6}	4.6	13
Input[e], mA	-40	-0.68	1.5×10^{-5}	28.8	40	-0.65	1.8×10^{-5}	34	52
	-60	-0.96	2.6×10^{-5}	46.8	45	-0.71	3.5×10^{-5}	66	77
	20	-0.73	1.1×10^{-5}	20.5	11	-0.67	3.9×10^{-5}	74	44
	50	-0.68	1.5×10^{-5}	28.8	40	-0.65	1.8×10^{-5}	34	52

Catalyst amount[f], mg	200	-0.67	3.7×10^{-6}	6.8	39	-0.64	4.4×10^{-6}	8	54
Solution	3	-0.61	1.3×10^{-5}	23.4	29	-0.57	1.6×10^{-5}	29	44
pH[g]	5	-0.68	1.5×10^{-5}	28.8	40	-0.65	1.8×10^{-5}	34	52
	10	-1.25	8.2×10^{-6}	15.5	24	-1.05	2.5×10^{-5}	46	95

[a] potential E with respect to Ag/AgCl (V)

[b] reaction rate calculated as shown in the supporting information

[c] turn over frequency calculated with the dispersion obtained by H_2 chemisorption

[d] electrical efficiency calculated as shown in the supporting information

[e] 50 mg of catalyst and pH of 5

[f] -40 mA and pH of 5

[g] 50 mg of catalyst and -40 mA

2.3.3. Impact of temperature on the ECH and thermal hydrogenation of phenol

The effect of temperature on the ECH of phenol was studied under galvanostatic and potentiostatic conditions with acetic acid as electrolyte (pH 5). In a preliminary study, the phenol ECH was explored on Pt/C in the temperature range of 5 - 80 °C with -40 mA. The conversion increased with temperature up to 50 °C. However, at 50 °C or above, the catalyst quickly deactivated. These results are shown in the supporting information (Figure A1). Deactivation of the catalyst has also been observed in Refs. [25, 26]. The activation energy, calculated from the conversion rates of phenol below 50 °C, was 7 kJ/mol. This unusual value is attributed to the reaction rate being limited by the supply of electrons due to the use of galvanostatic conditions (the proton reduction cannot be faster than the current input).

At potentiostatic conditions, the dependence of phenol conversion on temperature was determined on Pt/C and Rh/C from 5 °C to 40 °C as shown in Figure 2.7. The corresponding activation energies, calculated using TOF values were 29 kJ/mol on Pt/C, and 23 kJ/mol on Rh/C (the Arrhenius plots are presented in Fig. 2.7).
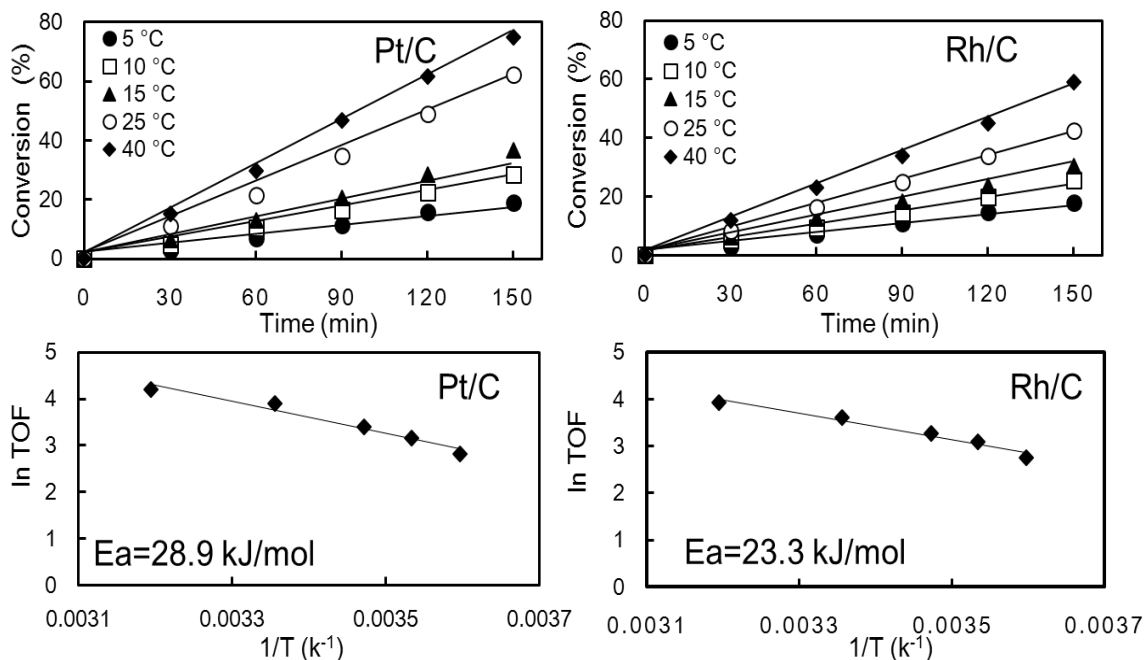
Figure 2.7. Conversion of phenol along with time at varying temperatures on Pt/C and Rh/C (upper panels). Arrhenius plots for the ECH of phenol on Pt/C (-0.75 V vs Ag/AgCl) and Rh/C (-0.62 V vs Ag/AgCl) (lower panels). The reactions were performed with 50 mg Pt/C or 20mg Rh/C in acetic acid at pH 5.

In order to understand the contributions of thermal pathways and the ECH mechanism, thermal hydrogenation (TH) of phenol was carried out on Pt/C. Namely, bubbling H_2 through the solution containing phenol, acetic acid, and the catalyst (Pt/C) in the absence of any electric potential. The variation of conversion with temperature and time, and the Arrhenius plot are presented in Figure 2.8. The apparent energy of activation corresponding to the TH of phenol at mild conditions

was 33 kJ/mol, which is in good agreement with the values reported for TH at high temperatures [27-29]. More importantly, this activation energy is very similar to that found for the ECH of phenol (29 kJ/mol, vide supra). This indicates that ECH and TH of phenol have the same rate-determining step (the mechanistic implications are further discussed below). Rates, TOFs and EE of the experiments performed at varying temperatures are summarized in Table 2.4. As previously noted, the EE increased with the rate of phenol conversion. Therefore, within the studied range, EE increase with increasing temperature.
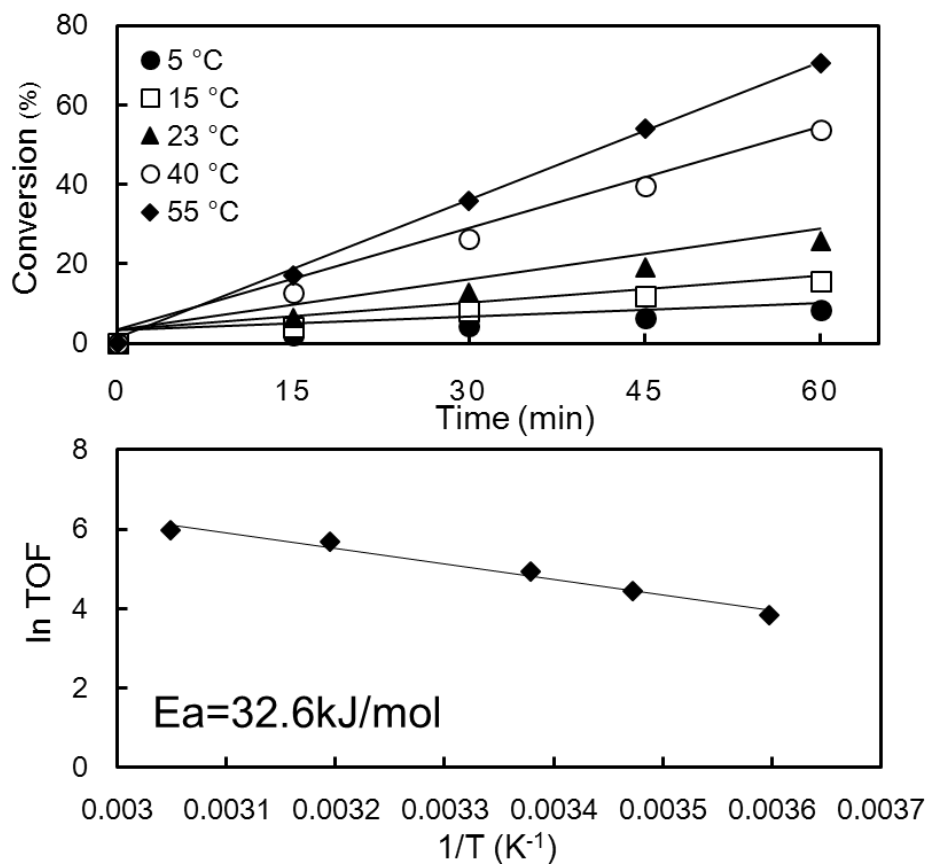
Figure 2.8. Conversion of phenol during thermal conversion along with time at varying temperatures on Pt/C (upper panels), and the corresponding Arrhenius plot (lower panels). The reactions were performed at atmospheric pressure, 20 mg of catalyst in acetic acid at pH 5.

Table 2.4. Reaction rate (mol/s·g_{metal}), TOF (h^{-1}), and EE (%), observed for the ECH of phenol at varying temperatures.

Temperature	Pt/C			Rh/C		
	Rate	TOF	E.E	Rate	TOF	EE
5°C	9×10^{-6}	16.6	26.4	8.5×10^{-6}	15.8	35
10°C	1.3×10^{-5}	23.5	36.1	1.2×10^{-5}	21.9	44.8
15°C	1.6×10^{-5}	30.2	41.8	1.4×10^{-5}	26.3	47.6
25°C	2.7×10^{-5}	49.5	55.4	2×10^{-5}	37.1	54.1
40°C	3.6×10^{-5}	67.4	62.1	2.7×10^{-5}	50.6	63.1

For comparison, the TH of phenol was performed at room temperature in pure water. The conversion rate of phenol was higher (7.6×10^{-5} mol/s·g_{metal}) in pure water than in the presence of acetic acid (6.4×10^{-5} mol/s·g_{metal}). The concentration profiles are presented in Figure A2 of the supporting information. This implies that acetic acid (needed as electrolyte for ECH), slows down the hydrogenation likely due to competitive adsorption on the metal.

2.3.4. Study of the reaction network and mechanism

During all the experiments reported in this work, the only products of the reaction were cyclohexanone and cylohexanol. Typical profiles of the concentrations of reactant and products are shown in Figure 2.9. As expected from the nature of the products, cyclohexanone is the primary product observed as well as an intermediate (the concentration of cyclohexanone increases and decreases with time reaching a maximum), whereas cyclohexanol is a secondary and stable product (the concentration of cyclohexanol increases exponentially with time up to an inflection point, which corresponds to the maximum in cyclohexanone concentration). Cleavage of the C-O bond was not observed under any reaction

conditions applied in this study. Thus, phenol is hydrogenated to cyclohexanone, which is in turn hydrogenated to cyclohexanol. The two steps need four and two atoms of hydrogen, respectively, which are provided by the reduction of protons from the solution (Scheme 2.1).
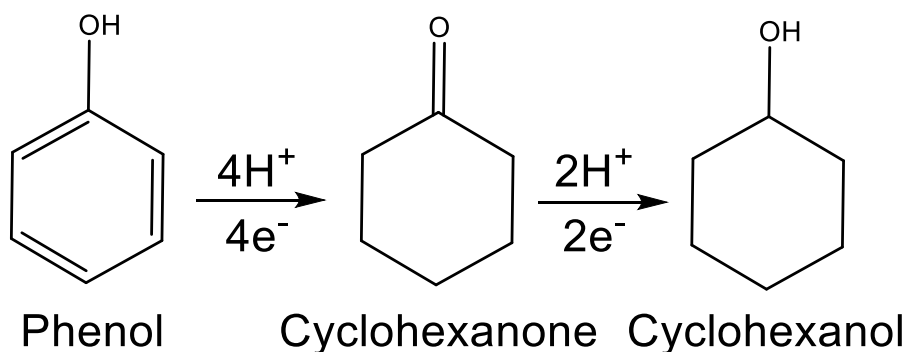
Scheme 2.1. Reaction network for the electrocatalytic hydrogenation of phenol on Pt/C, and Rh/C.

The ECH of phenol was carried out on Pt/C (50 mg of catalyst with acetic acid as electrolyte at pH 5) using three different experimental configurations in order to clarify the macroscopic mechanism of the reaction. The "suspension" configuration has been described in detail in the experimental part and consisted in suspending the catalyst in the reactant solution containing the working electrode (RVC electrode) and performing the reaction with stirring. The "filter" configuration consisted in introducing the catalyst inside a porous container into the reactant solution in order to avoid direct contact of the powder with the electrode. In the "ink" configuration, an ink containing the catalyst was prepared according to Ref. [30]. This ink was applied onto the RVC electrode in order to deposit the desired amount of catalyst directly on it. Figure A3 shows the phenol conversions observed with these three configurations. Table A1 summarizes the reaction rates, TOF and EE values. The "filter" configuration led to negligible phenol conversion, demonstrating that the direct contact between the catalyst grains and the electrode was needed to perform the reaction (the ECH process does not involved molecular

charged species). Another implication of this experiment was that the concentration of H_2 in solution (generated at the cathode during the experiment), was insufficient to hydrogenate phenol to a significant extent via thermal pathways (vide infra). The "ink" configuration led to about half of the phenol conversion rate with respect to the "suspension" configuration (although the same amount of catalyst was present in both kind of experiments), i.e., $1.5 \cdot 10^{-5}$ mol/s·g_{Pt} ("suspension") and $6 \cdot 10^{-6}$ mol/s·g_{Pt} ("ink"). This observation was unexpected as a constant and direct contact between the metal and the electrode should have ensured a continuous flow of electrons for the ECH (which may be not the case for the "suspension" configuration). We attribute this observation to possible agglomeration of the catalyst particles during the preparation and deposition of the ink, and covering of the metal particles with the polymers needed to prepare the ink. These could have easily reduced the proportion of metal accessible during the reaction.
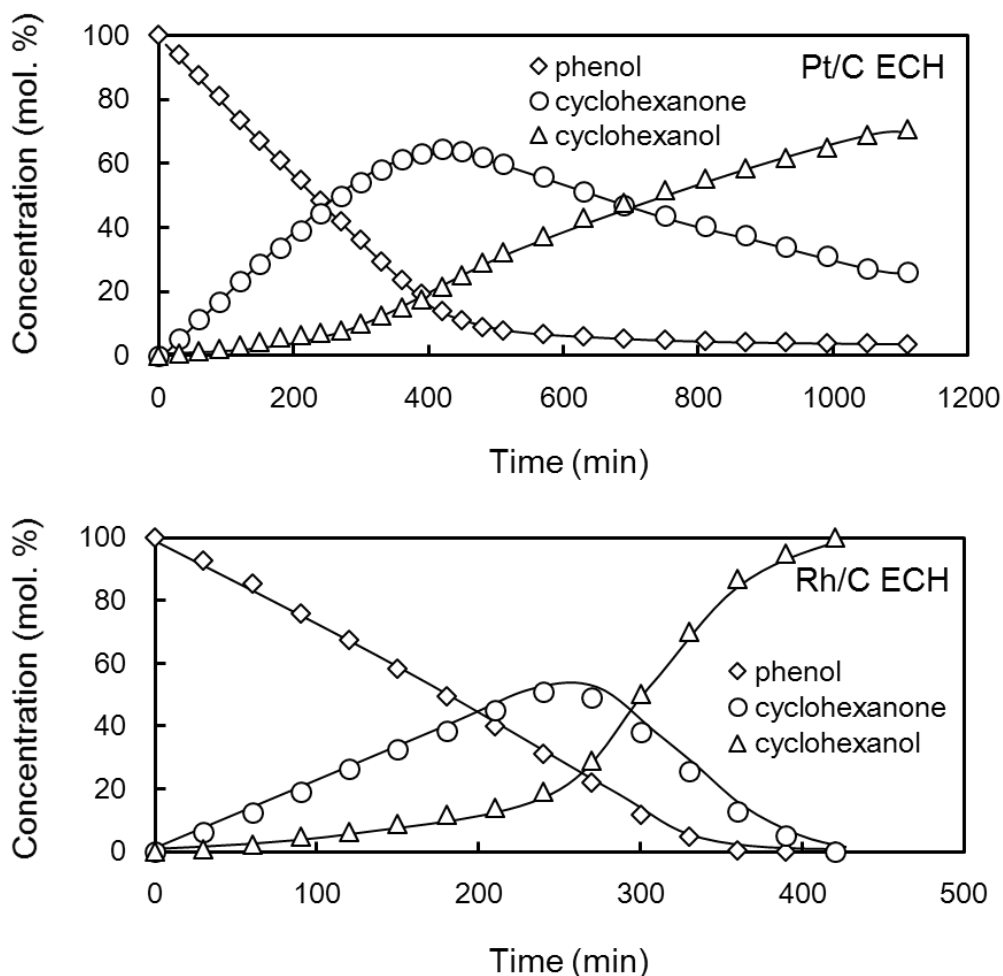
Figure 2.9. Concentration profiles of phenol and the products of ECH (cyclohexanone, and cyclohexanol) on Pt/C and Rh/C. The experiments were performed at -40 mA, room temperature, in acetic acid with pH 5.

Hence, the macroscopic ECH process during "suspension" operation is concluded to occur as shown in Figure 2.10. Phenol molecules and protons adsorb on the metal supported on carbon particles suspended in solution. The particles of the catalyst contact the electrode, which allows the transfer of electrons, which reduce the protons on the metal particles. Finally, there is a surface reaction between hydrogen radicals and adsorbed phenol producing the hydrogenated product, which desorbs.
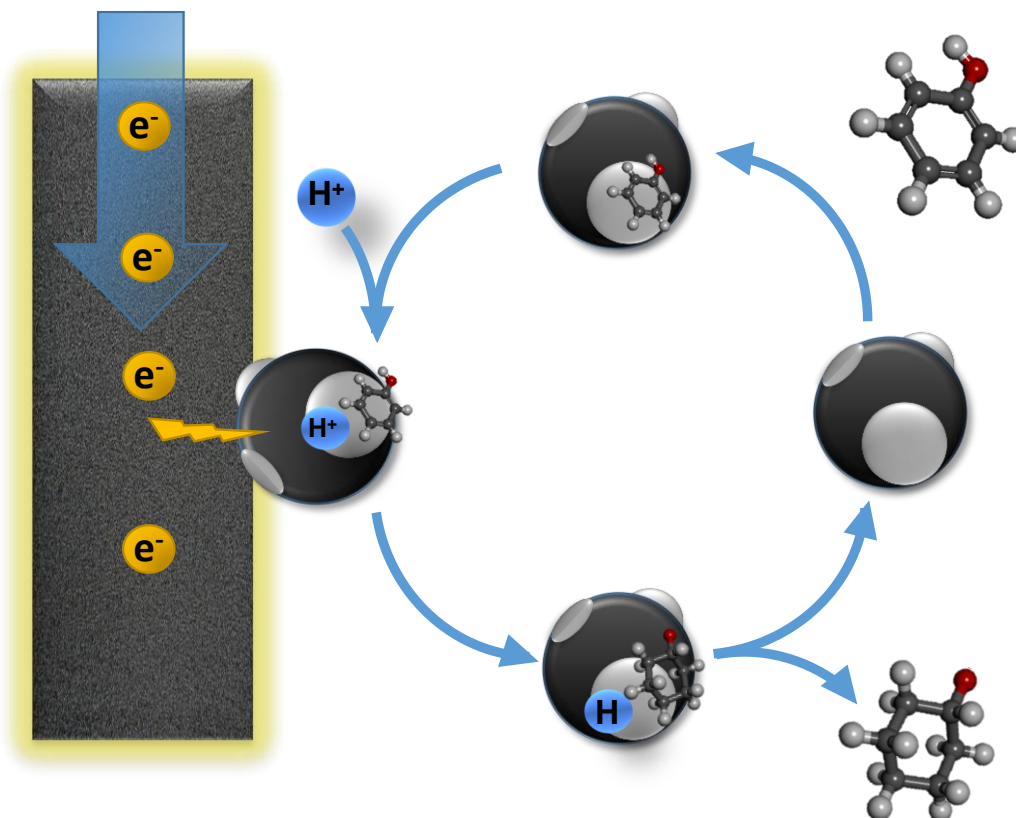
Figure 2.10. Visualization of the macroscopic process for the electrocatalytic hydrogenation of phenol with a carbon-supported metal catalyst is suspension.

In order to gain understanding on the microscopic mechanism of ECH, cyclic voltammetry (CV) studies were performed on bulk Pt and the Pt/C catalyst interacting with phenol. Cyclic voltammetry was performed on a Pt wire as cathode at pH 5 and a potential window between 1 V and -0.8 V vs Ag/AgCl. As shown in Figure 2.11 a, the typical curve of a Pt electrode was observed in pure electrolyte solution. The maxima in cathodic and anodic current correspond to the reactions (1)-(4), where *-H$^+$ and *-H denote protons and hydrogen atomos adsorb on metal sites, respectively. That is, hydrogen oxidation and oxide formation in the anodic part and oxide, and metal reduction and hydrogen evolution in the cathodic part [31, 32].

$$* + H^+ + e^- \rightleftharpoons *\text{-}H \qquad (1) \qquad \text{Reversible hydrogen underpotential deposition}$$

$$2H^+ + 2e^- \rightarrow H_2\uparrow \qquad (2) \qquad \text{Hydrogen evolution reaction}$$

Pt + H_2O +2e$^-$ $\rightleftharpoons$ Pt-O + ½ H_2O (3)   Reversible Pt hydroxide/oxide formation

H_2O → ½ O_2↑ + 2H$^+$ + 2e$^-$ (4)   Oxygen evolution reaction
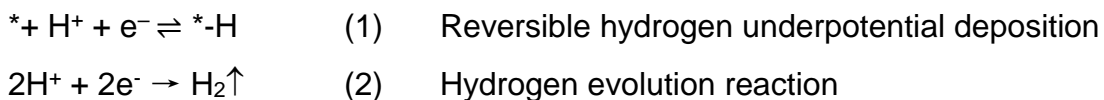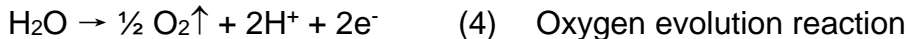
The potential of the H_2 evolution reaction (HER) shown in the voltagramm of Figure 11(a), at about -0.52 V (vs Ag/AgCl), is in good agreement with the value predicted by the Nernst equation. Figure 2.12 a shows the CV curves in the presence of increasing concentrations of phenol. Evidently, all current maxima fade out in the presence of phenol, i.e., the reacting substrate hinders all the surface reactions by adsorbing strongly on the metal surface.
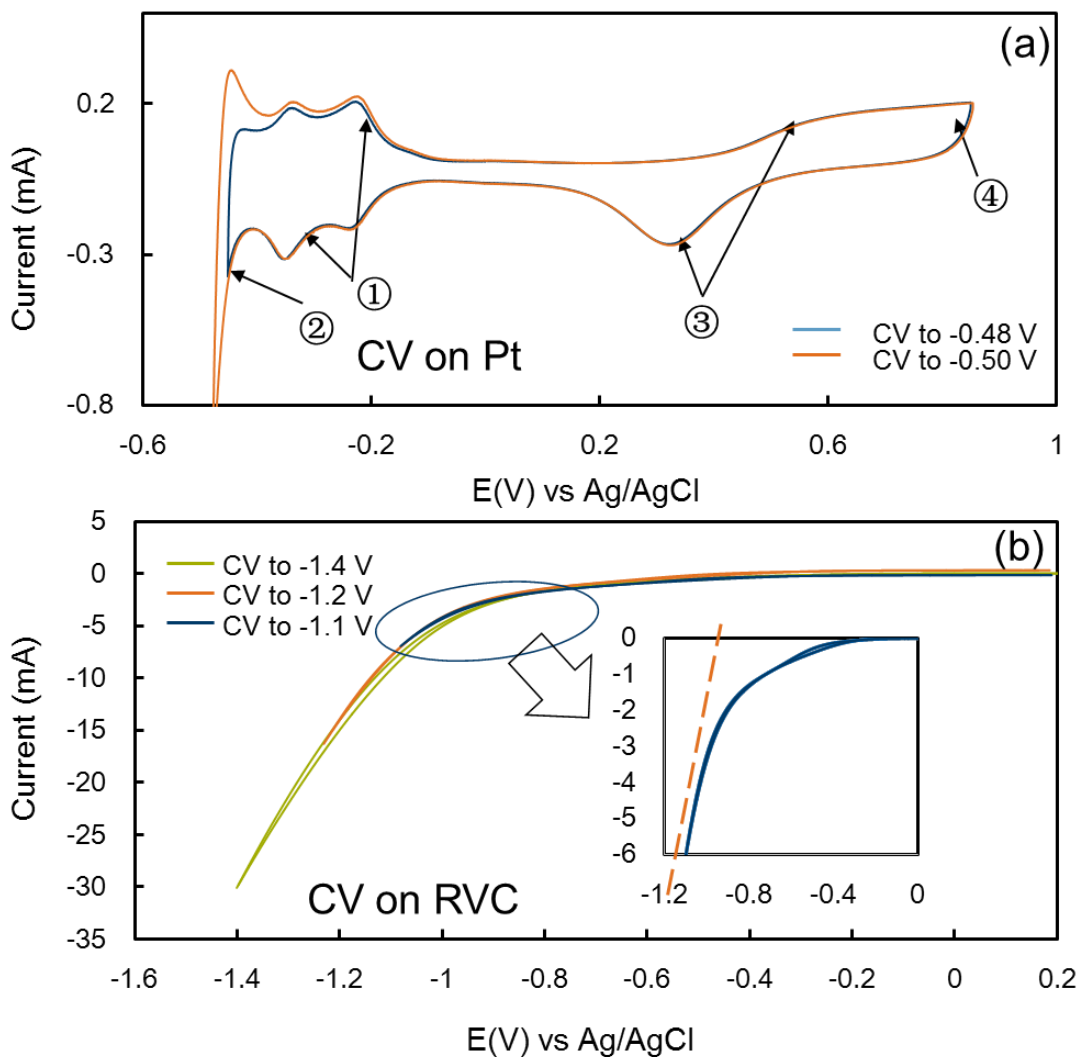
Figure 2.11. Cyclic voltamogramms on the Pt cathode at varying overpotential, (a). Cyclic voltamogramms on RVC cathode at varying overpotential, (b). CVs are performed in acetic acid with pH 5, at a scan rate of 20 mV/s.

The CV of the bare RVC electrode was also studied in the range of 0.2 V and -1.6 V as shown in Figure 11b. HER was observed at potentials more negative than -1.1 V (vs Ag/AgCl), much more negative to the one on bare Pt wire or in the presence of Pt/C (vide infra). Current peaks for the reversible hydrogen reduction-oxidation were not observed on bare RVC. Figures 12a and 12b show the CV curves obtained with an RVC electrode in the presence of Pt/C and increasing concentrations of phenol. The increase of cathodic current is observed at around -0.52 V, confirming that the transformations described along this work was driven by the proton reduction occurring on the Pt particles of the Pt/C powder in contact with the electrode. More interestingly, increasing concentrations of phenol lead to currents that are more negative. This indicates that the presence of phenol accelerates the reduction of protons. Note that the addition of phenol did not change the pH noticeably. In turn, we attribute this observation to the reduction of hydrocarbon species on the metal surface, which scavenges hydrogen atoms allowing faster adsorption and reduction of protons.
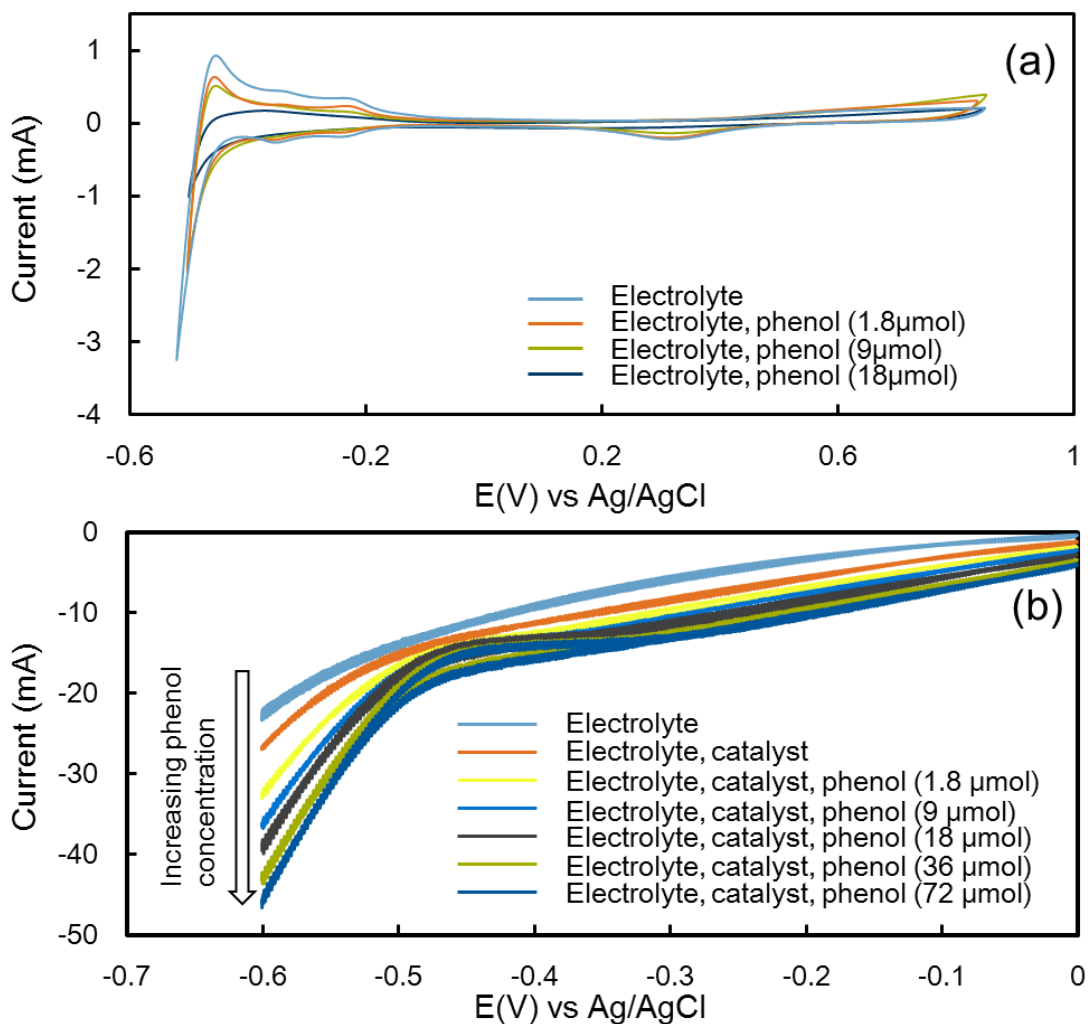
Figure 2.12. Cyclic voltagramms on the Pt cathode at varying concentration of phenol, (a). Cyclic voltagramms on the RVC cathode with Pt/C as catalyst, at different concentration of phenol. CVs are performed in acetic acid with pH 5, at a scan rate of 20 mV/s.

Thus, the microscopic mechanism of phenol hydrogenation under ECH can be described with the series of reactions (5)-(10), where the symbol "*-" denotes an adsorbed species, and "*" is an unoccupied metal site. C_nH_{2n-6}, and C_nH_{2n-4} denote an aromatic species and the corresponding hydrogenated product, respectively. Adsorbed hydrogen and molecular hydrogen are produced *via* Volmer, Herovsky,

and Tafel reactions (5)-(7) [33-35]. The hydrocarbon, on the other hand, adsorbs on the metal sites (8), and then undergoes hydrogenation with hydrogen radicals. Reaction (9) illustrates a one-step hydrogenation process for the sake of simplicity. However, the hydrogenation of adsorbed hydrocarbons is most likely stepwise. Finally, a stable hydrogenated species desorbs to give the product of the reaction (10). Clearly, the hydrogenation of adsorbed hydrocarbons and H_2 evolution (Heyrovsky and Tafel reactions) are parallel and competing reactions. Furthermore, the increasing EE values with increasing temperature (ECH experiments reported in Table 4), indicate that the rate of hydrocarbon hydrogenation increases faster than that of hydrogen evolution.

$$H^+ + e^- + * \rightarrow *\text{-}H \qquad\qquad (5) \qquad \text{Volmer reaction}$$

$$*\text{-}H + H^+ + e^- \rightarrow H_2 \qquad\qquad (6) \qquad \text{Heyrovsky reaction}$$

$$2*\text{-}H \rightleftharpoons H_2 \qquad\qquad (7) \qquad \text{Tafel reaction}$$

$$* + C_nH_{2n\text{-}6} \rightleftharpoons *\text{-}C_nH_{2n\text{-}6} \qquad\qquad (8)$$

$$2*\text{-}H + *\text{-}C_nH_{2n\text{-}6} \rightarrow *\text{-}C_nH_{2n\text{-}4} + * \qquad\qquad (9)$$

$$*\text{-}C_nH_{2n\text{-}4} \rightleftharpoons C_nH_{2n\text{-}4} + * \qquad\qquad (10)$$
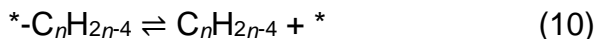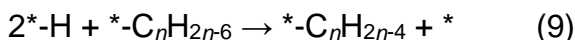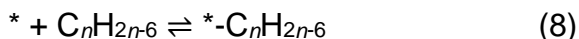
2.3.5. Comparison of ECH and TH of phenol

The thermal hydrogenation (TH) of phenol (in the absence of electric potential) follows a Langmuir-Hinshelwood mechanism. H_2 adsorbs on the metal dissociatively to form adsorbed hydrogen atoms, according to reaction (11):

$$H_2 + 2* \rightleftharpoons 2*\text{-}H \qquad\qquad (11)$$

The adsorption, subsequent hydrogenation of the hydrocarbon and evolution of the product proceed as described by reactions (8) - (10). Therefore, ECH and TH of phenol differ only in the origin of the adsorbed hydrogen species. The identical activation energies of ECH and TH on Pt/C, suggests that both processes

have the same rate determining step, i.e., one of the hydrogenation steps included in Reaction (9) [36, 37].

ECH and TH were compared by performing the hydrogenation of phenol on Pt/C and Rh/C under ECH, or TH conditions only, and ECH-TH, namely, ECH in the presence of H_2 (or thermal hydrogenation in the presence of the electric potential). The results of phenol ECH under typical galvanostatic reaction conditions (-40 mA in acetic acid at pH 5) are summarized Table 2.5 (concentration profiles are shown in Figure 2.13). The concentration profiles observed during TH are shown in Figure 2.13, whereas the rates of phenol conversion and TOFs on Pt/C and Rh/C are compiled in Table 2.5. Obviously, TH of phenol is much faster than phenol ECH, i.e., 4 and 5 times on Pt/C and Rh/C, respectively. The phenol conversion rates and TOFs obtained during the ECH-TH experiments are shown in Table 5, whereas the concentration profiles are shown in Figure 2.13. Remarkably, the rates and TOFs of the catalysts in the ECH-TH experiments equal the sum of the values observed during ECH and TH. This observation has several important implications, i.e., TH and ECH are independent pathways (hydrogen radicals for ECH are those produced from proton reduction instead of re-adsorbed H_2), and there is no synergy between electric potential and thermally catalyzed pathways.
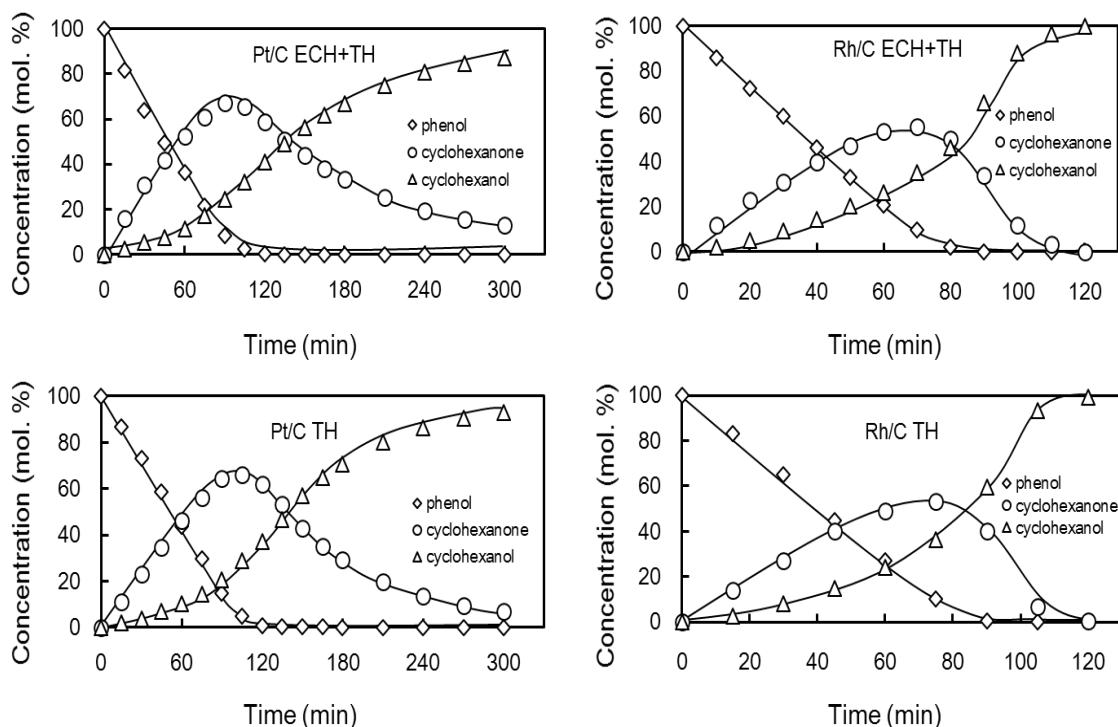
Figure 2.13. Concentration profiles of phenol and the products on Pt/C during TH (a), and ECH+TH (b). Concentration profiles of phenol and the products on Rt/C during TH (c), and ECH+TH (d). The ECH+TH experiments were performed at -40 mA, room temperature, in acetic acid (pH 5) under H_2 flow (atmospheric pressure). 50 mg Pt/C and 20mg Rh/C are chosen amount of catalyst. The TH experiments were performed at the same conditions in the absence of any electric potential.

Discussing concentration profiles observed on Pt/C and Rh/C highlights the similarities and differences of their intrinsic catalytic properties. On both catalysts, the decrease of phenol concentration is linear up to almost full conversion indicating that the reaction is zero order with respect to phenol. Furthermore, the concentration of cyclohexanone peaks at almost full conversion of phenol on both catalysts. This indicates that the rates of phenol hydrogenation are significantly faster than those of cyclohexanone hydrogenation, although the former step needs four H (consuming four electrons), whereas cyclohexanone hydrogenation consumes only two H (two electrons). Rh/C is 2-3 times more active than Pt/C.

Furthermore, the concentration of cyclohexanone peaks at shorter reaction time on Rh/C than on Pt/C. Also the hydrogenation of cyclohexanone was faster on Rh/C than on Pt/C, as the ratios of initial production rates cyclohexanone/cyclohexanone were ca. 5.2 and 3.9, respectively. The final product was cyclohexanol in all cases, e.g., C-O bond cleavage was not observed. It is speculated that the activation energy for hydrogenolysis is much higher than for hydrogenation. Therefore, it requires much higher temperatures and/or overpotentials than those accessed in this study.

Table 2.5. Reaction rates (mol/s·g_{metal}), and TOFs (h^{-1}), observed for the hydrogenation of phenol on Pt/C and Rh/C during different experimental conditions.

Reaction path	Pt/C		Rh/C	
	Rate	TOFs	rate	TOFs
ECH[a]	1.5×10^{-5}	28. 8	3.96×10^{-5}	73.5
TCH[b]	6.4×10^{-5}	118.8	2.05×10^{-4}	380.7
ECH+TCH[c]	8×10^{-5}	151.2	2.44×10^{-4}	452.8

[a] ECH was performed at -40 mA, and room temperature, in acetic acid (pH 5). 50 mg of Pt/C or 20 mg of Rh/C were used.

[b] TCH was performed in acetic acid (pH 5) with H_2 at atmospheric pressure and room temperature. 50 mg of Pt/C or 20 mg of Rh/C were used.

[c] ECH+TCH was performed at -40 mA, and room temperature, in acetic acid (pH 5) in the presence of flowing H_2 at atmospheric pressure. 50 mg of Pt/C or 20 mg of Rh/C were used.

2.4. Conclusions

This work explored the conversion of phenol on Pt/C, Rh/C, and Pd/C (5 wt. % metal) via electrocatalysis (electrocatalytic hydrogenation, ECH) and mild thermal catalysis (TH). The results show that electrocatalytic hydrogenation of phenol can be realized using suspensions of catalysts in the presence of a reticulated vitreous carbon electrode. Varying the electrolyte, the highest rates were found with acetic acid at pH 5.

In the temperature range studied (5 °C – 50 °C), TH and ECH have the same activation energy (~30 kJ/mol on Pt/C), which guides us to the conclusion that both pathways have the identical rate determining step. The electrocatalytic hydrogenation of phenol occurs via a Langmuir Hinshelwood mechanism in which H^+ and the substrate are adsorbed on the catalyst metal particles. The protons are reduced upon contact of the catalyst with the electrode, which produces adsorbed hydrogen radicals that hydrogenate the adsorbed hydrocarbons. Recombination of H· occurs in parallel (H_2 evolution reaction) competing with the hydrogenation. Compared to the ECH pathway, TH (where adsorbed H is produced by dissociation of H_2) is faster, likely due to much higher H coverages. The two pathways (ECH and TH) are independent, i.e., in the presence of the electrochemical reduction the evolved H_2 does not contribute in a measurable way to the overall reaction. In both pathways, the reaction network is phenol $\rightarrow$ cyclohexanone $\rightarrow$ cyclohexanol. C-O bond cleavage was not observed, in line with thermal catalysis in the absence of acid sites enabling deoxygenation via acid catalyzed dehydration. Electrocatalytic hydrogenation can be achieved under conditions similar to thermal conversions. The efficiency of the reaction depends markedly on the possibility to eliminate H_2 evolution.

2.5. Appendix

Calculations

Conversion, reaction rate, turnover frequency (TOF), electrical efficiency (EE), and overpotentials (E) were calculated according to the following equations.

$$\text{Conversion} = \frac{\text{Moles of phenol consumed}}{\text{Initial moles of phenol}} \times 100 \qquad [=] \ \%$$

$$\text{Reaction rate} = \frac{\text{Moles of phenol consumed}}{\text{Time} \times \text{Mass of catalyst} \times \text{Metal loading}} \qquad [=] \ \text{mol/s·g(metal)}$$

$$\text{TOF} = \frac{\text{Moles of phenol consumed}}{\text{Time} \times \text{Dispersion of metal} \times \text{Moles of metal in the catalyst}} \qquad [=] \ h^{-1}$$

$$\text{EE} = \frac{\text{Electrons consumed by hydrogenation of organic compounds}}{\text{Total electrons passed}} \times 100 \qquad [=] \ \%$$

$$E = E^{\theta} + \frac{RT}{zF} \ln \frac{a_{ox}}{a_{red}}, \quad \text{Nernst equation} \qquad [=] \ V$$

In which,

E is the half-cell reduction potential at the temperature of interest

$E^{\ominus}$ is the standard half-cell reduction potential

R is the universal gas constant: R=8.314 $K^{-1}mol^{-1}$

T is the absolute temperature

a_{ox} and a_{red} are reducing agent and oxidizing agent separately

F is the Faraday constant: F=9.65×10^4 $Cmol^{-1}$

z is the number of moles of electrons transferred in the reaction

At room temperature (25 ºC) RT/F can be treated as a constant 25.7 mV for cells, when using a 10 logarithms instead of natural logarithms, Nernst equation can be written as:

$$E = E^\theta - \frac{0.059V}{z} log_{10} \frac{a_{ox}}{a_{red}}$$

Thus, for hydrogen evolution reaction:

$2H^+ + 2e^- = H_2$ (g)
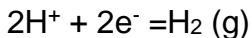
$$E = E^\theta - \frac{0.059V}{2} log_{10} \frac{[H^+]^2}{P_{H_2}}$$

As $log_{10} \frac{[H^+]^2}{P_{H_2}}$ equals to 2×pH, E≈ $E^\ominus$ – 0.06·pH

Theoretical potential of hydrogen evolution reaction (HER)

The potential for H_2 evolution (HER), according to ($H^+ + e^- \rightarrow \frac{1}{2}H_2$) is -0.223 V with respect of the Ag/AgCl electrode. The dependence of this potential on pH is:

E = $E^\ominus$ – 0.06·pH

E = -0.223 – 0.06·pH

Therefore, at pH of 5 the theoretical potential for HER is -0.523
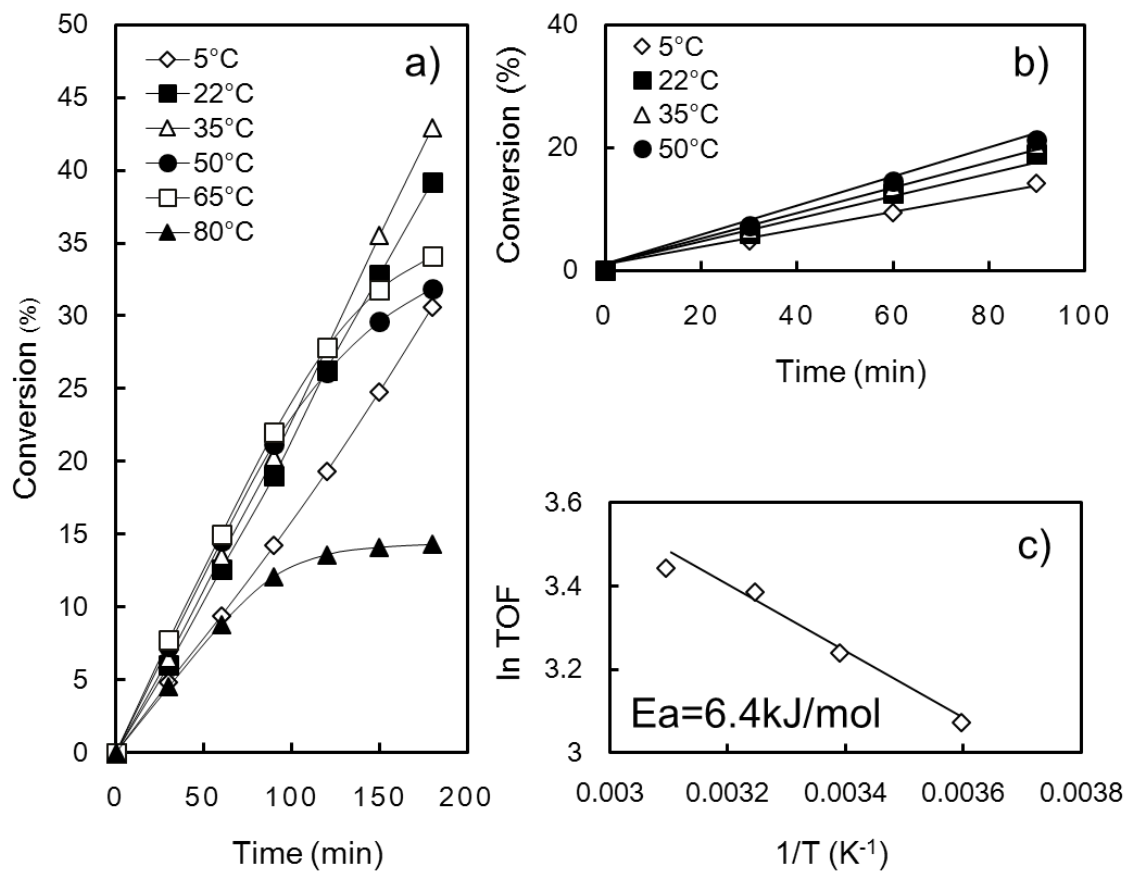
Figure A1. Conversion of phenol from 5°C to 80°C (a). Initial conversion of phenol from 5 °C to 50 °C (b). Arrhenius plot and apparent activation energy. ECH was performed at 40mA, in acetic acid at pH 5. 50mg of Pt/C catalyst is used for each.
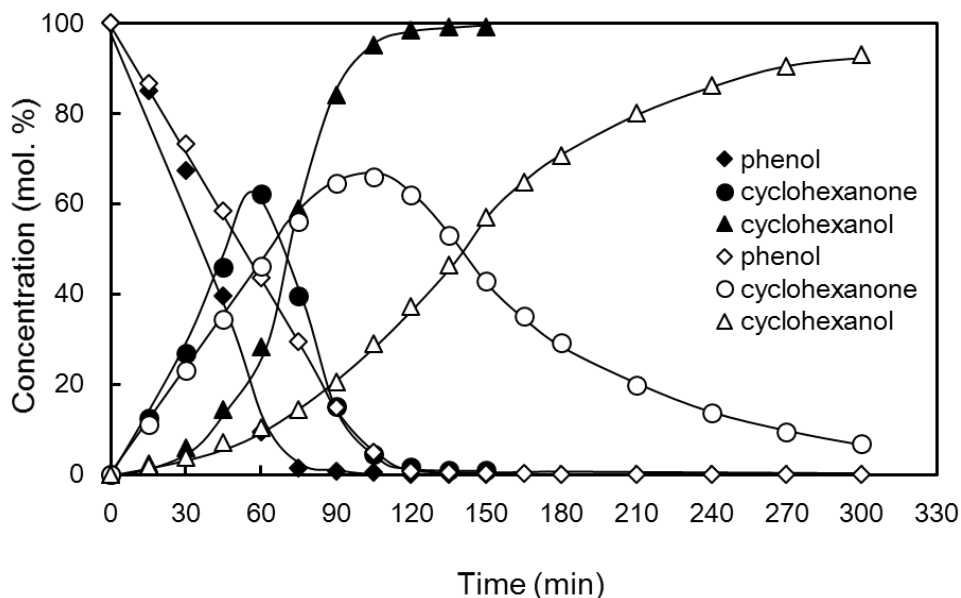
Figure A2. Thermal hydrogenation of phenol in pure water (black symbols) and in the presence of acetic acid (white symbols). The reactions were performed at room temperature at 1 bar H_2, with 50 mg of suspended Pt/C, pure water or a solution of acetic acid at pH 5 were used.
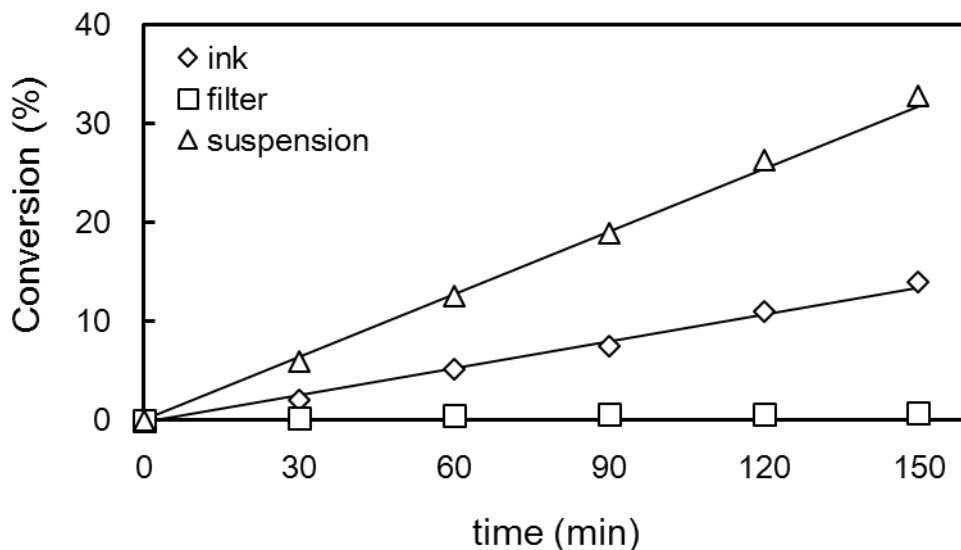
Figure A3. Phenol conversion during ECH at different experimental configurations. The experiments were performed at -40 mA in acetic acid (pH 5). The three configurations were: ink: (50mg Pt/C are mixed with isopropanol and Nafion solution, and the suspension is dropped on the RVC electrode), filter (50 mg Pt/C catalyst is dropped in electrolyte separated from the electrode with filter paper), and suspension (50 mg Pt/C powder is directly dropped into the electrolyte.

Table A1. Reaction rate (mol/s·g(Pt)), TOF (h^{-1}) and EE (%) observed with different experimental configurations.

configuration	rate	TOFs	E.E
suspension	1.5×10-5	28. 8	40
ink	6×10-6	11. 2	17.6
filter	0	0	0

2.6. References

[1] S. J. Davis, K. Caldeira, H. D. Matthews, Science 329 (2010) 1330-1333.

[2] A. J. Ragauskas, C. K. Williams, B. H. Davison, G. Britovsek, J. Cairney, C. A. Eckert, W. J. Frederick, J. P. Hallett, D. J. Leak, C. L. Liotta, J. R. Mielenz, R. Murphy, R. Templer, T. Tschaplinski, Science 311 (2006) 484-489.

[3] A. Corma, S. Iborra, A. Velty, Chem. Rev. 107 (2007) 2411-2502.

[4] K. Christopher, R. Dimitrios, Energy Environ. Sci. 5 (2012) 6640-6651.

[5] C. Zhao, J. He, A. A. Lemonidou, X. Li, J. .A Lercher, J. Catal. 280 (2011) 8-16.

[6] S. Czernik, A. V. Bridgwater, Energy Fuels 18 (2004) 590-598.

[7] C. Zhao, Y. Kou, A. A. Lemonidou, X. Li, J. A. Lercher, Angew. Chem. Int. Ed. 121 (2009) 4047-4050.

[8] D. Robin, M. Comtois, A. Martel, R. Lemieux, A. K. Cheong, G. Belot, J. Lessard, Can. J. Chem. 68 (1990)1218-1227.

[9] Z. Li, M. Garedew, C. H. Lam, J. E. Jackson, D. J. Miller, C. M. Saffron, Green Chem. 14 (2012) 2540-2549.

[10] X. Han, F. Cheng, T. Zhang, J. Yang, J. Hu, J. Chen, Adv. Mater. 26 (2014) 2047-2051.

[11] A. J. Ragauskas, G. T. Beckham, M. J. Biddy, R. Chandra, F. Chen, M. F. Davis, C. E. Wyman, Science 344 (2014) 1246843-1-1246843-10.

[12] C. Li, M. Zheng, A. Wang, T. Zhang, Energy Environ. Sci. 5 (2012) 6383-6390.

[13] X. Xu, Y. Li, Y. Gong, P. Zhang, H. Li, Y. Wang, J. Chem. Am. Soc. 134 (2012) 16987-16990.

[14] F. Laplante, L. Brossard, H. Ménard, Can. J. Chem. 81 (2003) 258-264.

[15] C. M. Cirtiu, A. Brisach-Wittmeyer, H. Ménard, J. Catal. 245 (2007) 191-197.

[16] J. M. Friedrich, C. Ponce-de-León, G. W. Reade, F. C. Walsh, J. Electroanal.Chem. 561 (2004) 203-217.

[17] J. Wang, Electrochim. Acta 26 (1981) 1721-1726.

[18] A. Martel, B. Mahdavi, J. Lessard, H. Ménard, L. Brossard, Can. J. Chem. 75 (1997) 1862-1867.

[19] P. S. Guin, S. Das, P. C. Mandal, Int. J. Electrochem. 2011 (2011) 1-22

[20] C. M. Cirtiu, H. O. Hassani, N. A. Bouchard, P. A. Rowntree, H. Ménard, Langmuir 22 (2006) 6414-6421.

[21] M. A. Casadei, D.Pletcher, Electrochim. Acta 33 (1988) 117-120.

[22] D. S. Santana, G. O. Melo, M. V. F. Lima, J. R. Daniel, M. C. Areias, M. Navarro, J. Electroanal. Chem. 569 (2004) 71-78.

[23] M. A. Casadei, D. Pletcher, Electrochim. Acta 33 (1988) 117-120.

[24] Y. Mao, B. M. Fung, J. Colloid Interface Sci. 191 (1997) 216-221.

[25] B. Zhao, M. Chen, Q. Guo, Y. Fu, Electrochim. Acta 135 (2014) 139-146.

[26] S. K. Green, J. Lee, H. J. Kim, G. A. Tompsett, W. B. Kim, G. W. Huber, Green Chem. 15 (2013) 1869-1879.

[27] J. He, C. Zhao, J. A. Lercher, J. Catal. 309 (2014) 362-375.

[28] J. He, C. Zhao, D. Mei, J. A. Lercher, J. Catal. 309 (2014) 280-290.

[29] F. Colmati, E. Antolini, E. R.Gonzalez, J. Power Sources 157 (2006) 98-103.

[30] T. J. Schmidt, H. A. Gasteiger, G. D. Stäb, P. M. Urban, D. M. Kolb, R. J. Behm, J. Electrochem. Soc. 145 (1998) 2354-2358.

[31] M. H. Miles, M. A. Thomason, J. Electrochem. Soc. 123 (1976) 1459-1461.

[32] S. A. Grigoriev, M. S. Mamat, K. A. Dzhus, G. S. Walker, P. Millet, Int. J. Hydrogen Energy 36 (2011) 4143-4147.

[33] Y. Kwon, M.Koper, ChemSusChem 6 (2013) 455-462.

[34] A. Bannari, P. Proulx, H. Ménard, C. M. Cirtiu, Appl. Catal. A: Gen. 345 (2008) 28-42.

[35] P. J. Rheinländer, J. Herranz, J. Durst, H. A. Gasteiger, J. Electrochem. Soc. 161 (2014) F1448-F1457.

[36] V. R. Stamenkovic, B. S. Mun, M. Arenz, K. J. Mayrhofer, C. A. Lucas, G. Wang, N. M. Markovic, Nat. Mater. 6 (2007) 241-247.

[37] M. Besson, P. Gallezot, C. Pinel, Chem. Rev. 114 (2013) 1827-1870.

2.7. Associated Content

Peer-Reviewed Publication

This chapter is based on the following article: Yang Song, Oliver Y. Gutiérrez, Juan Herranz, Johannes A. Lercher, Aqueous phase electrocatalysis and thermal catalysis for the hydrogenation of phenol at mild condition, Applied Catalysis B: Environmental, 2016, Vol. 182, 236-246.

Contributions

Oliver Y. Gutiérrez supervised the activites on aqueous-phase electrocatalysis and thermal catalysis for the hydrogenation of phenol at mild conditions. Yang Song contributed with the design of the experiments, operation of setups, experimental activities, data analysis, and draft writing. Juan Herranz supervised electrochemical experiments and participated in discussions. Johannes A. Lercher

was responsible for data discussion, supervising and manuscript preparation. Oliver Y. Gutiérrez and Johannes A. Lercher are the principal investigators of this work.

Clearance by the Publisher

Chapter 3

Integrated electrocatalytic conversion of substituted phenols and diaryl ethers

Electrocatalytic hydrogenation and catalytic thermal hydrogenation of substituted phenols and diaryl ethers were studied on carbon-supported Rh. The rates of electrocatalytic hydrogenation increase with increasingly negative potentials, which have been related with the coverage of adsorbed hydrogen. The lowest and highest negative potentials in electrocatalytic hydrogenation correspond to the onset of H_2 evolution and to the onset of reactions involving the electrolyte, respectively. For electrocatalytic and catalytic thermal hydrogen addition reactions, the dominant reaction pathway is hydrogenation to cyclic alcohols and cycloalkyl ethers. The presence of substituting methyl or methoxy groups led to lower rates compared to unsubstituted phenol or diphenyl ether. Methoxy or benzyloxy groups, however, undergo C-O bond cleavage via hydrogenolysis and hydrolysis (minor pathway). The surface chemical potential of hydrogen can be increased also by generating a H_2 atmosphere above the reaction media, supporting the conclusion that thermal and electrochemical routes share the same reaction pathways.

3.1. Introduction

Electrocatalytic hydrogenation of biomass feedstocks is a promising approach for the synthesis of zero-carbon-footprint energy carriers by coupling electrocatalytic H^+ reduction using renewable energy with reductive processing of biomass-derived intermediates to fuels. In order to realize such a pathway, the synthesis has to occur decentralized, as the renewable electric energy is generated decentralized and with relatively low power. The local, small-scale reductive conversions must be performed under milder conditions than typical hydrotreating processes [1-8].

Formally, electrocatalytic hydrogenation consists of integrating the reduction of protons (Reaction I) and the hydrogenation of organic compounds at the cathode. The reduction at the cathode occurs, while O_2 (Reaction II) is formed or another oxidation reaction occurs at the anode.

$$2H^+_{(aq)} + 2e^- \rightarrow H_{2\,(g)} \qquad E^0 = 0 \text{ V} \qquad\qquad (I)$$

$$2H_2O_{(l)} \rightarrow O_{2\,(g)} + 4H^+ + 4e^- \qquad E^0 = 1.23 \text{ V} \qquad (II)$$

Mechanistically, electrocatalytic hydrogenation (ECH) could proceed through two main different pathways, i.e., stepwise proton/electron addition or simultaneous electron-proton (neutral) hydrogenation. In turn, the stepwise hydrogenation may consist of electron addition followed by protonation of the oxygenated hydrocarbon, or by direct protonation of the hydrocarbon followed by electron transfer. Direct electron addition to an aromatic hydrocarbon followed by proton addition is not likely, because higher negative overpotentials are required for the direct reduction of aromatic molecules than for proton reduction, as shown, e.g., for the reduction of benzene in Reaction III [9]. A pathway started by protonation of the aromatic would depend on the strength of the acid present in the environment and the proton affinity of the hydrocarbon in solution. We can rule out such a pathway for phenolic compounds (model molecules used in this study), because the pK_a of, e.g., protonated phenol and protonated benzene are -6 and -24, respectively. Thus,

very high activation barriers are expected in stepwise hydrogenation mechanisms, compared to neutral pathways [10].

$$C_6H_6 + e^- \rightarrow (C_6H_6)^- \qquad E^0 = -3.18 \text{ V} \qquad \text{(III)}$$

The mechanistic steps for the cathode reaction in water electrolysis comprise of the formation of adsorbed H (Volmer step, Reactions IV and V), the combination of H to H_2 (Tafel step, Reaction VI) and the concerted reductive H_2 production (Heyrovsky steps, Reactions VII and VIII).

$$H^+ + e^- \rightleftharpoons H_{ads} \text{ (in acid)} \qquad \text{(IV)}$$

$$H_2O + e^- \rightleftharpoons H_{ads} + OH^- \text{ (in base)} \qquad \text{(V)}$$

$$2H_{ads} \rightleftharpoons H_2 \qquad \text{(VI)}$$

$$H_{ads} + H^+ + e^- \rightleftharpoons H_2 \text{ (in acid)} \qquad \text{(VII)}$$

$$H_{ads} + H_2O + e^- \rightleftharpoons H_2 + OH^- \text{ (in base)} \qquad \text{(VIII)}$$
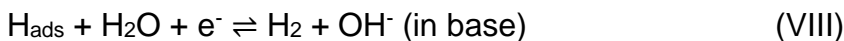
The simultaneous electron-proton transfer to the hydrocarbon as hydrogenation mechanism may proceed *via* concerted electron-proton transfer or *via* H-atom transfer [11,12]. Reaction IX exemplifies a first concerted hydrogenation step to adsorbed phenol, whereas Reaction X shows the hydrogenation of phenol to cyclohexanone by H atoms. It is difficult to determine unequivocally the nature of the hydrogenation step. However, phenol can be hydrogenated at the metal surface with adsorbed H in the absence of electric potential [13]. Thus, under our conditions, the hydrogenation pathway is hypothesized at this point to be equivalent to the thermally induced catalyzed reaction between H_2 and the reactant thermal hydrogenation (thermal catalytic hydrogenation, TCH). In this instance, the (reversible) Volmer step, would establish the surface chemical potential of H that drives the hydrogenation and product desorption.

$$C_6H_5OH^* + H^+ + e^- \rightarrow C_6H_6OH^* \qquad \text{(IX)}$$

$$C_6H_5OH + 4H_{ads} \rightarrow C_6H_{10}O \qquad \text{(X)}$$

Therefore, the ECH in this case is equivalent to the metal catalyzed hydrogenation of hydrocarbons in aqueous phase with the adsorbed hydrogen generated *in situ*.

ECH of phenol has been reported on Pd-, Ni-, and Rh-based catalysts [13-15]. C-O bond cleavage has been observed for the electrochemical conversion of benzophenone, diaryl ethers, and hydroxymethylfurfural [15,16]. However, the reaction pathways, mechanisms that operate at such mild conditions and the impact of the molecular structure on the pathways have hardly been explored. A detailed molecular level understanding of the reaction pathways is required to advance this important reaction step in an overall concept of a decentralized synthesis of carbon-neutral fuels.

As a step in this direction, we report here on the catalytic hydrogenation of increasingly complex aromatic molecules containing oxygen, ranging from phenol to substituted di-aryl ethers on carbon-supported Rh (Rh/C). We compare reaction pathways and kinetic parameters obtained when the adsorbed hydrogen is formed from proton reduction (ECH) or H_2 dissociation (TCH).

3.2. Experimental and theoretical methods

3.2.1. Chemicals and catalytic materials

All chemicals were obtained from Sigma Aldrich and used as received: phenol (≥99.0%), 4-methylphenol (Sigma-Aldrich, ≥99.0%), 3-methylphenol (Sigma-Aldrich, ≥99.0%), 2-methylphenol (Sigma-Aldrich, ≥99.0%), 4-methoxyphenol (Sigma-Aldrich, ≥99.0%), 3-methoxyphenol (Sigma-Aldrich, ≥99.0%), 2-methoxyphenol (Sigma-Aldrich, ≥99.0%), diphenyl ether (Sigma-Aldrich, ≥99.0%), cyclohexyl phenyl ether (Sigma-Aldrich, ≥99.0%), *p*-tolyl ether (Sigma-Aldrich, ≥99.0%), benzyl phenyl ether (Sigma-Aldrich, ≥99.0%), acetate buffer solution (Sigma-Aldrich, pH 4.6), methanol (Sigma-Aldrich, ≥99.9%, HPLC), ethanol (Sigma-Aldrich, ≥99.9%, HPLC), isopropanol (Sigma-Aldrich, ≥99.9%, HPLC), ethyl acetate (Sigma-Aldrich, ≥99.9%, HPLC), dimethoxyethane (Sigma-Aldrich, ≥99.9%, HPLC), Na_2SO_4 (Sigma-Aldrich, ≥99.9%), NaCl (Sigma-Aldrich, ≥99.9%),

and KCl (Sigma-Aldrich, ≥99.9%). High purity water, obtained with a Milli-Q water purification system with a resistivity of 18.2 MΩ·cm, was used for all experimental procedures. H_2 (Air Liquide, >99.99%) is used for thermal hydrogenation, He (Air Liquide, >99.99%) is used as protection gas to remove oxygen from the electrolyte before ECH. The catalyst used in this study, Rh/C with a metal content of 5 wt. %, was purchased from Sigma Aldrich.

3.2.2. Catalyst characterization

The surface area and pore diameter of the catalyst were measured by N_2 physisorption, which was performed at 77 K on a PMI automated BET sorptometer. The samples were outgassed before measurements at 523 K for 20 h. The surface area and pore distribution were calculated according to BET and BJH models.

The dispersion of the metal phase was determined by H_2 chemisorption. Prior to the measurement, the material was treated in vacuum at 588 K for 1h and then cooled to 313 K. An adsorption isotherm was measured at from 1 to 40 kPa. Afterwards, the sample was outgassed at 313 K for 1h and a second isotherm was measured to determined physisorbed H_2. The concentration of hydrogen chemisorbed on the metal was determined by extrapolating the difference isotherms to zero hydrogen pressure. The dispersion of the supported metal was estimated from the concentration of chemisorbed hydrogen assuming a stoichiometry of 1:1 metal to hydrogen atoms.

The dispersion of the metal was also explored by transmission electron microscopy (TEM). Samples of the catalysts were ground, and ultrasonically dispersed in ethanol. Drops of the suspensions were applied on a copper-carbon grid and the measurements were carried out in a JEOL JEM-2011 electron microscope with an accelerating voltage of 120 keV. Statistical treatment of the metal particle size was done by counting at least 200 particles detected in several places of the grid. The morphology of the working electrode (activated carbon felt)

before and after incorporating the catalyst was investigated by a scanning electron microscope (JSM-7500F from JEOL).

3.2.3. Electrocatalytic hydrogenation (ECH)

In a previous contribution, ECH was slower than TCH by one order of magnitude [10]. The reason for the low rates of was the particular experimental configuration in which the large distance between electrodes and the concomitant resistance to ion transport led to significant voltage losses. In order to minimize internal Ohmic resistance, in this work all experiments were carried out in a two-compartment galvanostatic cell with very short distance between electrodes and the membrane. A diagram of the cell used to perform the reactions is shown in Figure A1. Cathodic and anodic compartments of the cell were separated by a Nafion 117 proton exchange membrane (Ion Power, Inc.), which was pretreated in a H_2O_2 solution (3 vol.%) and in sulfuric acid (2 M) before reaction. A piece of carbon felt (Alfa Aesar >99.0%, 3.2 mm thickness, shown in Figure A2) connected to a graphite rod (Sigma Aldrich) was used as working electrode in the cathode compartment. A platinum wire (Alfa Aesar, 99.9 %) was used as counter electrode in the anodic compartment. The reference electrode was a home-made Ag/AgCl electrode with a double junction. For ECH of phenol, methylphenol and methoxyphenol, the cathode compartment was filled with acetate buffer at pH 5. 20 mg of the Rh/C catalyst were added into the cathode compartment. All reactions were performed at atmospheric pressure at 296 K. The stirring at 500 rpm allowed complete incorporation of the powder into the carbon felt. Prior to ECH, polarization of the catalyst was performed under a constant current of -40 mA for 30 min. For ECH, phenolic solution was added into the cathode compartment to obtain a final concentration of 16 mmol/L. Owning to the poor solubility of di-aryl ethers in water at room temperature a mixture of acetate buffer (30 vol.%) in isopropanol was used as solvent for ECH of diphenyl ether, p-tolyl ether, and benzyl phenyl ether. For the ECH of these compounds, solutions with $5 \cdot 10^{-4}$ mol reactants were mixed with

50 mg of Rh/C. ECH experiments were performed at constant potential while a flow of He was kept through the cell. During all described procedures, the anode compartment contained mixtures of acetate buffer (pH 5) as the electrolyte. All electrochemical procedures were performed with an electrochemical workstation (VSP-300, Bio Logic). Before each ECH test, the cell compartments and other materials were cleaned with concentrated H_2SO_4 and immersed in boiling water for 2 h several times. Prior to the reactions, the electrodes were alternatively immersed in H_2SO_4 (5 M) and KOH (5 M) for 15 min. After each immersion, the materials were thoroughly cleaned (Pt electrodes were further ultrasonically treated) in ultrapure water for 15 min. ECH with recycling hydrogen were performed in the cell depicted in as Figure A1. The cell was closed gas-tight and equipped with a recycling gas pump on top of the cathodic chamber to recycle the hydrogen produced via hydrogen evolution reaction during ECH.

3.2.4. Thermal catalytic hydrogenation (TCH)

Catalytic thermal reactions were carried out at atmospheric pressure with H_2 (20 mL/min) flowing through the reactant solution in the cathode compartment at 296 K. The preparation of the different reactant solutions and their concentrations were the same as those described for ECH. For coupled ECH and TCH experiments, a recycling pump was connected to the cell in order to feed in the H_2 produced by the hydrogen evolution reaction, whereas the cell was closed to allow building up of the pressure.

3.2.5. Product analysis

The course of the ECH and TCH experiments was followed by periodically withdrawing aliquots of 1 mL from the cathode compartment. The products were extracted with 3 mL of ethyl acetate. A 2 mL of 1 mol/L Na_2SO_4 solution was needed for the extraction of diaryl ethers, owning to the presence of ethanol in the solution. The organic phase was separated from the aqueous phase by decantation and dried on Na_2SO_4. A sample of the dry organic phase was mixed

with a solution containing a standard. Quantitative analyses of those samples were performed by gas chromatography coupled with mass spectrometry (Shimadzu GCMS-QP2010), equipped with a plot Q capillary column (30m x 250 μm) and a thermal conductivity detector (TCD).

3.3. Results and discussion

The catalyst used in this work was carbon-supported Rh with a metal loading of 5 wt.% and average Rh particle size of 3.4 nm. During the experiments, this catalyst was infiltrated in an activated carbon felt. Experimental procedures (Figures A1), calculation details, and catalyst characterization (Figures A2) are described in the supporting information. In the following the Faradaic efficiencies (FE) is defined as the percentage of the current producing the adsorbed hydrogen that reacts with oxygenates, i.e., reactant and intermediates of ECH. The turnover frequencies (TOF) correspond to the moles of ECH reactant converted per surface metal atom per hour. ECH and rates of the hydrogen evolution reaction (HER) are defined as the moles of organic reactant converted and moles of molecular H_2 produced, respectively, per second and gram of Rh. Adsorbed hydrogen (H_{ads}) consumption rates of ECH, TCH, and HER are defined as the moles of adsorbed H that react with organic compounds *via* ECH or TCH or that produce molecular H_2 in HER, respectively, per second and gram of Rh.

3.3.1. Manipulating the electrocatalytic hydrogenation of phenol with potential

In the conversion of phenol at varying potentials, the cathodic current increased linearly from 18 mA to 220 mA with potentials varying from -0.4 V to -0.9 V (vs Ag/AgCl) (Table 3.1). In this potential range, the sum of hydrogen reacted with oxygenates and evolved as H_2 (only product detected in the gas phase) equaled the measured currents. Thus, electrons were only consumed in the reduction of protons, which solely participate in ECH as well as in HER. The ohmic loss was 1.8 Ohm as determined by impedance measurements. Upon taking into account this loss, the current showed an exponential increase with increasingly negative HFR-free potentials as shown in Table A2 and Figure A3.

Table 1. Measured current, current density, rate of electrocatalytic hydrogenation (ECH), TOF, Faradaic efficiency (FE), and rates of hydrogen evolution (HER) observed during the catalytic hydrogenation of phenol at varying potentials. The reactions were performed in mixtures of water and acetic acid at room temperature and atmospheric pressure on Rh/C.

Potential (V vs Ag/AgCl)	-0.4	-0.5	-0.6	-0.7	-0.8	-0.9
Current (mA)	-18	-50	-100	-140	-175	-220
Current density[a] ($mA \cdot cm^{-2}$)	0.02	0.06	0.11	0.16	0.20	0.25
ECH ($\cdot 10^{-5}\, mol \cdot s^{-1} \cdot g_{Rh}^{-1}$)	0.81	7.5	16	26	28	34
TOF (h^{-1})	15	138	296	475	538	629
FE (%)	20	58	68	70	68	66
HER ($\cdot 10^{-5}\, mol \cdot s^{-1} \cdot g_{Rh}^{-1}$)	7.5	11	16	22	29	38

[a] The electrode area is defined as the metal surface as determined *via* H_2 chemisorption.

For comparison, the rates of hydrogen equivalents consumed during ECH (converting the reactant and intermediate) and during HER are shown in Figure 3.1 (for values see Table A3). The low rates of ECH and HER at -0.4 V are caused by the overpotential needed for generating surface hydrogen at pH of 4.6 (-0.45 V

vs Ag/AgCl). Between -0.4 V and -0.9 V, the changes of HER and ECH rates with potential increased linearly with 3 $\mu molH_{ads} \cdot s^{-1} \cdot g_{Rh}^{-1}$ of H consumed in HER and 1.2 $\mu molH_{ads} \cdot s^{-1} \cdot g_{Rh}^{-1}$ of H consumed in ECH (0.61 $\mu mol \cdot s^{-1} \cdot g_{Rh}^{-1}$ of H_2 evolved and 0.68 $\mu mol \cdot s^{-1} \cdot g_{Rh}^{-1}$ of phenol converted), per 1 mV of negative potential. ECH rates increasing faster than HER rates with increasing negative potentials suggesting a surprisingly stronger dependence of phenol hydrogenation than HER on concentration of adsorbed hydrogen.
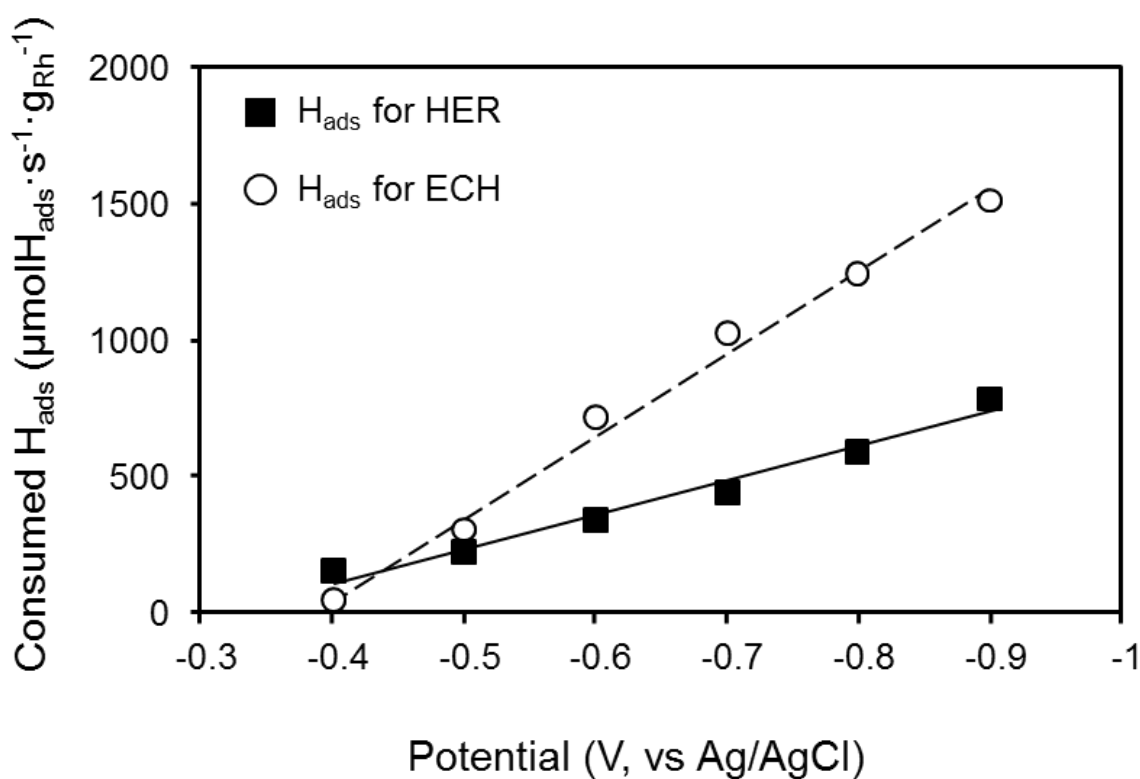
Figure 3.1. Dependence of electrocatalytic phenol hydrogenation (ECH) and hydrogen evolution rates (HER), expressed as rate of adsorbed hydrogen consumed, on potential. The reactions were performed in a water-acetic acid mixture at room temperature and atmospheric pressure on Rh/C.

The rate of H addition to oxygenates in TCH was $10 \cdot 10^{-4}$ $molH_{ads} \cdot (s \cdot g_{Rh})^{-1}$ (TOF of 385 h^{-1}) at 298 K and 1 bar H_2 (Figure 2). In ECH, the conversion of the organic

compounds was controlled by potential and could reach rates, which were up to 1.6 times higher than TCH at a H_2 pressure of 1 bar, i.e., $15 \cdot 10^{-4}$ $molH_{ads} \cdot (s \cdot g_{Rh})^{-1}$ (TOF of 629 h^{-1}) at -0.9 V.

The reaction order in phenol from -0.4 V to -0.9 V was zero (Figure 3.2). Thus, the coverage of reactive hydrogen on the metal surface determines the ECH rates. In turn, faster ECH than TCH implies that the concentration of adsorbed H under ECH is higher than the equilibrium value corresponding to 1 bar H_2.
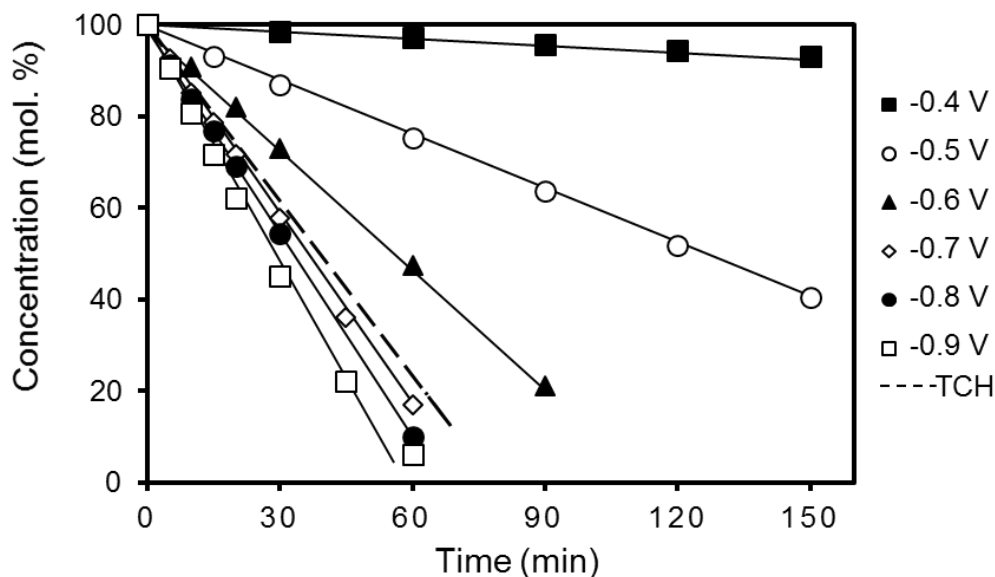
Figure 3.2. Decrease in phenol concentration during thermal catalytic hydrogenation (TCH), and electrocatalytic hydrogenation under varying potentials (from -0.4 V to -0.9 V vs Ag/AgCl). The reactions were conducted in a water-acetic acid mixture at room temperature and atmospheric pressure on Rh/C.

At conditions where only HER occurs (Reaction I), the hydrogen coverage at the metal surface at -0.23 V (or -0.52 V at pH 5), vs Ag/AgCl is equivalent to 1 bar of H_2 gas. However, the ECH conditions are far from ideal, as protons must compete with hydrocarbons for adsorbing at the metal, where H recombination occurs in parallel to hydrogenation. This has to require high over potentials to sustain hydrogen coverages. Follow this rationale, if the role of the potential in

ECH is to provide the adsorbed hydrogen that reacts with phenol, a potential must exist (more negative than that required for ideal HER) at which the hydrogen coverage is identical to that corresponding to 1 bar of H_2 in the presence of the hydrocarbon. We identified -0.7 V as that potential, because all rates of TCH and ECH of the reaction of intermediates were similar at that point (Figure 3.2). Figure 3.3 shows that the concentration profiles of TCH and ECH at -0.7 V were equivalent. In contrast, the concentration profiles of TCH and ECH at e.g., -0.6 V are clearly different. The cyclohexanol to cyclohexanone molar ratio at, e.g., ~20% phenol conversion, increased from 0.31 to 0.4 with increasingly negative potentials. This shows that increasing hydrogen coverage enhances the production of cyclohexanol, which is formed after addition of 6 H to the initial reactant phenol.
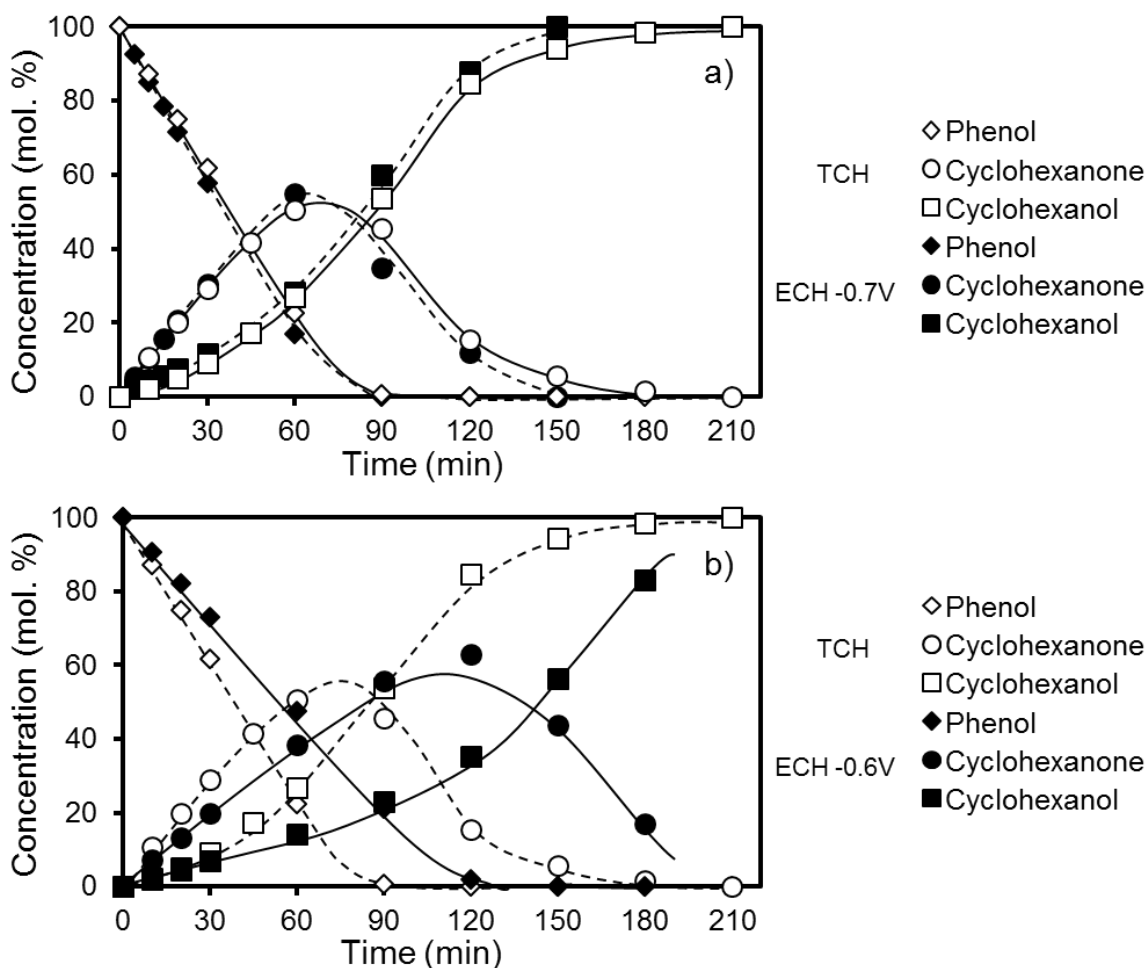
Figure 3.3. Concentration profiles observed during thermal catalytic hydrogenation (TCH) and electrocatalytic hydrogenation (ECH) of phenol. a) Comparison between TCH and ECH at -0.7 V, b) comparison between TCH and ECH at -0.6 V (vs Ag/AgCl).

3.3.2. Electrocatalytic hydrogenation and catalytic hydrogenation of substituted phenolic compounds

The conversion rates of methylphenol and methoxyphenol were lower than that of phenol under identical TCH and ECH conditions (Table 3.2). In ECH, the FEs of methylphenol and methoxyphenol were lower than the ones observed of phenol at the same potential, whereas the observed currents did not vary significantly. This indicates that the surface concentration of the hydrocarbons decreased with increasing substitutions, allowing for the rates of HER to increase twofold compared to the HER parallel to the ECH of phenol (Table 3.2). Indeed, the presence of a methyl or methoxy group decreases the adsorption energy of the aromatic compound on noble metals by 10-30 kJ·mol^{-1} [17]. This effect is caused by repulsive interactions between the substituent groups and the metal surface, whereas their induction effect on the adsorption of the ring is minor. In agreement with this, we observed that the position of the substituents (*o*, *m*, or *p*) had a small influence on the hydrogenation rates (Table A4 and Figure A4 of the appendix).

Table 3.2. Potential, current, current density, reaction rate, TOF, and Faradaic efficiency observed during the conversion of phenol, 4-methylphenol, and 4-methoxyphenol during ECH and TCH. The reactions were performed in a water-acetic acid mixture at room temperature and atmospheric pressure on Rh/C.

	Phenol		4-Methylphenol		4-Methoxylphenol	
	ECH	TCH	ECH	TCH	ECH	TCH
Potential (V vs Ag/AgCl)	-0.6	-	-0.6	-	-0.6	-
Current (mA)	-100	-	-105	-	-95	-
Current density^a (mA·cm^{-2})	0.11		0.12		0.11	
Reaction rate ($\cdot 10^{-5}$ mol·s^{-1}·g$_{Rh}^{-1}$)	16	20	8.1	10	7.4	11
TOF (h^{-1})	296	374	151	191	138	212
FE (%)	68	-	31	-	35	-
HER rate ($\cdot 10^{-5}$ mol·s^{-1}·g$_{Rh}^{-1}$)	17	-	38	-	32	-

[a] The electrode area is defined as the metal surface as determined *via* H_2 chemisorption.

Complete removal of O from hydroxyl groups at room temperature was not observed. This concluded to be absent, because the energy of activation to cleave the C-O bond is too high for secondary alcohols [18, 19]. Thus, the conversion of phenol and methylphenol is limited to hydrogenation to cyclohexanones and cyclic alcohols (Figure A5, and Figure 3.4 a and 3.4 c). The concentrations of cyclohexanones pass through maximum values indicating that they are primary and intermediate products. In contrast, the concentration of alcohols increased exponentially with time indicating that these are stable products [20-22]. Note that the concentration profiles in TCH and ECH are not identical, because coverages

of adsorbed hydrogen in TCH and ECH differ under the experimental conditions. At sufficiently long reaction time, complete conversion of reactant and intermediates was achieved.

The ECH and TCH of methoxyphenol produced hydrogenated products, (i.e., methoxy cyclohexanone and methoxy cyclohexanol), as well as phenol, cyclohexanone, cyclohexanol, and methanol (Figure 3.4 b and 3.4 d). Thus, the presence of the methoxy group opened a C-O hydrogenolysis pathway, yielding methanol (not reacting under these conditions) and phenol, which reacts further along the hydrogenation pathway described before. The selectivity was 90 % to hydrogenation, and 10 % to hydrogenolysis under ECH and TCH.
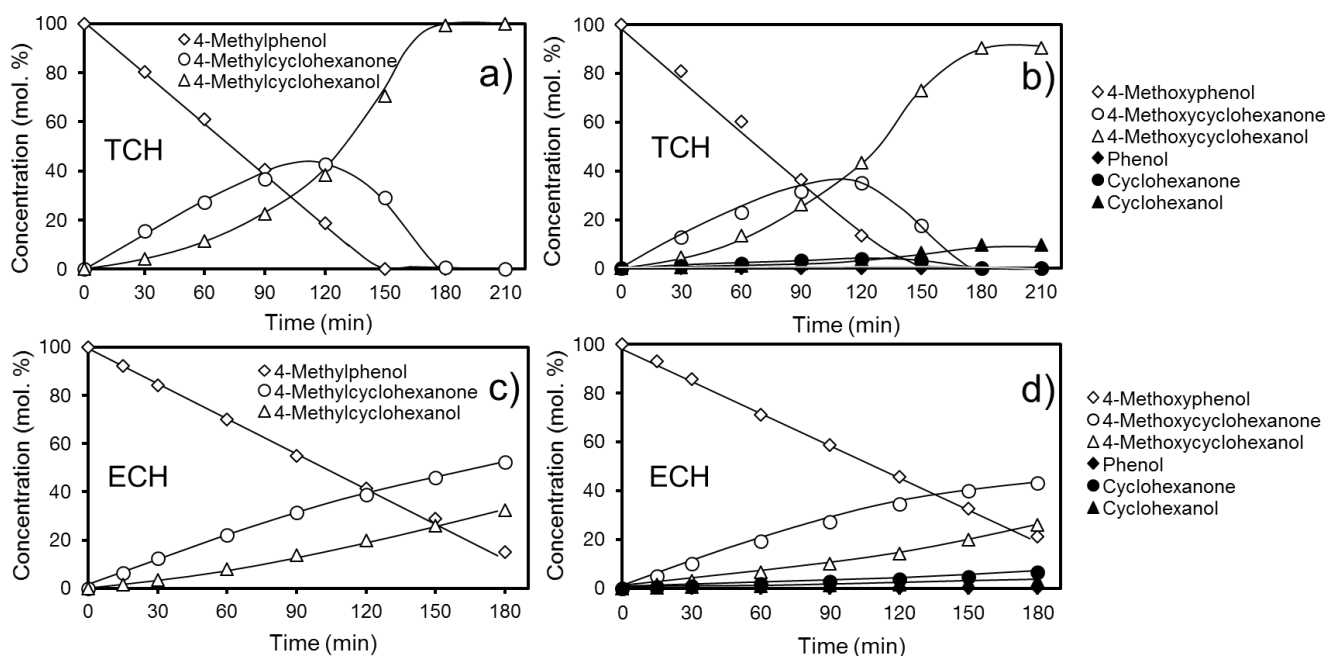
Figure 4. Concentration profiles observed during thermal catalytic hydrogenation (TCH, upper panels) and electrocatalytic hydrogenation (ECH bottom panels) of 4-methylphenol (a, c) and 4-methoxyphenol (b, d). The reactions were performed in water at room temperature and atmospheric pressure on Rh/C. The potential in ECH was -0.6 V (vs. Ag/AgCl).

Scheme 3.1 shows the reaction networks for the conversion of phenolic compounds by ECH and TCH. The only pathway for phenol, and methyl phenol, and main pathway for methoxyphenol is the consecutive 4- and 2-hydrogen additions to the corresponding cyclohexanones and cyclic alcohols, respectively. 4-Methoxyphenol undergoes C-O bond hydrogenolysis as a minor pathway. We hypothesize that the C-O bond was cleaved between the methoxy group and phenol in 4-methoxyphenol due to its lower strength (410 kJ·mol^{-1}) compared to the bond between the hydroxyl group and the aromatic ring (480 kJ·mol^{-1}). Cleavage of the methoxy group in the hydrogenated products was not observed.
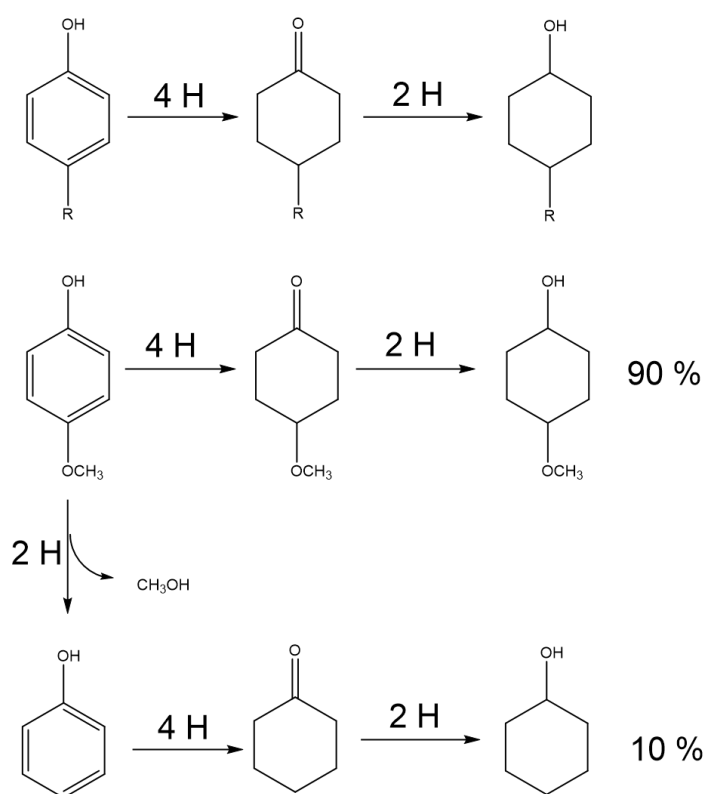
Scheme 1. Reaction networks of the conversion of phenol (R=H) 4-methylphenol (R=CH$_3$) (up) and 4-methoxyphenol (bottom) under catalytic thermal hydrogenation and electrocatalytic hydrogenation.

3.3.3. Electrocatalytic hydrogenation and catalytic thermal hydrogenation of di-aryl ethers

The conversion of the aryl ethers (representative of lignin-derived bio-oils): diphenyl ether (DPE), *p*-tolyl ether (PTE), and benzyl phenyl ether (BPE), was performed *via* TCH and ECH. The supporting information describes the effect of the solvent on rates and the choice of isopropanol-water mixtures as solvent. Under TCH and ECH modes, the reactivities of the aryl ethers increased following the ranking PTE < DPE < BPE (Table 3 and Figure A6 of the supported information). PTE is the least reactive, because of the steric repulsion induced by the methyl groups, decreasing the adsorption enthalpy by 75 kJ·mol^{-1} compared to DPE [23]. In contrast, the high reactivity of BPE is related to the relatively low dissociation energy of the α-O-4 bond (218 kJ·mol^{-1}), compared to, e.g., that of the 4-O-5 bond in DPE (314 kJ·mol^{-1}).

In TCH and ECH, the conversion of di-aryl ethers was slower than the conversion of phenolic compounds (Tables 3.2, 3.3, and A5). This was caused by the fact that the conversion of di-aryl ethers was carried out in the presence of large concentrations of isopropanol (needed to dissolve the ether), which is expected to strongly solvate the ethers and strongly adsorb on the metal reducing the aryl ether coverage [24]. In line with this conclusion, the conversion of aryl ethers in TCH and ECH followed a first order dependence on the hydrocarbon (Figure A6), reflecting their low coverage. The conversion rates during TCH were higher than during ECH by factors of up to 1.7 (Table 3.3), which is attributed to differences in hydrogen coverage as shown for phenol.

Although usage of organic solvents has profound effects on ECH rates (detail studies regarding the effect of solvent has been discussed in the supporting information), it does not affect HER strongly. Similarly, HER rates during the ECH of di-aryl ethers (performed in isopropanol-electrolyte mixtures) were between 33

and $42 \cdot 10^{-5}$ mol·s^{-1}·g$_{Rh}$$^{-1}$, while the HER rate in phenol was $38 \cdot 10^{-5}$ mol·s^{-1}·g$_{Rh}$$^{-1}$ at a potential of -0.9 V (vs Ag/AgCl) (Tables 3.1 and 3.3).

Table 3.3. Current, current density, reaction rate, TOF, and Faradaic efficiency of the conversion of di-aryl ethers via electrocatalytic hydrogenation (ECH) and thermal catalytic hydrogenation (TCH). The reactions were performed in water-isopropanol mixtures at room temperature and atmospheric pressure on Rh/C.

	Diphenyl ether		p-Tolyl ether		Benzyl phenyl ether	
	ECH	TCH	ECH	TCH	ECH	TCH
Potential (V vs Ag/AgCl)	-0.9	-	-0.9	-	-0.9	-
Current (mA)	-100	-	-100	-	-100	-
Current density^{b} (mA·cm^{-2})	0.11		0.11		0.11	
Reaction rate ($\cdot 10^{-5}$ mol·s^{-1}·g$_{Rh}$$^{-1}$)	3.2	4.5	2.3	2.8	4.7	8.2
Initial TOF (h^{-1})	60	85	43	50	88	155
FE (%)	25	-	18	-	36	-
HER rate ($\cdot 10^{-5}$ mol·s^{-1}·g$_{Rh}$$^{-1}$)	39	-	42	-	33	-

[a] C-O cleavage TOF was estimated from the sum of the selectivities to hydrolysis and hydrogenolysis.

[b] The electrode area is defined as the metal surface as determined *via* H$_2$ chemisorption.

In the conversion of DPE *via* ECH or TCH (Figure 3.5), the concentrations of cyclohexyl phenyl ether, phenol, cyclohexanone, and benzene passed through maxima, which indicate that they are intermediates and reactive products. Dicyclohexyl ether, cyclohexanol, and cyclohexane are secondary and stable

products. The product profiles observed in the ECH and TCH of PTE (Figure 3.6) indicate that 4-methylphenyl 4-methylcyclohexyl ether, 4-methylphenol, 4-methylcyclohexanone, and toluene are primary and intermediate products, whereas di 4-methylcyclohexyl ether, 4-methylcyclohexanol, and methylcyclohexane are final products.
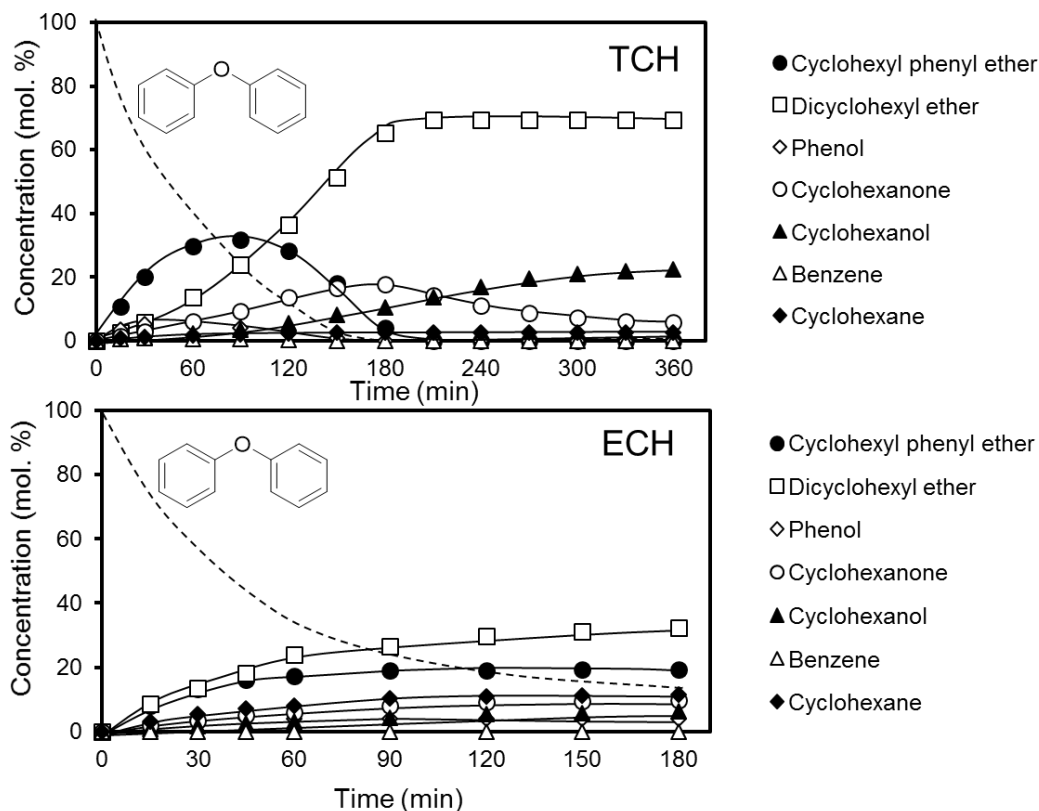
Figure 3.5. Concentration profiles observed during catalytic thermal catalytic hydrogenation (TCH) and electrocatalytic hydrogenation (ECH) of diphenyl ether. The reactions were performed in water-isopropanol-acetic acid mixtures at room temperature and atmospheric pressure on Rh/C.

The products identified in the conversion of DPE and PTE point to three reaction pathways, i.e., hydrogenation (yielding hydrogenated ethers), hydrogenolysis, and hydrolysis (both yielding oxygenated as well as O-free

hydrocarbons with only one aliphatic or aromatic ring). Hydrolysis was inferred by mass balances applied to the concentrations of the compounds with only one ring. The selectivity to the different pathways was similar for the conversions of DPE and PTE in ECH and TCH (Figure A7). This is attributed to the similarity of the structure and bond energies of both molecules and to identical elemental steps occurring on the metal surface under either ECH or TCH.

Scheme 3.2 shows the reaction network for DPE and PTE and the selectivity to the different reaction pathways. In the hydrogenation route (selectivity of ~70%) both rings are hydrogenated in consecutive steps, each of them involving the addition of six hydrogen atoms. C-O bond cleavage does not occur on this route, which yields ethers as final products. In the hydrogenolysis route (selectivity of 7-13%), a C-O bond is cleaved to produce phenolic and phenyl compounds as primary products, which are hydrogenated in subsequent parallel routes. The hydrolysis pathway (selectivity of 15-25%) leads to phenolic compounds, which undergo consecutive hydrogenation yielding cyclic alcohols as final products (as shown for phenol and methylphenol in Scheme 3.1). Additional experiments using cyclohexyl phenyl ether, and 4-mehylphenyl 4-methylcyclohexyl as starting reactants showed that the C-O bond between benzyl and ether groups are cleaved yielding O-free aromatics and cyclic alcohols (indicated in Scheme 3.2 with the doted red line). The selectivity towards complete hydrogenation, however, from those partially hydrogenated ethers is higher than 90% (Figure A8 supporting information).
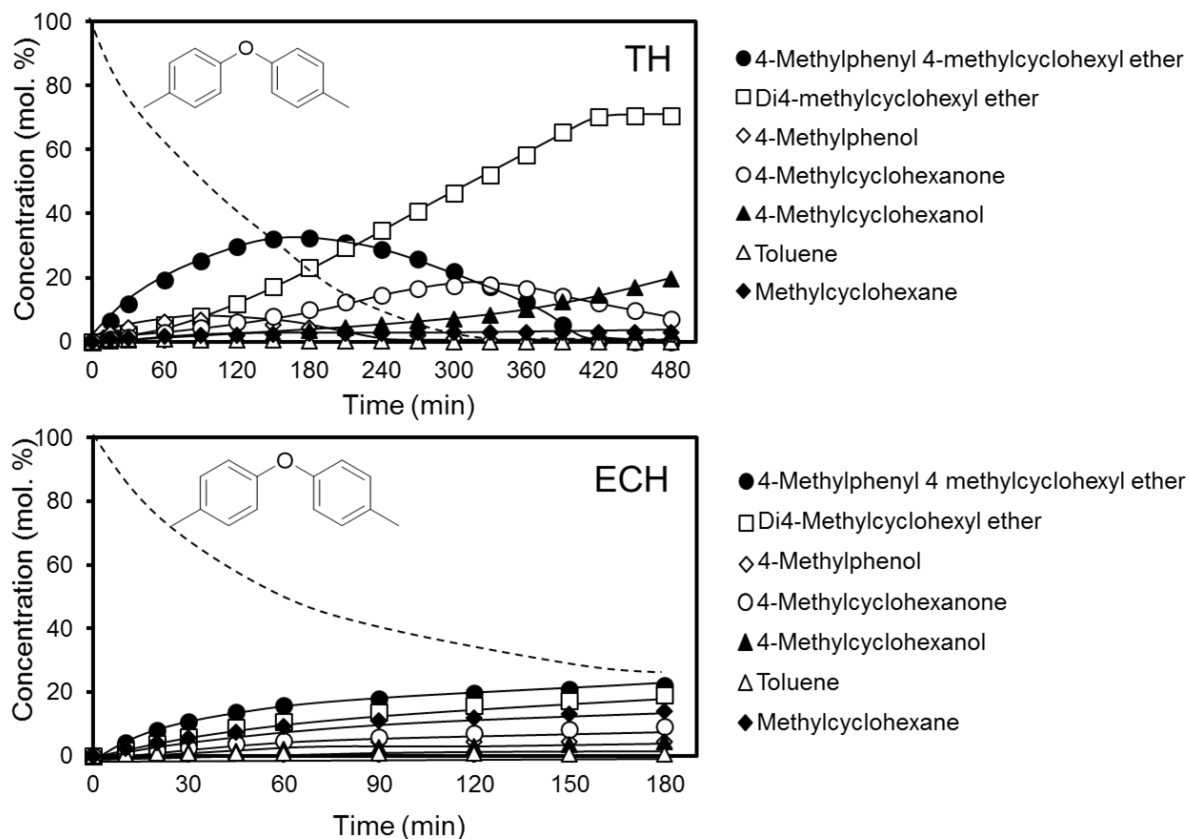
Figure 3.6. Concentration profiles observed during thermal catalytic hydrogenation (TCH) and electrocatalytic hydrogenation (ECH) of p-tolyl ether during of diphenyl ether. The reactions were performed in water-isopropanol-acetic acid mixtures at room temperature and atmospheric pressure on Rh/C.
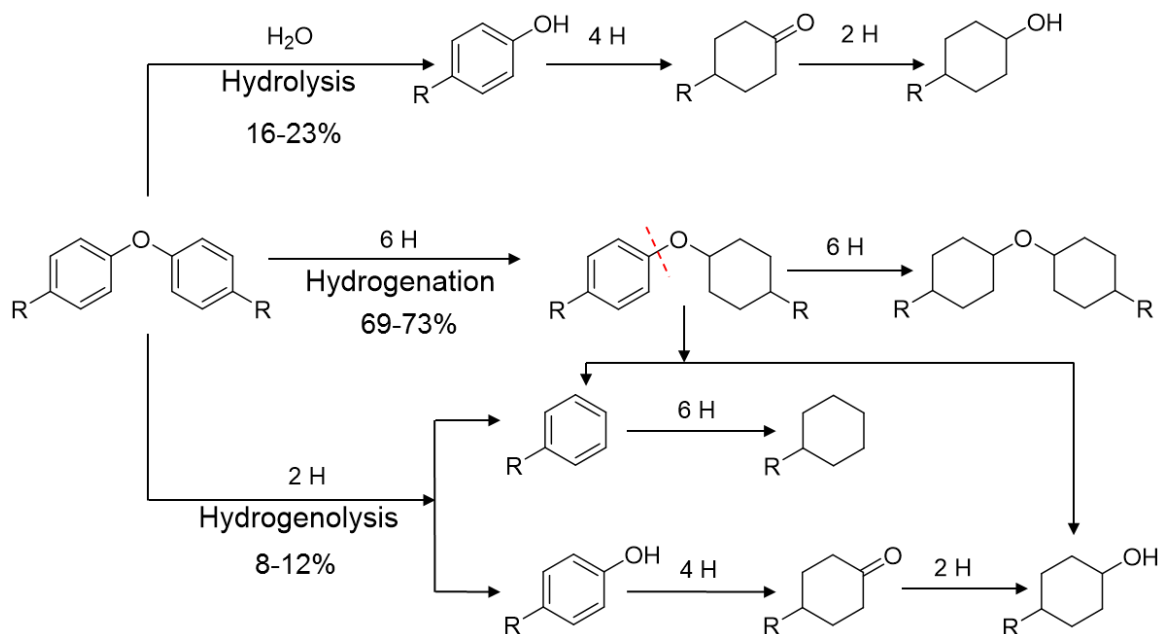
Scheme 3.2. Reaction network of the conversion of diphenyl ether (R=H) and p-tolyl ether (R=CH$_3$) under catalytic thermal hydrogenation and electrocatalytic hydrogenation.

The product profiles observed during the TCH and ECH of benzyl phenyl ether (BPE) are shown in Figure 7. The hydrogenated ethers, methyl cyclohexyl phenyl ether, cyclohexyl benzyl ether were primary and reactive products, whereas cyclohexyl methyl cyclohexyl ether was a stable product. Within the products with one functionalized ring, phenol, cyclohexanone, and benzyl alcohol, were secondary intermediates, whereas cyclohexanol, and cyclohexylmethanol were final products. The oxygen-free hydrocarbons toluene and methylcyclohexane were intermediate and final products, respectively.
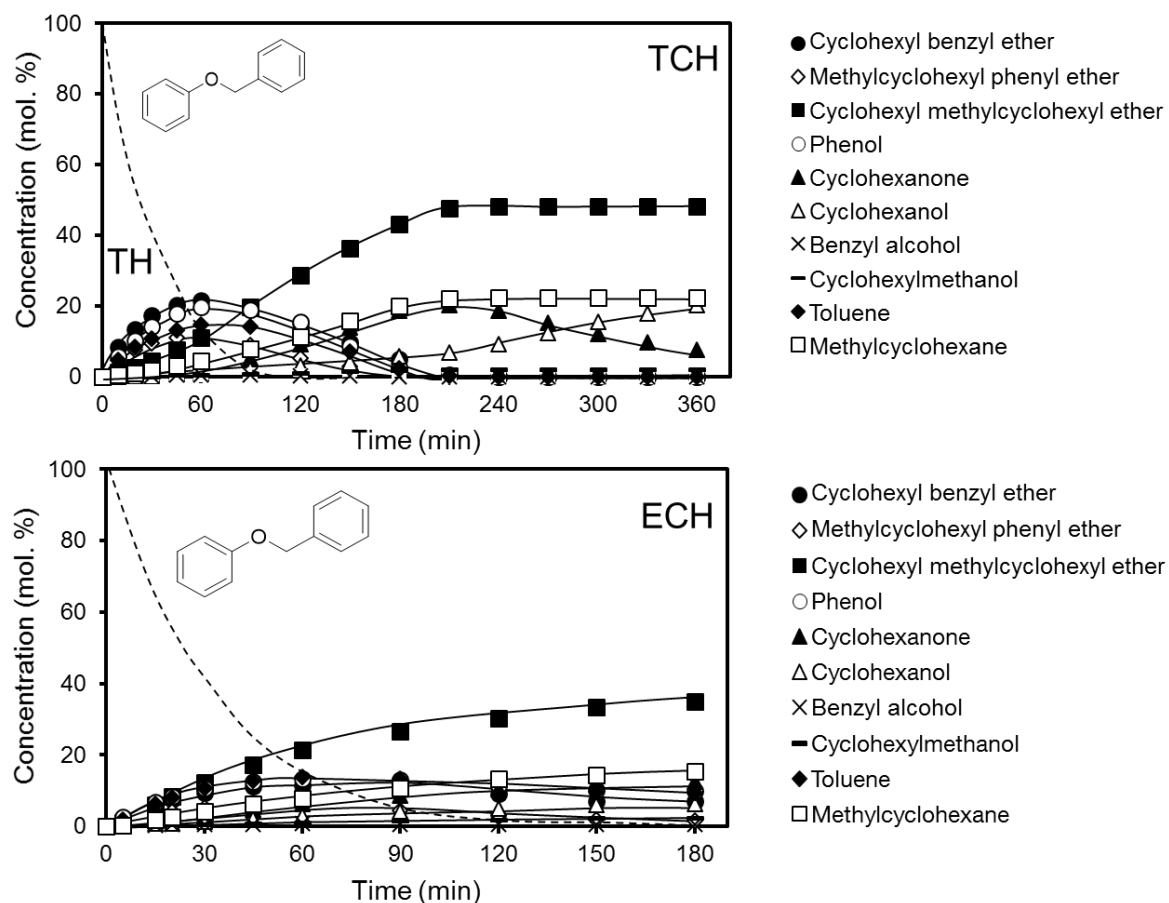
Figure 3.7. Concentration profiles observed during catalytic thermal hydrogenation of benzyl phenyl ether. The reactions were performed in a water-ethanol mixture at room temperature and atmospheric pressure on Rh/C.

The concentrations profiles and structure of the products allowed us to conclude that the conversion of BPE follows a reaction network that includes hydrogenation, hydrogenolysis, and hydrolysis as in the case of the symmetric ethers (Scheme 3.3). The selectivities to these three pathways in ECH and TCH are similar (Figure A7). The hydrogenation pathway (selectivity of ~38%) yields partially and fully hydrogenated ethers in consecutive steps. Cyclohexyl benzyl ether is the dominant primary product (over methyl cyclohexyl phenyl ether) suggesting that the phenyl ring is more facile to hydrogenate than the benzyl ring. This is because the sp^3 hybridized -CH$_2$- group induces looser bonding of the aromatic ring to the surface. Hydrogenolysis (selectivity of 59-63%) yields phenol

and toluene on the cleavage of the α-O-4 bond. The same bond is cleaved by hydrolysis (selectivity of ~2%) yielding phenol and benzyl alcohol. The primary products of hydrogenolysis and hydrolysis undergo hydrogenation of the aromatic ring and carbonyl groups without further C-O bond cleavage (as shown in Scheme 1 for phenol). Neither benzene nor cyclohexane were observed, indicating that the C_{sp}^2-O bond in BPE was not cleaved. This is attributed to the large difference in bond energies, i.e., 218 kJ·mol^{-1} for C_{sp}^3-O and 334 kJ·mol^{-1} for C_{sp}^2-O.
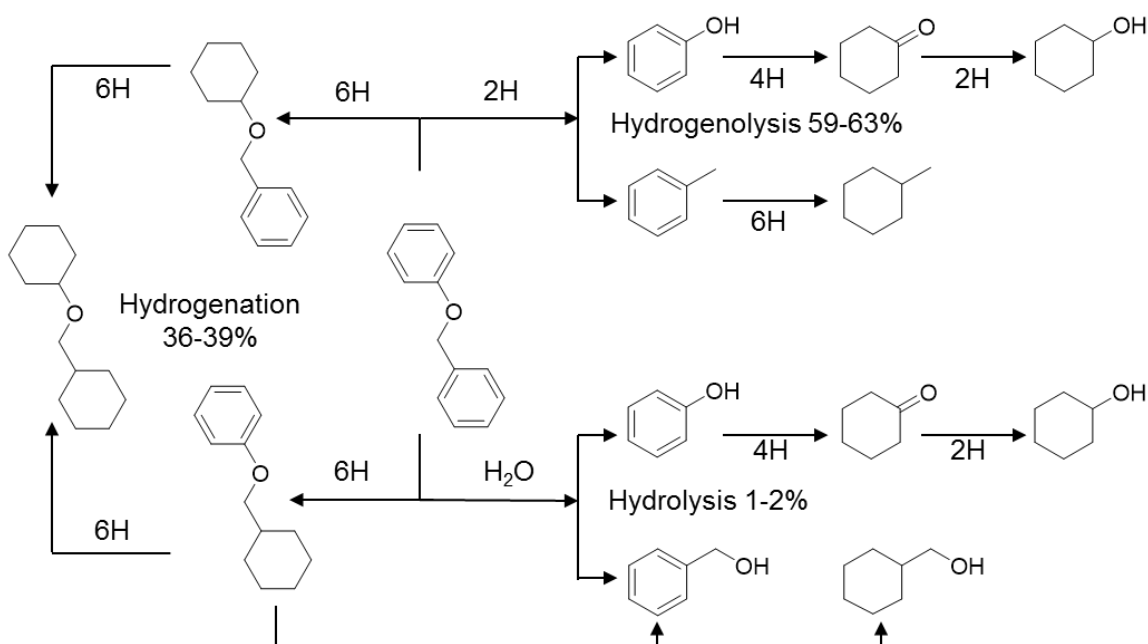
Scheme 3.3. Reaction network of the conversion of benzyl phenyl ether under catalytic thermal catalytic hydrogenation and electrocatalytic hydrogenation.

Let us analyze the particular initial conversion rates of the selected di-aryl ethers by ECH and TCH (Table 3.4). Comparisons between the rates of DPE and PTE conversion shows that the strong impact of the methyl groups on the adsorption of PTE is reflected in the rates of all pathways, which decreased by 20-50%. BPE was converted much faster than DPE and PTE, mainly via hydrogenolysis, which proceeded at 4.7·10^{-5} mol·s^{-1}·g$_{Rh}^{-1}$ in TCH (2.1·10^{-5} mol·s^{-1}·g$_{Rh}^{-1}$ in ECH). That is, from 4 to 8 times faster than the hydrogenolysis of DPE

$(6 \cdot 10^{-6} \, mol \cdot s^{-1} \cdot g_{Rh}^{-1}$ in TCH and $5 \cdot 10^{-6} \, mol \cdot s^{-1} \cdot g_{Rh}^{-1}$ in ECH) and from 5 to 19 times faster than the hydrogenolysis of PTE ($2.5 \cdot 10^{-6} \, mol \cdot s^{-1} \cdot g_{Rh}^{-1}$ in TCH and $4 \cdot 10^{-6} \, mol \cdot s^{-1} \cdot g_{Rh}^{-1}$ in ECH). In contrast, the hydrogenation rate of BPE was identical to that of DPE ($\sim 3.3 \cdot 10^{-5} \, mol \cdot s^{-1} \cdot g_{Rh}^{-1}$ in TCH and $\sim 2.5 \cdot 10^{-5} \, mol \cdot s^{-1} \cdot g_{Rh}^{-1}$ in ECH). Hence, the hydrogenation of the aromatic rings is not influenced by the presence of the methylene bridge group. The rates of BPE hydrolysis ($1 \cdot 10^{-6} \, mol \cdot s^{-1} \cdot g_{Rh}^{-1}$ in TCH and ECH) are lower than those of DPE ($7 \cdot 10^{-6} \, mol \cdot s^{-1} \cdot g_{Rh}^{-1}$ in TCH and $3 \cdot 10^{-6} \, mol \cdot s^{-1} \cdot g_{Rh}^{-1}$ in ECH) and even lower than those of PTE ($6 \cdot 10^{-6} \, mol \cdot s^{-1} \cdot g_{Rh}^{-1}$ in TCH and $2 \cdot 10^{-6} \, mol \cdot s^{-1} \cdot g_{Rh}^{-1}$ in ECH). This is attributed to the preference of a $PhCH_2\cdot$ fragment to combine with $H\cdot$ but not $OH\cdot$ [25]. We note in passing that hydrolysis did not occur in the absence of adsorbed hydrogen (via H_2 dissociation or H^+ reduction). Thus, the C-O cleavage for hydrolysis appears to be related to that in hydrogenolysis, whereas the difference relates to the probability of $H\cdot$ or $OH\cdot$ being added to the adsorbed hydrocarbon moiety [25].

Table 3.4. Reaction rate ($mol \cdot s^{-1} \cdot g_{Rh}^{-1}$) of di-aryl ethers *via* different pathways in electrocatalytic hydrogenation. The reactions were performed in a water-isopropanol-acetic acid mixture at room temperature and atmospheric pressure on Rh/C.

	Hydrogenation		Hydrolysis		Hydrogenolysis	
	ECH	TCH	ECH	TCH	ECH	TCH
DPE	$2.4 \cdot 10^{-5}$	$3.2 \cdot 10^{-5}$	$3 \cdot 10^{-6}$	$7 \cdot 10^{-6}$	$5 \cdot 10^{-6}$	$6 \cdot 10^{-6}$
PTE	$1.6 \cdot 10^{-5}$	$1.9 \cdot 10^{-5}$	$2 \cdot 10^{-6}$	$6 \cdot 10^{-6}$	$4 \cdot 10^{-6}$	$2.5 \cdot 10^{-6}$
BPE	$2.5 \cdot 10^{-5}$	$3.4 \cdot 10^{-5}$	$1 \cdot 10^{-6}$	$1 \cdot 10^{-6}$	$2.1 \cdot 10^{-5}$	$4.7 \cdot 10^{-5}$

3.3.4. Coupling electrocatalytic and catalytic conversion

We have established that the rates of ECH increase with increasingly negative potentials due to changes in the concentration of adsorbed hydrogen. At potentials less negative than -0.9 V, the hydrogen coverages are low (-0.7 V equals to only 1 bar H_2 pressure). Thus, we hypothesized that the Tafel step could be reverted even with small H_2 pressure increases in order to increase the concentration of adsorbed hydrogen. In order to test this hypothesis, ECH was performed at optimum conditions keeping the H_2 *ex* HER in the reaction media, while monitoring the associated pressure increase. Namely, combined ECH/TCH experiments of phenol and PTE (the most reactive compound and the least reactive compound, respectively, used in this study) at -0.7 and -0.9 V, respectively, while recycling the evolved H_2 into the reactor.
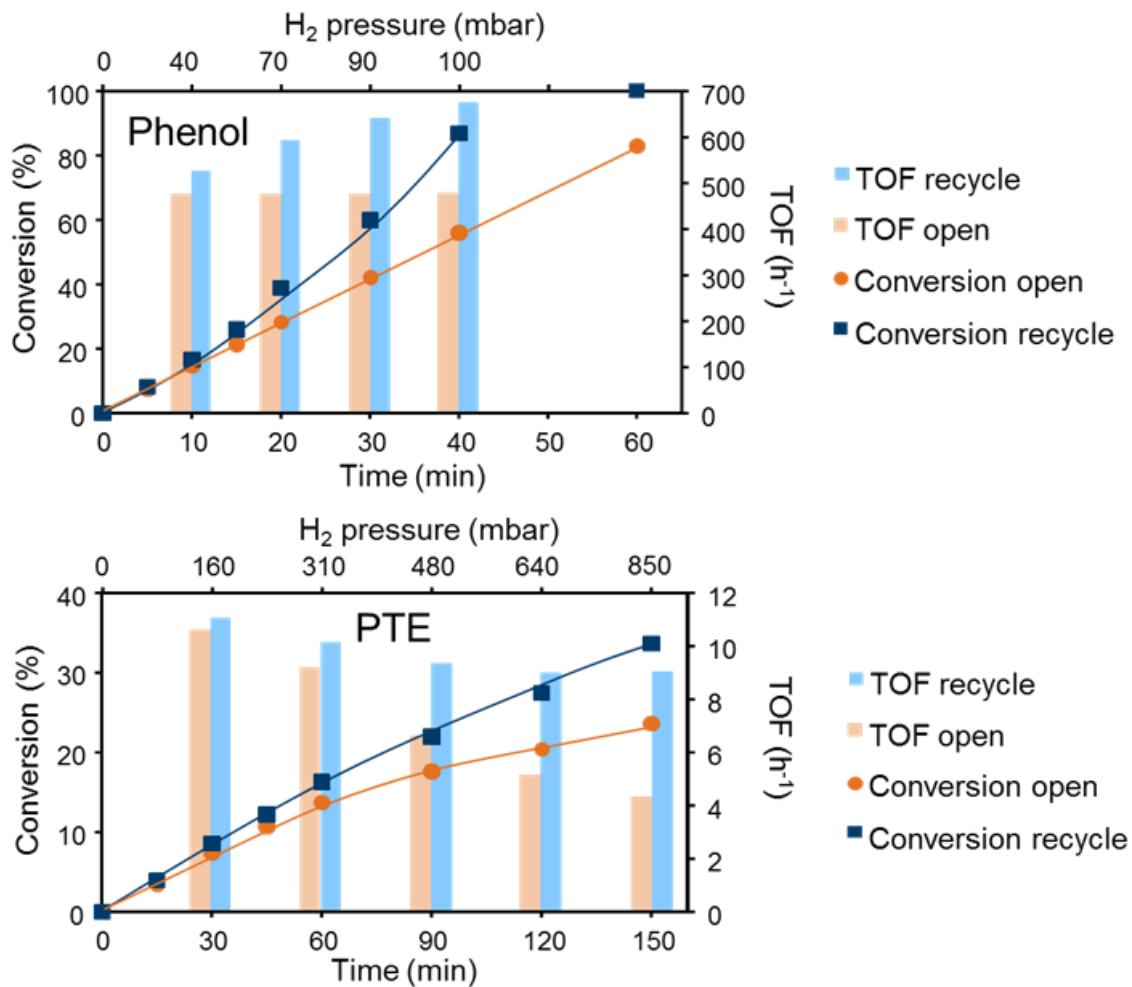
Figure 3.8. Comparison of electrocatalytic reduction of phenol and p-tolyl ether (PTE) (at -0.7 V and -0.9 V, respectively). Orange columns, lines and symbols represent results obtained at normal ECH conditions. Blue columns, lines and symbols represent results obtained when recycling the evolved H_2.

3.4. Conclusions

The rates of electrocatalytic hydrogenation (ECH) of functionalized aromatic molecules on carbon supported Rh are proportional to the negative potential of the electrode at ambient reaction conditions. Reaction rates of ECH rise with increasing cathodic potentials (above the potential needed for H_2 evolution) up to values that trigger the formation of compounds that adsorb strongly on the metal. ECH rates were higher than those of thermal catalytic hydrogenation (TCH). The concentration of adsorbed hydrogen can be sustained at values above that corresponding to 1 bar H_2 by employing higher cathodic potentials. This coverage, however, seems low and can be increased by keeping H_2 (ex-H_2 evolution reaction) in the reaction media favoring the inverse Tafel step to aid the oxygenate transformation instead of competing with it.

Electrocatalytic and thermal hydrogenation of phenolic compounds and diaryl ethers follow identical routes, i.e., hydrogenation, hydrogenolysis, and hydrolysis, with similar selectivity. Comparison with high temperature hydrodeoxygenation studies allows concluding that the presence of substituents in the aromatic rings reduces ECH and TCH rates due to repulsion with the metal, whereas the rate of C-O bond cleavage is inversely proportional to the corresponding bond energy. Hydrogenation, the dominant route (the only one for phenol and methylphenol), yields cyclic alcohols and cycloalkyl ethers as final products. Hydrogenolysis and hydrolysis (minor pathway) allow C-O bond cleavage of methoxy groups and ether bonds. This allows obtaining O-free hydrocarbons in a reaction path, which can reach significant selectivities.

3.5. Appendix

3.5.1. Calculations

Conversion, reaction rate, adsorbed hydrogen (Hads) consumption rate, turnover frequency (TOF), and Faradic efficiency (FE) were calculated according to the following equations.

$$\text{Conversion} = \frac{\text{Moles of phenol consumed}}{\text{Initial moles of phenol}} \times 100 \qquad [=] \%$$

$$\text{ECH Reaction rate} = \frac{\text{Moles of reactant consumed via ECH}}{\text{Time} \times \text{Mass of catalyst} \times \text{Metal loading}} \qquad [=] \text{mol/s·g(metal)}$$

$$\text{TH Reaction rate} = \frac{\text{Moles of reactant consumed via TH}}{\text{Time} \times \text{Mass of catalyst} \times \text{Metal loading}} \qquad [=] \text{mol/s·g(metal)}$$

$$\text{HER Reaction rate} = \frac{\text{Moles of hydrogen gas produced via HER}}{\text{Time} \times \text{Mass of catalyst} \times \text{Metal loading}} \qquad [=] \text{mol/s·g(metal)}$$

$$\text{Hads consumption rate of ECH} = \frac{\text{Moles Hads consumed via ECH}}{\text{Time} \times \text{Mass of catalyst} \times \text{Metal loading}} [=] \text{mol/s·g(metal)}$$

$$\text{Hads consumption rate of HER} = \frac{\text{Moles of Hads consumed via HER}}{\text{Time} \times \text{Mass of catalyst} \times \text{Metal loading}} [=] \text{mol/s·g(metal)}$$

$$\text{Hads consumption rate of TH} = \frac{\text{Moles of Hads consumed via TH}}{\text{Time} \times \text{Mass of catalyst} \times \text{Metal loading}} \ [=] \text{mol/s·g(metal)}$$

$$\text{TOF} = \frac{\text{Moles of phenol consumed}}{\text{Time} \times \text{Dispersion of metal} \times \text{Moles of metal in the catalyst}} \qquad [=] \text{h}^{-1}$$

$$\text{FE} = \frac{\text{Electrons consumed by hydrogenation of organic compounds}}{\text{Total electrons passed}} \times 100 \qquad [=] \ \%$$

Scheme of the cell for electrocatalytic hydrogenation

Cathode and anode chambers are separated by a proton exchange membrane (Nafion 117). Working electrode (ACF), and reference electrode (Ag/AgCl) are used in the cathodic compartment, with a Helium gas flow bubbling through the liquid volume. The stirring speed is achieved by a magnetic bar. In the anodic chamber, a platinum wire is used as counter electrode. Stirring is also applied in this side of the cell.
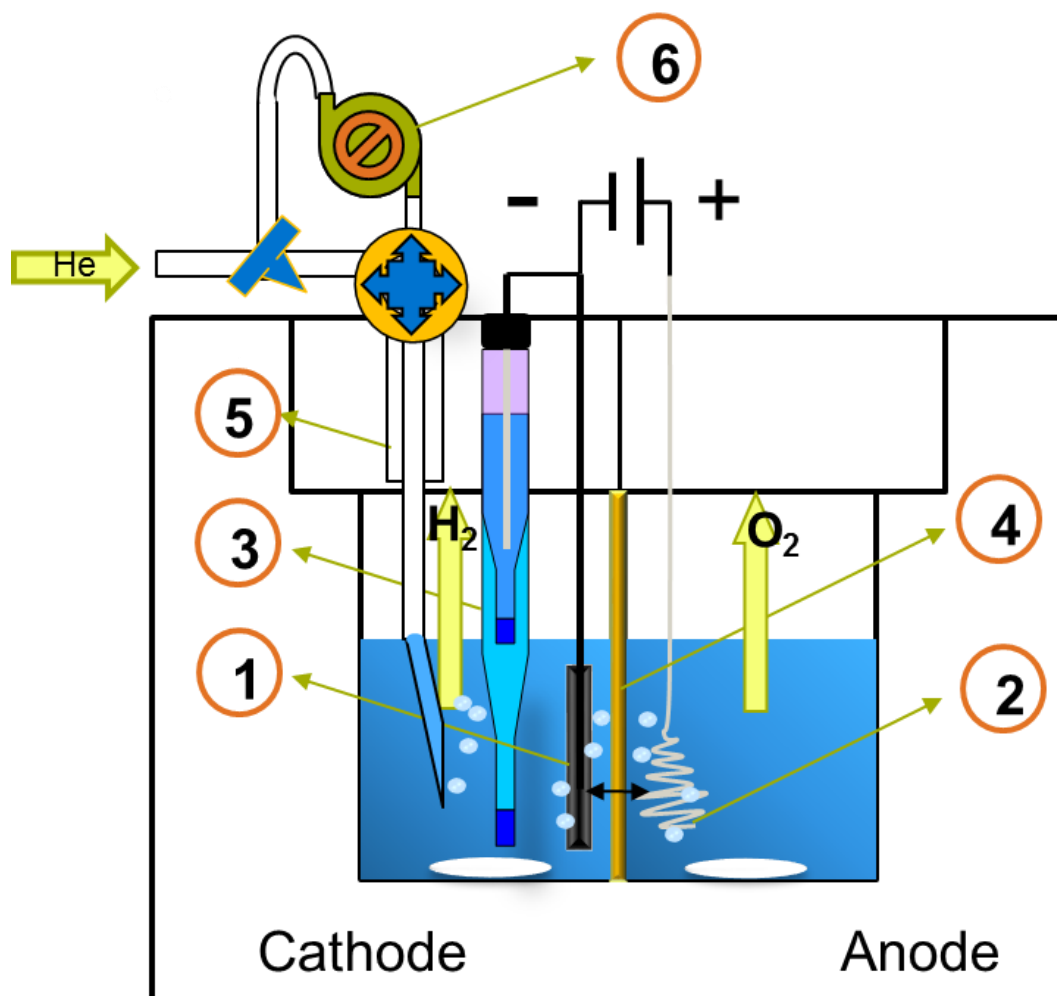
Figure A1. Schematic diagram of the ECH cell. Working electrode (ACF) (1); Counter electrode (Pt wire) (2); Reference electrode (Ag/AgCl) (3); Proton exchange membrane (Nafion 117) (4); Inert gas inlet (5); recycling pump connected in selected experiments (6).

3.5.2. Physicochemical properties of the catalyst

The Rh/C catalyst exhibited surface area of 301 $m^2 \cdot g^{-1}$ and pore volume of 0.34 $cm^3 \cdot g^{-1}$. The average particle size of the supported metal, as determined by H_2 chemisorption, was 3.4 nm, which was in good agreement with the size estimated from TEM images (3.9 nm). Activated carbon felt (ACF) was chosen as working electrode. The fibrous structure of ACF retained the powder catalyst by simple mechanical stirring before reaction. This allowed maximum contact between catalyst and electrode without losses of exposed surface area (expected when an ink is used). The microscopic morphology of ACF is shown in Figure A2, carbon fibers with diameters of around 10 µm are clearly observed, and Rh/C with particle sizes from 1 to 5 µm, are deposited into the network of ACF.
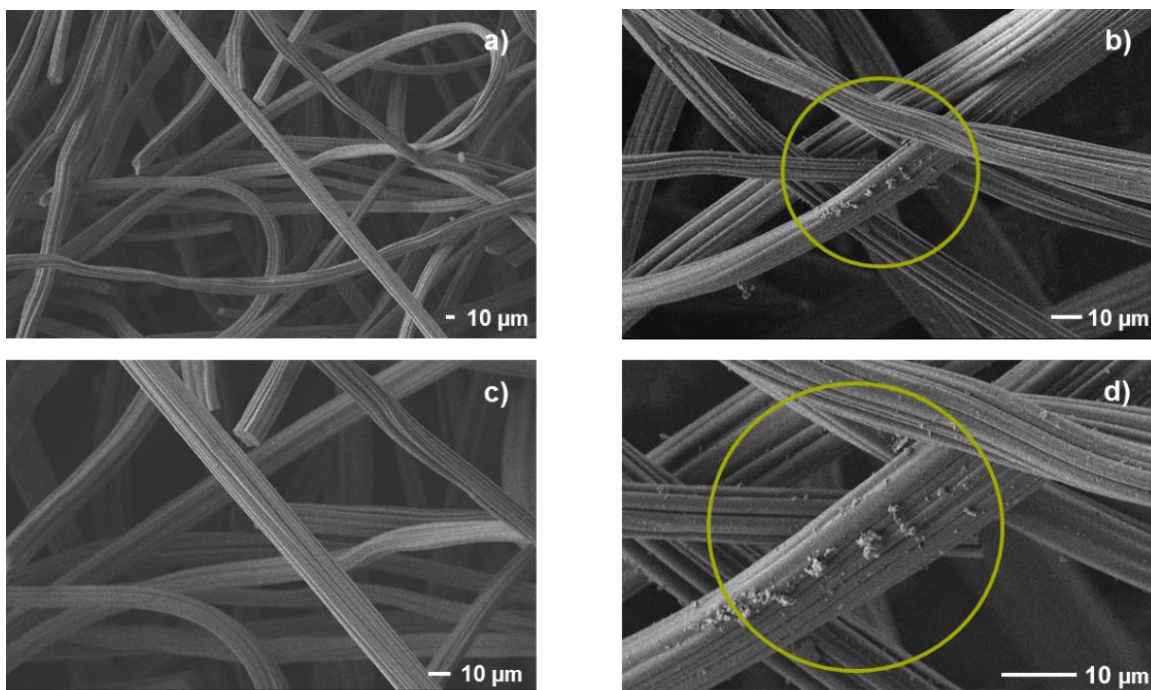
Figure A2. SEM images of bare activated carbon felt before (a) and (c) after incorporation (b) and (d) of Rh/C (highlighted by the circles).

3.5.3. Manipulating the electrocatalytic hydrogenation of phenol with potential

Potential in the absence of ohmic loss

The ohmic loss of the system was determined by impedance measurements (Nyquist plot) as 1.8 Ohm. The corrected potential, $E_{corrected}$ (HFR-free potentials), is related to the applied one by the equation:

$E_{corrected} = E_{applied} - i \cdot R$,

where $E_{applied}$ is the potential applied, i is the current, and R is the ohmic resistance. Table A2 shows the corrected potentials and the corresponding currents and applied potentials. The correlation between current and corrected potentials is shown in Figure A3.

Table A2. Corrected potential and current density calculations.

Potential$_{applied}$ (V)	-0.4	-0.5	-0.6	-0.7	-0.8	-0.9
Potential$_{corrected}$ (V)	-0.37	-0.41	-0.42	-0.44	-0.47	-0.5
Current (mA)	-18	-50	-100	-140	-175	-220
Current density (mA·cm^{-2})	-0.02	-0.06	-0.11	-0.16	-0.20	-0.25
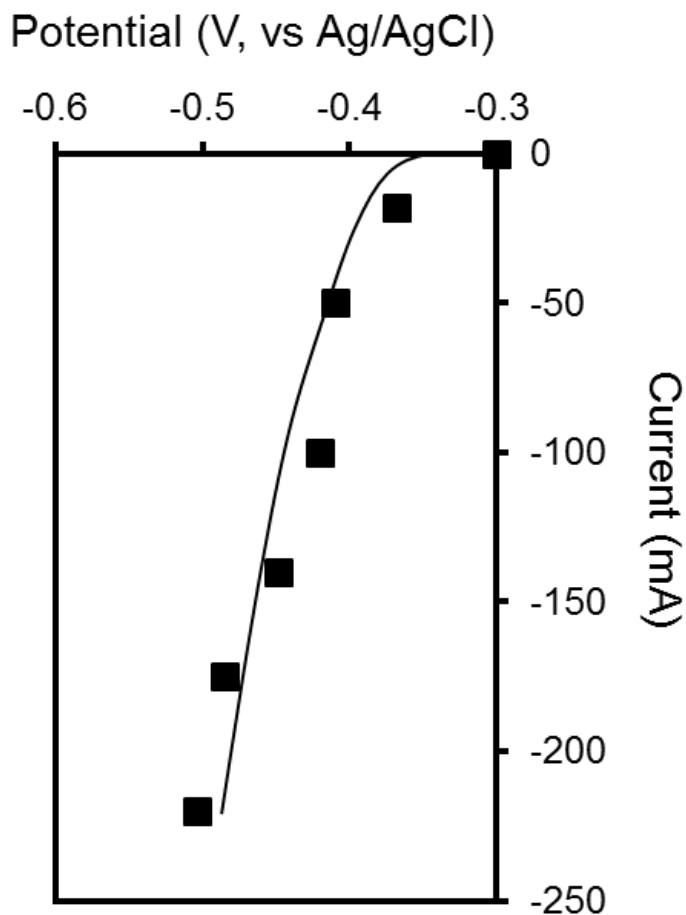
Figure A3. Polarization curve showing the dependence of current on corrected potential (E$_{iR-free}$).

Dependence of electrocatalytic phenol hydrogenation (ECH) and hydrogen evolution rates (HER) on potential.

Table A3. Adsorbed hydrogen (H$_{ads}$) consumption rate of electrocatalytic hydrogenation (ECH), hydrogen evolution reaction (HER) under different potentials, and thermal catalytic hydrogenation (TH).

Potential (V)	-0.4	-0.5	-0.6	-0.7	-0.8	-0.9	TCH

ECH ($\cdot 10^{-5}$ molH$_{ads}$·s^{-1}·g$_{Rh}^{-1}$)	3.7	30	70.5	101.6	123.3	150.5	-
HER ($\cdot 10^{-5}$ molH$_{ad}$·s^{-1}·g$_{Rh}^{-1}$)	14.9	21.8	33.2	43.5	58	77.5	-
TH ($\cdot 10^{-5}$ molH$_{ad}$·s^{-1}·g$_{Rh}^{-1}$)	-	-	-	-	-	-	100.9

[a] Potentials applied for ECH (V, vs Ag/AgCl).

3.5.4. Electrocatalytic hydrogenation and catalytic thermal hydrogenation of substituted phenolic compounds
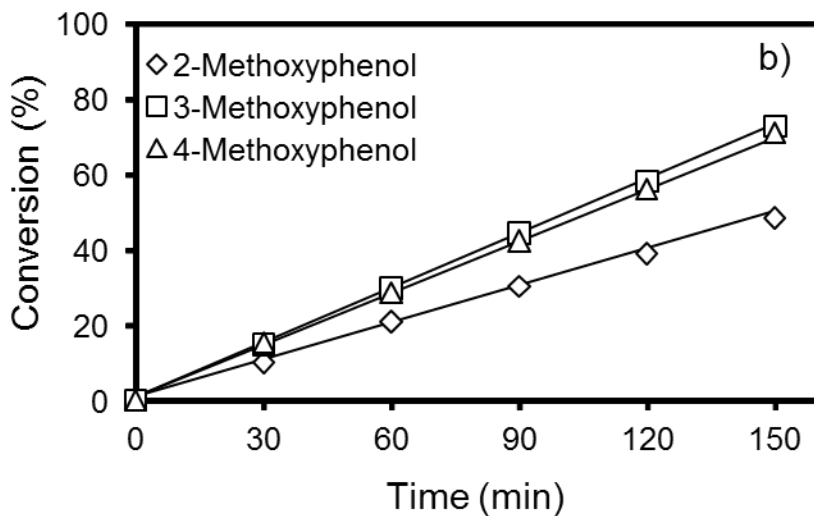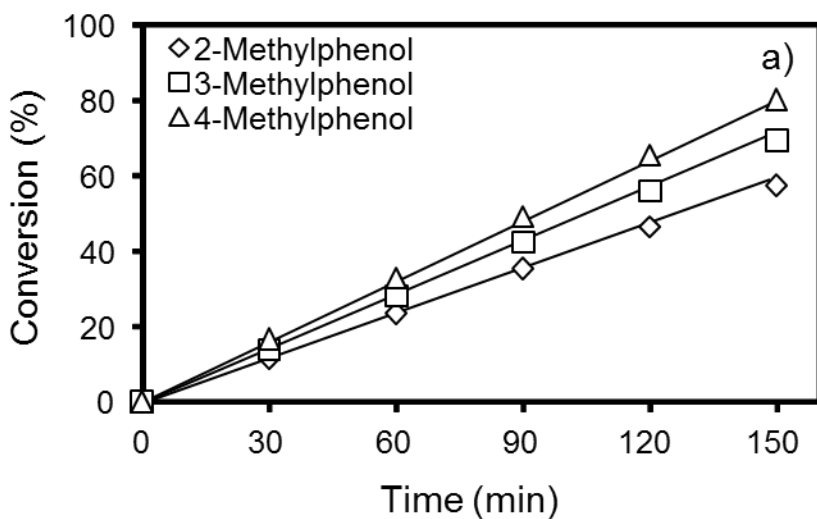
Figure A4. Conversion of methylphenol a) and methoxyphenol b), with substituents in different positions during electrocatalytic hydrogenation at -0.6 V in acetic acid buffer at room temperature and ambient pressure on Rh/C.
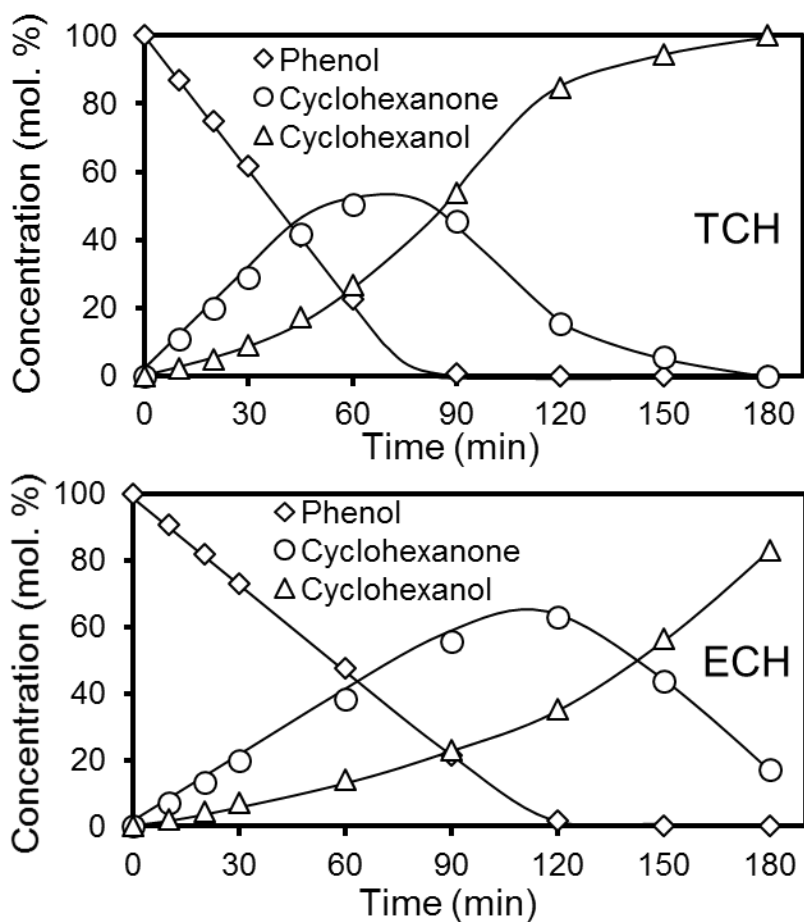
Figure A5. Concentration profiles observed during catalytic thermal catalytic hydrogenation (TCH), and electrocatalytic hydrogenation (ECH) of phenol. The reactions were performed in water at room temperature and atmospheric pressure on Rh/C.

Table A4. Current, reaction rates, TOF, hydrogen evolution rates (HER), rates of consumed adsorbed hydrogen (H_{ads}) and Faradaic efficiency observed during the conversion of 4-methylphenol, and 4-methoxyphenol isomers during ECH.

	2-Methylphenol	3-Methylphenol	4-Methylphenol	2-Methoxyphenol	3-Methoxyphenol	4-Methoxyphenol
Potential (V vs Ag/AgCl)	-0.6	-0.6	-0.6	-0.6	-0.6	-0.6
Current (mA)	-100	-102	-105	-98	-100	-95
Reaction rate ($\cdot 10^{-5} mol \cdot s^{-1} \cdot g_{Rh}^{-1}$)	6	7.1	8.1	5.4	7.8	7.5
TOF (h^{-1})	112	130	151	98	145	138
FE (%)	28	33	31	26	34	35
HER rate ($\cdot 10^{-5} mol \cdot s^{-1} \cdot g_{Rh}^{-1}$)	37	35	38	38	34	32
ECH ($\cdot 10^{-5} molH_{ads} \cdot s^{-1} \cdot g_{Rh}^{-1}$)	29	34.9	33.7	26.4	35.2	34.5
HER ($\cdot 10^{-5} molH_{ad} \cdot s^{-1} \cdot g_{Rh}^{-1}$)	74.6	70.8	75.1	75.2	68.4	64

Table A5. Adsorbed hydrogen (H_{ads}) consumption rate of electrocatalytic hydrogenation (ECH), hydrogen evolution reaction (HER), and thermal catalytic hydrogenation (TCH) of phenolic compounds and di-aryl ethers.

Reactant	Phenol		4-Methylphenol		4-Methoxyphenol		DPE		PTE		BPE	
	ECH	TCH	ECH	TCH	ECH	TCH	ECH	TCH	ECH	TCH	ECH	TCH
ECH ($\cdot 10^{-5}$ molH$_{ads}$ $\cdot$s^{-1}$\cdot$g$_{Rh}$$^{-1}$)	71	-	34	-	35	-	26	-	19	-	37	-
HER ($\cdot 10^{-5}$ molH$_{ads}$ $\cdot$s^{-1}$\cdot$g$_{Rh}$$^{-1}$)	33	-	73	-	64	-	78	-	85	-	66	-
TCH ($\cdot 10^{-5}$ molH$_{ads}$ $\cdot$s^{-1}$\cdot$g$_{Rh}$$^{-1}$)	-	101	-	50	-	54	-	41	-	26	-	71

3.5.5. Electrocatalytic hydrogenation and catalytic thermal hydrogenation of di-aryl ethers
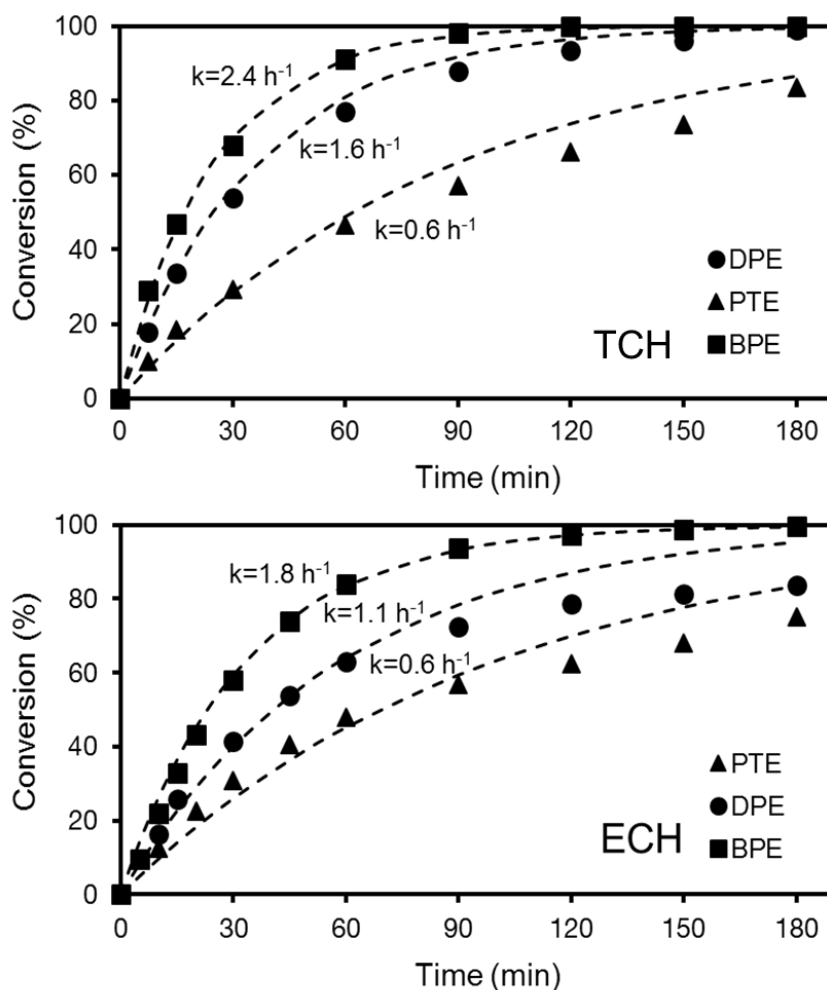
Figure A6. Comparison of the conversions of di-aryl ethers *via* electrocatalytic hydrogenation (ECH) and thermal catalytic hydrogenation (TCH). The reactions were performed in water-isopropanol acetic solution at room temperature and atmospheric pressure on Rh/C, in TH with 1 bar H2 inlet, and in ECH with -0.9 V potential. The Figure shows the values of first order rate constants fitting the experimental data. Deviations from the first order kinetics for DPE and PTE at high conversions are attributed to competitive adsorption of the products.
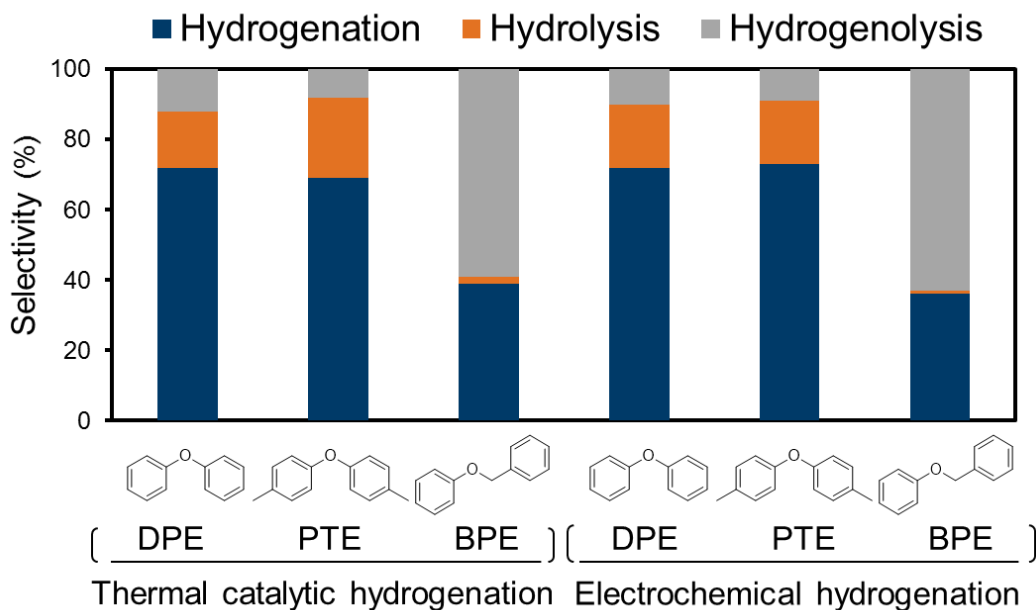
Figure A7. Selectivity towards the pathways observed in the conversion of di-aryl ethers under thermal catalytic hydrogenation and electrochemical hydrogenation for diphenyl ether (DPE), p-tolyl ether (PTE) and benzyl phenyl ether (BPE).
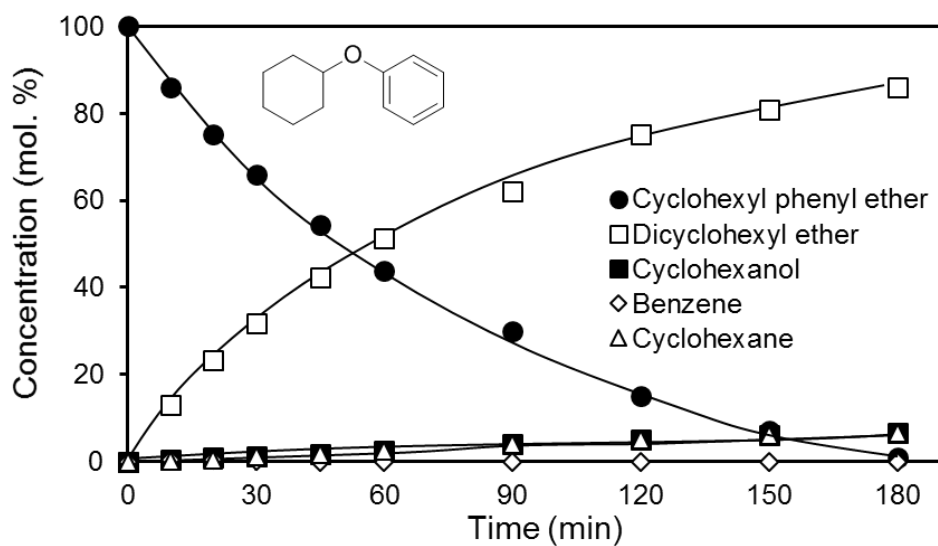
Figure A8. Concentration profiles observed during catalytic hydrogenation of cyclohexyl phenyl ether. The reaction was performed in a water-ethanol-acetic acid mixture at room temperature and atmospheric pressure of H_2 on Rh/C. Selectivties were calculated, giving 93% via hydrogenation and 7% via hydrogenolysis.

3.5.6. Coupling electrocatalytic and catalytic conversion
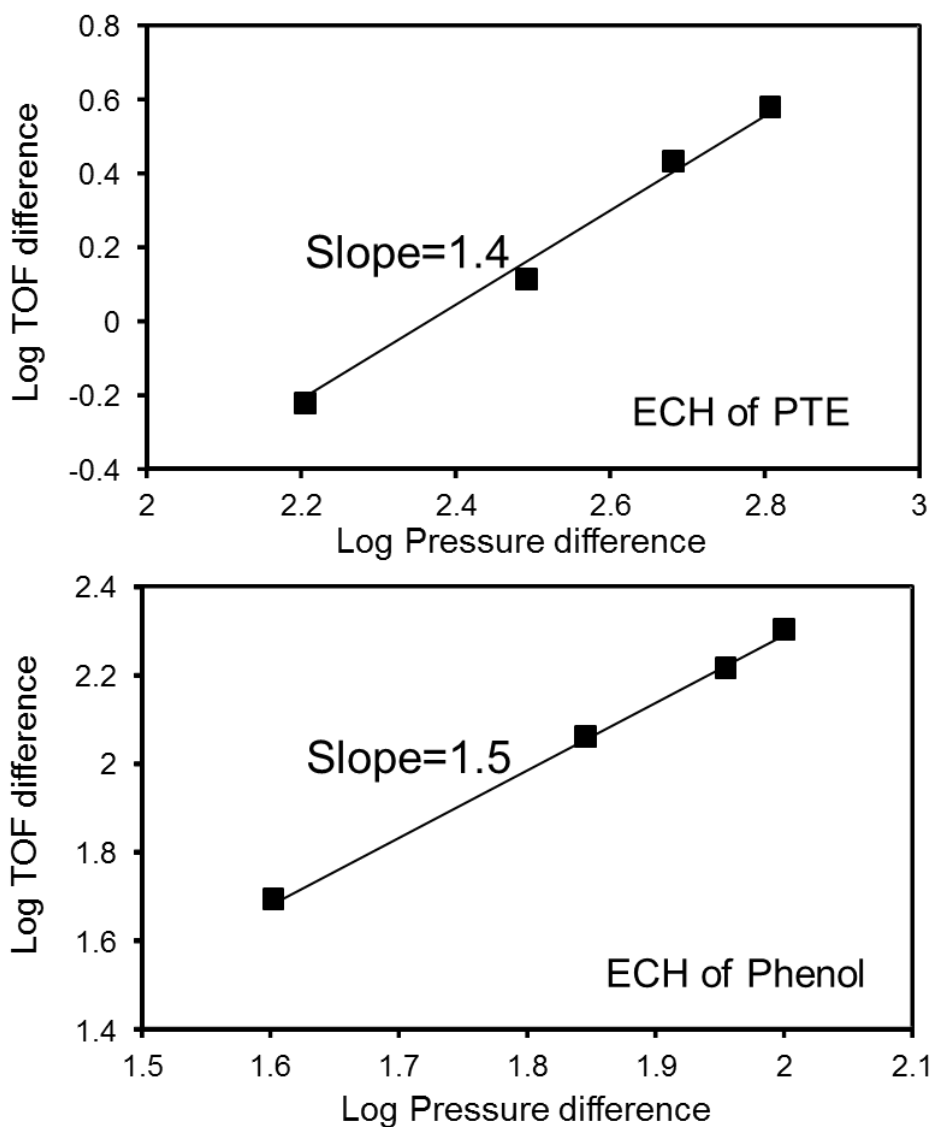
Figure A9. Logarithmic plot of TOF increases (differences of TOFs in "open" and "recycle" operations) vs. pressure of H_2 accumulated in "recycle" operation.

3.5.7. On the inhibiting effect of the solvent

We observed that the ECH of di-aryl ethers at -1 V (vs Ag/AgCl) in water-ethanol mixtures was much slower than TH. Table A6 shows the results of ECH obtained in such conditions. Note that the ECH rates are lower than those obtained at optimized conditions (-0.9 V using water-isopropanol mixtures, Table 3 in the main text) by 50-70%. In some cases, even signs of deactivation were noted as shown in Figure A10 for the ECH of diphenyl ether (DPE), and *p*-tolyl ether (PTE). Note that more negative potentials are required in the ECH of di-aryl ethers (-1 V or -0.9 V) than in the ECH of phenolic compounds (-0.6) in order to obtain measurable conversions. This is because of the need of using water-alcohols mixtures in order to dissolve the ethers. Whereas the mixtures decrease the concentration of the electrolyte, the alcohols hinder the accessibility of reactants to the metal as described in the main text.

Table A6. Current, reaction rate, TOF, Faradaic efficiency, and rates of consumed adsorbed hydrogen (H_{ads}) of the conversion of di-aryl ethers via electrocatalytic hydrogenation. The reactions were performed in a water-ethanol-acetic acid mixture at room temperature and atmospheric pressure on Rh/C.

	Diphenyl ether	*p*-Tolyl ether	Benzyl phenyl ether
Potential (V vs Ag/AgCl)	-1	-1	-1
Current (mA)	-110	-90	-80
Reaction rate ($\cdot 10^{-5}$ mol$\cdot$(s$\cdot$g)$^{-1}$)	1.6	0.7	2.6
Initial TOF (h^{-1})	30	14	49
FE (%)	25	9	30
ECH ($\cdot 10^{-5}$ molH$_{ads}\cdot$s$^{-1}\cdot$g$_{Rh}^{-1}$)	29	8	25
HER ($\cdot 10^{-5}$ molH$_{ads}\cdot$s$^{-1}\cdot$g$_{Rh}^{-1}$)	86	85	58

To understand the low conversions and the phenomena of deactivation during the conversion of di-aryl ethers, we hypothesized that at -1 V side reactions occur, which produce strongly adsorbing species. In order to test the hypothesis, the ECH of PTE was performed until the catalyst was deactivated. Then the reaction was stopped and the reactant solution was replaced and/or the electrode was washed with water prior to further application of potential. The activity was recovered for certain time although rapidly set in again (Figure A11). This observation suggested that a compound was formed which hindered the adsorption of the reactant. In an additional experiment, the ECH of phenol was conducted in an ethanol-water mixture at -1 V. Surprisingly, at such conditions, phenol was not converted while H$_2$ still evolved (the observed current was 95 mA). This indicated that the species affecting ECH were produced by the combination of ethanol and acetic acid at very negative potentials. During all the described experiments we identified the increase in the concentration of ethyl acetate. In further experiments, the ECH (or TCH) of phenol was carried out at optimum conditions (-0.7 V) and a volume of ethyl acetate was injected into the reactor. As a consequence, the hydrogenation of p-tolyl ether stopped (Figure A12). Thus, we conclude that the activity loss is due to the formation of ethyl acetate *via* esterification of ethanol and acetic acid [13]. Activity losses, attributed to the presence of the electrolyte [26], are more severe in

presence of reduction products, because these adsorb competitively on active sites [27].
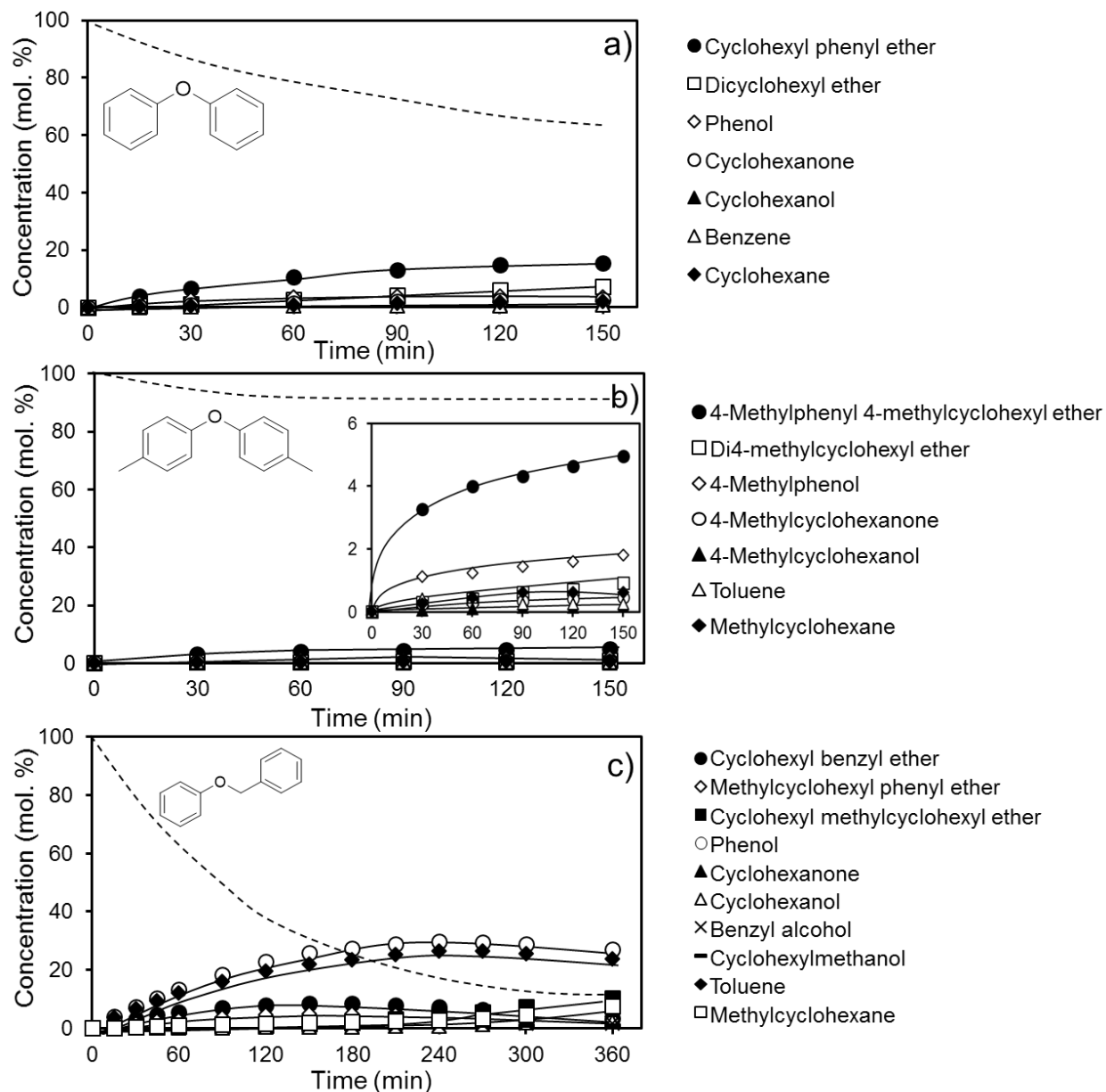
Figure A10. Concentration profiles observed during electrocatalytic hydrogenation of diphenyl ether (a), *p*-tolyl ether (b), and benzyl phenyl ether (c). The reactions were performed in a water-ethanol-acetic acid mixture at -1 V, room temperature and atmospheric pressure on Rh/C.

Once identified the reason for deactivation, we tested alternative reaction conditions. Replacing acetic acid as electrolyte is not attractive because ECH rates are lower in the presence of, e.g., sulfuric acid, and phosphoric acid [13]. Instead, we tested alternative solvents for the conversions of di-aryl ethers. Exploratory experiments with mixtures of the electrolyte solution and 1,2-dimethoxyethane, a solvent that is used in electrochemical studies of aromatic compounds owning to its good solubility and high electrochemical stability [28] were unsuccessful (phenol was not converted). In contrast, when the ECH of di-aryl ethers was performed in mixtures of water and isopropanol, much higher conversion rates and Faradaic efficiencies were observed than in mixtures of water and ethanol. Note that, whereas the rate of reactant conversion was affected by the solvent, the evolution profiles of the products indicate that the selectivity and reaction network remain invariant.
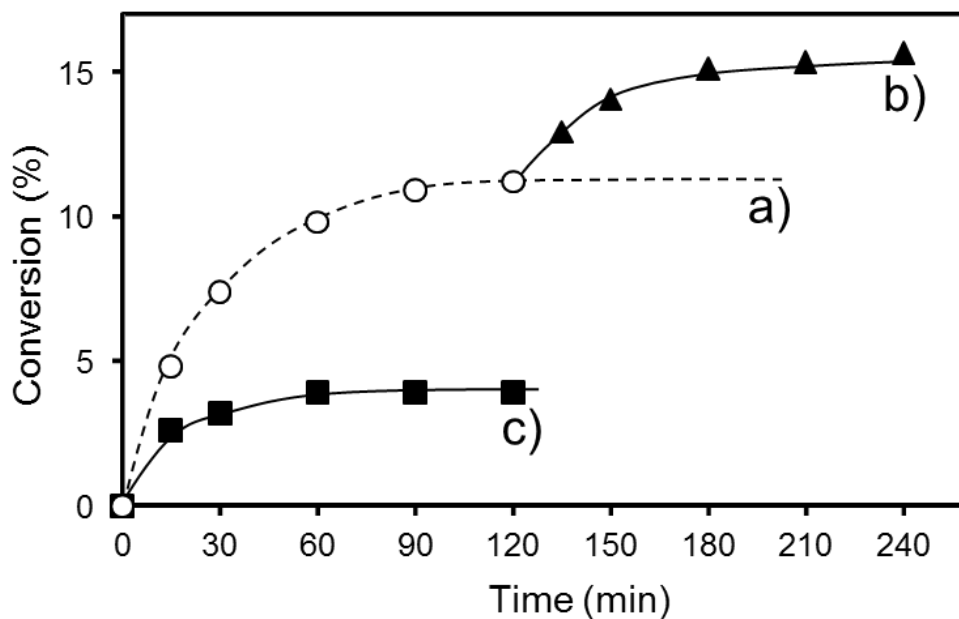
Figure A11. PTE conversions via ECH under -1 V a) until deactivated, b) electrode was washed with pure water and put back for further ECH, c) electrode was washed again, the reactant and electrolyte were refreshed.
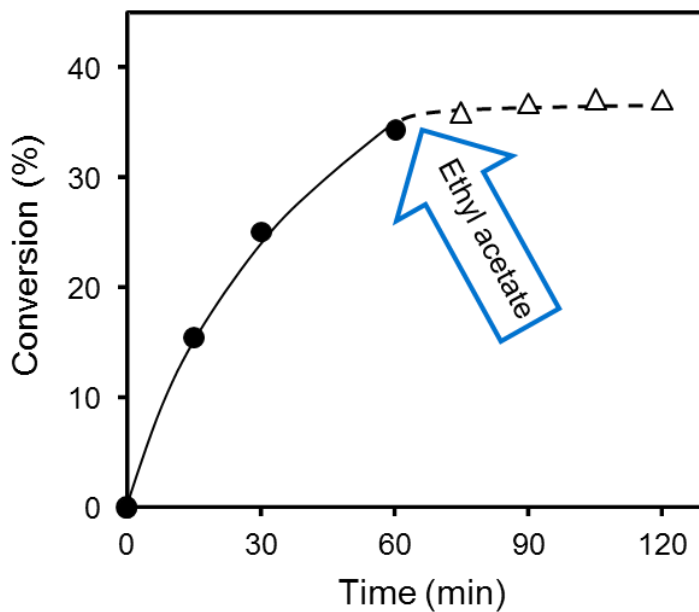
Figure A12. Conversion of p-tolyl ether via catalytic thermal hydrogenation in the mixture of acetic acid and ethanol. After 60 min, 2 mL ethyl acetate was added to the reaction.

3.6. References

[1] M. Chatterjee, T. Ishizaka, A. Suzuki, H. Kawanimi, Chem. Commun. 49 (2013) 4567-4569.

[2] S. Czernik, A.V. Bridgwater, Energy Fuels. 18 (2004) 590-598.

[3] C. Zhao, Y. Kou, A.A. Lemonidou, X. Li, J.A. Lercher, Angew. Chem. Int. Ed. 48 (2009) 4047-4050.

[4] M. Chatterjee, A. Chatterjee, T. Ishizaka, H. Kawanami, Catal. Sci. Technol. 5 (2015) 1532-1539.

[5] A. J. Ragauskas, C. K. Williams, B. H. Davison, G. Britovsek, J. Cairney, C. A. Eckert, W. J. Frederick, J. P. Hallett, D. J. Leak, C. L. Liotta, J. R. Mielenz, R. Murphy, R. Templer, T. Tschaplinski, Science 311 (2006) 484-489.

[6] S. J. Davis, K. Caldeira, H. D. Matthews, Science 329 (2010) 1330-1333.

[7] A. Corma, S. Iborra, A. Velty, Chem. Rev. 107 (2007) 2411-2502.

[8] X. Wang, R. Rinaldi, Energy Environ. Sci. 5 (2012) 8244-8260.

[9] J. Mortensen, J. Heinze, Angew. Chem. Int. Ed. Engl. 23 (1984) 84-85.

[10] M. Bourrez, R. Steinmetz, S. Ott, F. Gloaguen, L. Hammarström, Nat. Chem. 7 (2015) 140-145.

[11] D. Weinberg, C. Gagliardi, J. Hull, C. Murphy, C. Kent, B. Westlake, A. Paul, D. Ess, D. McCafferty, T. Meyer, Chem. Rev. 112 (2012) 4016-4093

[12] M. Hang, V. Huynh, T. Meyer, Chem. Rev. 107 (2007) 5004-5064.

[13] Y. Song, O. Gutiérrez, J. Herranz, J. A. Lercher, Appl. Catal. B. 182 (2016) 236-246.

[14] C. Cirtiu, H. Hassani, N. Bouchard, P. A. Rowntree, H. Ménard, Langmuir. 22 (2006) 6414-6421.

[15] C. M. Cirtiu, A. Brisach-Wittmeyer, H. Ménard, Catal. Commun. 8 (2007) 751-754.

[16] J.J. Roylance, K.-S. Choi, Green Chem. DOI: 10.1039/c6gc00533k.

[17] S. J. Jenkins, Proc. R. Soc. A. 465 (2009) 2949-2976.

[18] B. Güvenatam, O. Kurşun, E. H. Heeres, E. A. Pidko, E. J. Hensen, Catal. Today. 233 (2014) 83-91.

[19] D. J. Rensel, S. Rouvimov, M. E. Gin, J. C. Hicks, J. Catal. 305 (2013) 256-263.

[20] C. Lam, C. Lowe, Z. Li, K. Longe, J. Rayburn, M. Caldwell, C. Houdek, J. Maguire, C. Saffron, D. Miller, H. Jackson, Green. Chem. 17 (2015) 601-609.

[21] X. Wang, R. Rinaldi, ChemSusChem. 5 (2012) 1455-1466.

[22] W. Wu, J. Huang, J. Org. Chem. 79 (2014) 10189-10195.

[23] J. He, C. Zhao, D. Mei, J.A. Lercher, J Catal. 309 (2014) 280-290.

[24] J. He, C. Zhao, J.A. Lercher, J Catal. 309 (2014) 362-375.

[25] J. He, C. Zhao, J. Lercher, J. Am. Chem. Soc.134 (2012) 20768-20775.

[26] A. Darlington, W. Guenther, J. Chem. Eng. Data, 12 (1967) 605–607.

[27] M. El-Deab, F. Kitamura, T. Ohsaka, J. Electrochem. Soc, 160 (2013), F651-F658.

[28] Z. Song, H. Zhan, Y. Zhou, Chem. Commun, (2009) 448-450.

3.7. Associated Content

<u>Clearance by the Publisher</u>

Elsevier gave approval to non-commercially reproduce the accepted article both in print and online.

Chapter 4

Hydrogenation of benzaldehyde via electrocatalysis and thermal catalysis on carbon-supported metal catalysts

The hydrogenation of benzaldehyde to benzyl alcohol was performed on C-supported Pt, Rh, Pd, and Ni in aqueous phase. The reduction equivalents were provided either by H_2 (thermal catalytic hydrogenation, TCH) or electric potential (electrocatalytic hydrogenation, ECH). In TCH, the intrinsic activity of the metals at room temperature and 1 bar H_2 increases as Rh/C < Pt/C < Pd/C, whereas Ni/C is inactive at these conditions. The reaction follows a Langmuir-Hinshelwood mechanism with the second hydrogen addition to the adsorbed hydrocarbon being the rate determining step. All tested metals were active in ECH of benzaldehyde although it competes with the hydrogen evolution reaction (HER). The minimum cathodic potentials to obtain appreciable ECH rates are identical to the onset potentials of HER. The selectivity to ECH and TCH is determined by the relative rates of H reacting to H_2 and H addition to the hydrocarbon. Accordingly, the selectivity of the metals towards ECH increases in the order Ni/C < Pt/C < Rh/C < Pd/C, the latter having exceptionally high ECH selectivity.

4.1. Introduction

Producing bio-fuels from renewable lignocellulosic biomass has a great potential to substantially reducing the anthropogenic carbon footprint. Hydrogenation of biomass-derived bio-oils is an important step towards their upgrading to fuels. In this context, electrocatalytic hydrogenation (ECH) is an attractive alternative for low-temperature bio-oil treatment as adsorbed hydrogen, or reduction equivalents for hydrocarbon conversion, are produced in-situ on the electrode *via* e.g., proton reduction to adsorbed hydrogen or coupled electron and proton addition. With this approach, the power supply for electrocatalysis could be obtained from renewable electric energy such as photovoltaics, wind power and tidal energy [1-6]. However, the search for suitable catalysts at the cathode demands the understanding of metal functionalities and reaction mechanisms in condensed phases and in the presence of electric potentials. A special issue to be understood in ECH is the mutual influence of pathways for hydrocarbon hydrogenation and for the H_2-evolution reaction (HER).

Fundamental studies of metal electrocatalysts require model oxygenated compounds as reactants. Noble metals such as Pt, Pd, and Rh are reported active for the reduction of carbonyl groups to alcohols [7], hydrogenation of phenolic rings, hydrogenation and C-C bond cleavage of diaryl ethers [8, 9]. For the latter two examples, Pd showed much lower activity than Pt and Rh. Besides, high surface Pd cathodes have been shown of interest for the hydrogenation of C=C bond in the steroid field as well [10]. Faradaic efficiency on noble metals is usually reported below 80% and is usually controlled by reaction parameters instead of the nature of the metal. Metals with high overpotentials for HER (i.e., base metals and post-transition metals) have been also tested for reduction of carbonyl groups showing dissimilar activities and faradaic efficiencies, which indicate stronger dependence on the nature of the metal. Pb cathodes, for instance, are efficient for the reduction of levulinic acid, whereas Cu is inactive [11]. Ni and Ni-containing alloys have been active for ECH of conjugated substrates sucn as benzene, acetophenone and styrene, while not active for ECH of non-conjugated olefins such as cyclohexene and geraniol. [12, 13], and Raney Ni catalyst have been reported as an active

material for ECH of phenolic and aromatic compounds, as well as of ß-O-4 lignin models, including hydrogenolysis of phenolic ß-arylethyl-aryl ethers [14, 15].

Aromatic aldehydes are common in bio-oils (0-18 % in carbon yield) [16, 17] and are prone to polymerization, which makes their conversion at high temperature challenging [18]. Thus, benzaldehydes are an ideal group of compounds to target by low temperature hydrogenation in order to stabilize lignin-derived bio-oil. TCHs of benzaldehyde on Pt metals were performed by Vannice et al., showing that benzaldehyde was hydrogenated to benzyl alcohol following the Langmuir-Hinshelwood model invoking the addition of the second H atom to benzaldehyde as the rate determining step [19]. A zero reaction order for TCH of benzaldehyde on Pd/C was also confirmed by Pinna et al. [20]. ECH of benzaldehyde on Pd/C was much less reported, one showed that ECH involved two parallel steps through which alcohol and hydrocarbon are generated from the reactant adsorbed on different active sites, and the kinetics was described by means of the Langmuir-Hinshelwood mechanism [21].

Thus, in this study we performed the hydrogenation of benzaldehyde as model compound on Pt/C, Rh/C, Pd/C and Ni/C under ECH and TCH conditions. The former three metals are known noble active metals for hydrogenation and hold the best promise for low temperature applications. In contrast, Ni is an abundant base metal with high barriers for hydrogenation [22-24]. Thus, optimizing its activity at low temperature is desirable for technical realization of ECH technology. Based on previous results, we hypothesized that at relatively low cathodic potentials (below the potentials required for direct reduction of the hydrocarbons) ECH and TCH follow the same reaction mechanism. Furthermore, we hypothesize that the tradeoffs between HER and ECH depend on the overpotential for H_2 evolution of the metal. To verify these hypotheses, we performed the hydrogenation of benzaldehyde at varying temperatures, cathodic potentials (ECH) and H_2 partial pressure (TCH). Kinetic parameters such as intrinsic rates, energies of the activation, and reaction orders allowed to propose reaction mechanisms on the different metals.

4.2. Experimental section

4.2.1. Chemicals and catalytic materials

Chemicals were obtained from Sigma Aldrich and used as received: benzaldehyde (Sigma-Aldrich, ≥99.0%), acetate buffer solution (Sigma-Aldrich, pH 4.6), ethyl acetate (Sigma-Aldrich, ≥99.9%, HPLC), Na_2SO_4 (Sigma-Aldrich, ≥99.9%), NaCl (Sigma-Aldrich, ≥99.9%), and KCl (Sigma-Aldrich, ≥99.9%). $Ni(NO_3)_2 \cdot 6H_2O$ (Sigma-Aldrich, 99.999%), activated carbon powder (Sigma-Aldrich) awere used as received to prepare the Ni/C catalyst. High purity water, obtained with a Milli-Q water purification system with a resistivity of 18.2 MΩ·cm, was used for all experimental procedures. H_2 (Air Liquide, >99.99%) is used for thermal hydrogenation, He (Air Liquide, >99.99%) is used as protection gas to remove oxygen from the electrolyte before ECH and Ar (Air Liquide, >99.99%) is used to change the partial pressure for determination of reaction partial orders in TCH.

4.2.2. Preparation and Ni/C catalysts

Ni/C, with 5 wt. % metal, was prepared by impregnating activated carbon powder with an aqueous solution of $Ni(NO_3)_2$. After drying at 383 K, the impregnated material was treated in in flowing H_2 at 723 K for 5 h, the heating rate was maintained at 2 K·min^{-1}.

4.2.3. Catalyst characterization

The specific surface area and pore diameter of the catalysts were derived (according to BET and BJH models) from N_2 physisorption isotherms, which were measured at 77 K on a PMI automated BET sorptometer. The samples were outgassed before measurements at 523 K for 2 h.

The dispersions of the metals were determined by H_2 chemisorption. Prior to the measurement, the materials were treated in vacuum at 588 K for 1h and then cooled to 313 K. A first set of adsorption isotherms were measured from 1 to 40 kPa. Afterwards, the samples were outgassed at 313 K for 1h and a second set of isotherms were measured, which corresponded to physisorbed H_2. The concentrations of hydrogen chemisorbed on the metal were determined by extrapolating the difference isotherms to zero hydrogen pressure. The dispersions of the supported metals were estimated from the concentration of chemisorbed hydrogen assuming a stoichiometry of 1:1 metal to hydrogen atoms.

The dispersions of the metals were also explored by transmission electron microscopy (TEM). Samples of the catalysts were ground, and ultrasonically dispersed in ethanol. Drops of the suspensions were applied on a copper-carbon grid and the measurements were carried out in a JEOL JEM-2011 electron microscope with an accelerating voltage of 120 keV. Statistical treatment of the metal particle size was done by counting at least 300 particles detected in several places of the grid. The morphology of the working electrode (activated carbon felt) before and after incorporating the catalysts was investigated by a scanning electron microscope (JSM-7500F from JEOL). The X-ray diffraction measurements (XRD) were carried out with an Analytical X'Pert Pro diffractometer, using Cu K_α radiation (λ = 1.54056 Å), operating at 45 kV and 40 mA. All the measurements were carried out in a 2Θ range of 25-85º.

4.2.4. Eletrocatalytic hydrogenation

Electrocatalytic hydrogenation (ECH) experiments were carried out in a two-compartment galvanostatic cell described in Ref. [10]. Cathodic and anodic

compartments were separated by a Nafion 117 proton exchange membrane (Ion Power, Inc.), which was treated in a H_2O_2 solution (3 vol.%) and in sulfuric acid (2 M) before reaction. A piece of carbon felt (Alfa Aesar >99.0%, 3.2 mm thickness) connected to a graphite rod (Sigma Aldrich, 99.99%) was used as working electrode in the cathode compartment. A platinum mesh (Alfa Aesar, 99.9 %) was used as counter electrode in the anodic compartment. The reference electrode was a home-made Ag/AgCl electrode with a double junction protection. For ECH of phenol and benzaldehyde, the cathode compartment was filled with 60 mL acetate buffer at pH 5. 10 mg of the Rh/C, Pt/C, Pd/C or Ni/C catalyst were added into the cathode compartment. All reactions were performed at atmospheric pressure at varying potentials. Prior to ECH, the stirring at 500 rpm allowed complete incorporation of the powder into the carbon felt. Polarization of the catalyst was performed under a constant current of -40 mA for 30 min. Benzaldehyde was typically added into the cathode compartment to obtain a final concentration of 20 mmol/L. This concentration was varied $\pm$ 25% to determine reaction orders in benzaldehyde. ECH experiments were performed at fixed potential while a flow of He was kept through the reactant solution. Temperature was controlled with a cooling/heating circulator (Julabo F25-ED). During all procedures, the anode compartment contained mixtures of acetate buffer (pH 5) as the electrolyte. All electrochemical procedures were performed with an electrochemical workstation (VSP-300, Bio Logic). Prior to the reactions, the electrodes were alternatively immersed in H_2SO_4 (5 M) and KOH (5 M) for 15 min. After each immersion, the materials were thoroughly cleaned (Pt electrodes were further ultrasonically treated) in ultrapure water for 15 min. Ohmic loss was measured by using IR compensation (PEIS) high frequency impedance method from Bio-Logic potentiostat, scanning from 100 mHz to 800 kHz.

4.2.5. Thermal catalytic hydrogenation

Thermal catalytic hydrogenation (TCH) was carried out in a glass batch reactor with 10 mg samples of Pt/C, Rh/C, Pd/C and Ni/C, stirring at 500 rpm. Typical measurements were performed at atmospheric pressure with H_2 (10 mL/min)

flowing through the reactant solution at 296 K. The preparation of the different reactant solutions and the concentrations of benzaldehyde were the same as those described for ECH. Partial reaction orders in H_2 were performed by changing the partial pressure of H_2 (0.8 atm, 0.9 atm and 1 atm) using N_2 as diluting gas. Gas flows were controlled by mass-flow controllers (El-Flow, Bronkhorst) and temperature was controlled with the cooling/heating circulator Julabo F25-ED.

4.2.6. Product analysis

The course of the ECH and TCH experiments was followed by periodically withdrawing aliquots of 1 mL from the cathode compartment. The products were extracted with 3 mL of ethyl acetate. The organic phase was separated from the aqueous phase by decantation and dried on Na_2SO_4. A sample of the dry organic phase was mixed with a solution containing phenol as standard. Quantitative analyses of the samples were performed by gas chromatography coupled with mass spectrometry (Shimadzu GCMS-QP2010), equipped with a plot Q capillary column (30m x 250 μm) and a thermal conductivity detector (TCD).

4.3. Results and Discussion

4.3.1. Catalysts characterization

The catalysts used in this work (metal loadings of 5 wt. %) were C-supported Pt, Rh, Pd, and Ni with dispersions of 26 %, 20 %, 30 %, and 0.5 % respectively, which corresponds to average particle sizes of 3.8 nm for Pt, 4.2 nm for Rh, 3.3 nm for Pd and 200 nm for Ni. Details of the physicochemical properties of the catalysts are described in the supporting in formation (Tables A1-A2).

4.3.2. Thermal catalytic hydrogenation of benzaldehyde

Benzaldehyde was quantitatively converted via 2H-hydrogen addition to benzyl alcohol on Pt/C, Rh/C and Pd/C, whereas no conversion was observed on Ni/C (Figure 4.1 shows the conversion profiles observed at room temperature). As Ni can activate H_2 at room temperature, we attribute the inactivity of Ni/C to oxidization in the slightly acidic solution (pH 5). The rates of benzaldehyde conversion were 158 $\mu mol \cdot s^{-1} \cdot g_M^{-1}$, 520 $\mu mol \cdot s^{-1} \cdot g_M^{-1}$, and 928 $\mu mol \cdot s^{-1} \cdot g_M^{-1}$ on Pt/C, Rh/C, and Pd/C, respectively, at 298 K and 1 bar H_2. The corresponding intrinsic activities followed the same trend with TOFs of 427 h^{-1}, 964 h^{-1}, and 1062 h^{-1}, on Pt/C, Rh/C, and Pd/C, respectively.
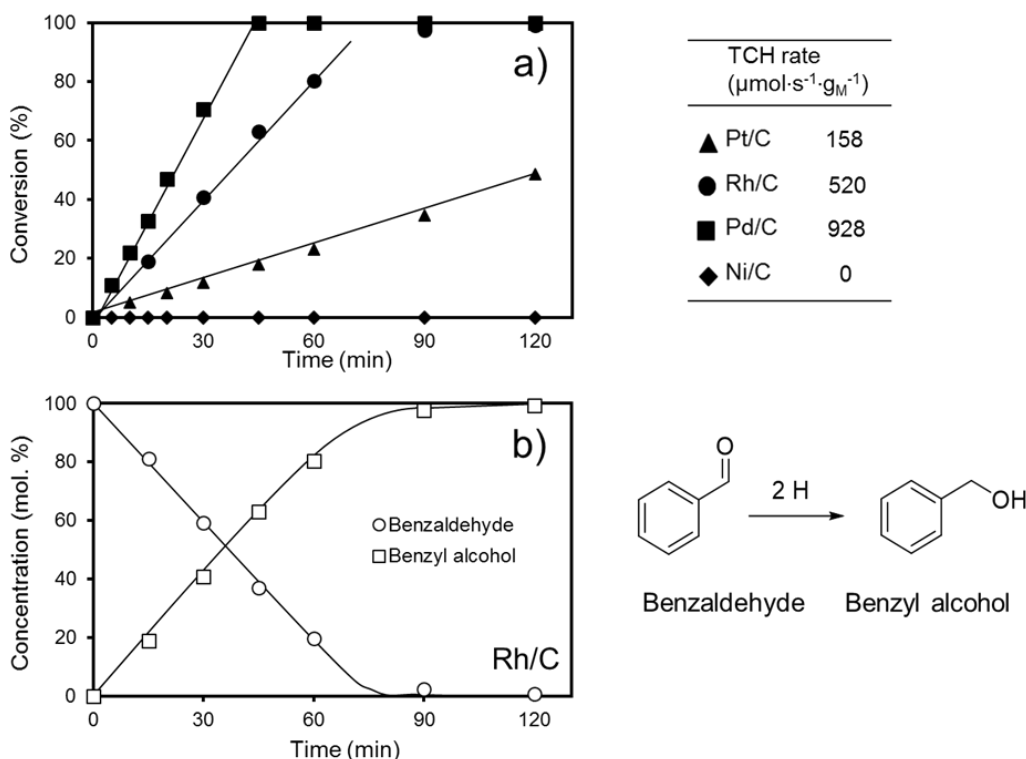
Figure 4.1. Conversion of benzaldehyde on different metal catalysts (a), and product distribution of benzaldehyde performed on Pd/C (b). TCH reactions are performed at room temperature with 1 bar of H2 inlet, the stirring speed is 500 rpm.

The apparent zero reaction order in benzaldehyde observed in the concentration profiles (Figure 4.1) was confirmed with a series of experiments with

varying starting concentrations of benzaldehyde (Figure A1). The reaction orders in H_2 (determined by varying its partial pressure) were 0.8 on Rh/C and Pt/C and 1 on Pd/C (Figure A1). The reaction orders are in good agreement with the Langmuir-Hinshelwood mechanism shown in Scheme 4.1. H_2 and benzaldehyde adsorb on the same kind of metal sites (H_2 adsorbs dissociatively). The adsorption of the two reactants is quasi-equilibrated (reactions (1) and (2) in scheme 4.1). The first hydrogen addition to the adsorbed hydrocarbon is fast and, thus, it is in quasi-equilibrium (reaction (3) in Scheme 4.1). This first H addition probably takes place on the O of the carbonyl [25]. The second H addition (reaction (4) in Scheme 4.1), which leads to the product benzyl alcohol, is the rate determining step [20]. The desorption of alcohol might be equilibrated (reaction (5) in Scheme 4.1) but it is kinetically irrelevant.

$$H_2 + 2\,{*} \rightleftharpoons 2\,H^* \tag{1}$$

$$C_6H_5CHO + {*} \rightleftharpoons C_6H_5CHO^* \tag{2}$$

$$C_6H_5CHO^* + H^* \rightleftharpoons C_6H_5CH_2O^* + {*} \tag{3}$$

$$C_6H_5CH_2O^* + H^* \rightarrow C_6H_5CH_2OH^* + {*} \tag{4}$$

$$C_6H_5CH_2OH^* \rightleftharpoons C_6H_5CH_2OH + {*} \tag{5}$$
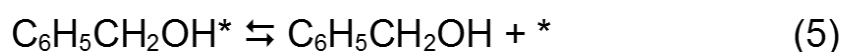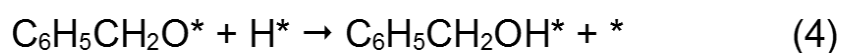
Scheme 4.1. Reaction mechanism proposed for the catalytic thermal hydrogenation of benzaldehyde at near room temperature and 1 bar. Metal active sites are represented by "*".

The reaction mechanism in Scheme 4.1 leads to the rate equation (*i*), where "k" is the rate constant of the rate determining step; "K_{BZH}" and "K_{H2}" are the adsorption equilibrium constants of benzaldehyde and H_2, respectively; "C_{BZH}" and "C_{H2}" are the concentrations of benzaldehyde and H_2 (in equilibrium with the gas phase), respectively. "K_3" is the equilibrium constant of reaction 3 in Scheme 4.1.

Equation (*i*) predicts that the rate is first order in H_2 and in benzaldehyde. The experimental zero order in benzaldehyde indicates that the coverage of the hydrocarbon is high under reaction conditions but not high enough to hinder H_2 adsorption.

$$r = \frac{kK_3K_{H2}K_{BZH}C_{H2}C_{BZH}}{\left(1+K_{BZH}C_{BZH}+K_{H2}^{1/2}C_{H2}^{1/2}+K_3K_{BZH}C_{BZH}K_{H2}^{1/2}C_{H2}^{1/2}\right)^2} \qquad (i)$$

The activity trend Pt/C < Rh/C ≤ Pd/C prevailed in the temperature range from 285 K to 310 K (Figure 4.2). The corresponding activation energies were 32 kJ·mol^{-1}, 27 kJ·mol^{-1}, and 21 kJ·mol^{-1} for Pt/C, Rh/C, and Pd/C, respectively. This trend corresponds to the activity trend of the three catalysts. The determined activation energies are higher than those reported for benzaldehyde hydrogenation at 393 K and 1 bar H_2 on Pt and Pd catalysts (between 10-16 kJ·mol^{-1}) [26, 27]. The adsorption enthalpies of benzaldehyde on the three catalysts were -39 kJ·mol^{-1}, -44 kJ·mol^{-1}, and -61 kJ·mol^{-1} on Pt/C, Rh/C, and Pd/C, respectively. Although this arameters do not influence the true activation energies (the reaction is zero order in benzaldehyde), they hint to stronger adsorption of benzaldehyde on Pd than on Rh and Pt.
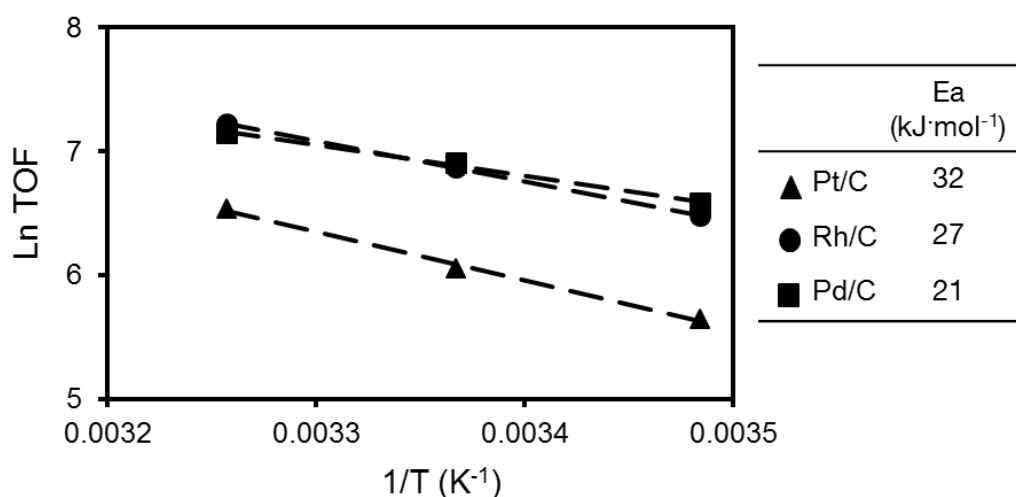
Figure 4.2. Variation of TOF for the hydrogenation of benzaldehyde with temperature and the corresponding activation energies.

4.3.3. Electrocatalytic hydrogenation of benzaldehyde

Electrocatalytic hydrogenation (ECH) of benzaldehyde was performed in the potential range from -0.5 V to -0.9 V (vs Ag/AgCl) on Pt/C, Rh/C and Pd/C, and from -0.8 V to -1.1 V (vs Ag/AgCl) on Ni owning to its different onset potential for the hydrogen evolution reaction (HER). In all ECH experiments, as in TCH, the only product of benzaldehyde hydrogenation was benzyl alcohol (2H hydrogenation), which did not convert further. On the other hand, the hydrogen evolution reaction (HER) competes with hydrocarbon hydrogenation for reduction equivalents. HER proceeds as shown in Scheme 4.2. Adsorbed H is first produced by the reduction of protons from solution (Volmer step). HER produces molecular H_2 via the combination of adsorbed H (Tafel step) or the reaction of the adsorbed H with protons and electrons (Heyrovsky step). Thus, in the following the faradaic efficiency is defined as the percentage of the total current that is consumed for the hydrogenation of benzaldehyde. On the other hand, the current was utilized only for benzaldehyde hydrogenation or H_2 evolution as showed by quantitatively analysis of the gas phase with a mass spectrometer.

$$H^+ + e^- + * \leftrightarrows H* \qquad (1)$$

$$2\,H* \leftrightarrows H_2 + * \qquad (2)$$

$$H* + H^+ + e^- \leftrightarrows H_2 + * \qquad (3)$$

Scheme 4.2. Reaction mechanism for the H_2 evolution reaction. The Volmer, Tafel, and Heyrovsky steps are shown in Reactions (1), (2), and (3), respectively. Metal active sites are represented by "*".

The observation of benzyl alcohol being the only product from benzaldehyde hydrogenation contrasts the conversion of the aromatic ring of phenol, which proceeds via cyclohexanone (4 H additions) to cyclohexanol (2 H additions) under identical conditions on Pt/C, Rh/C, and Pd/C [9, 28]. In benzaldehyde, only the carbonyl group is hydrogenated (2 H additions) to alcohol without hydrogenation of the aromatic ring. We propose that this difference originates from the different adsorption modes of both compounds. Phenol adsorption is favored in a mode parallel to the metal surface [29, 30], while benzaldehyde adsorbs perpendicular to the metal interacting via the carbonyl group [31, 32]. Scheme 4.1 shows the representation of the coplanar η^6 adsorbed state of phenol and the η^1 or η^2 adsorption of benzaldehyde that hinders ring hydrogenation. On the other hand, it surprises that the sole presence of the hydroxymethyl group in benzyl alcohol hinders the η^6 adsorption needed for the consecutive hydrogenation of the aromatic ring. According to previous investigations, the hydrogenation of benzyl alcohol can be achieved at high H_2 pressure (60 bar) and relative mild temperatures (between 50 °C to 120 °C), although higher than those accessed in this work. Moreover, salvation effects could also affect the reactivity of benzyl alcohol [33, 34].

Phenol   a)   Cyclohexanone

coplanar state

adsorption η^6 desorption

Benzaldehyde   b)   Benzyl alcohol

non-planar state

adsorption η^2 η^1 desorption
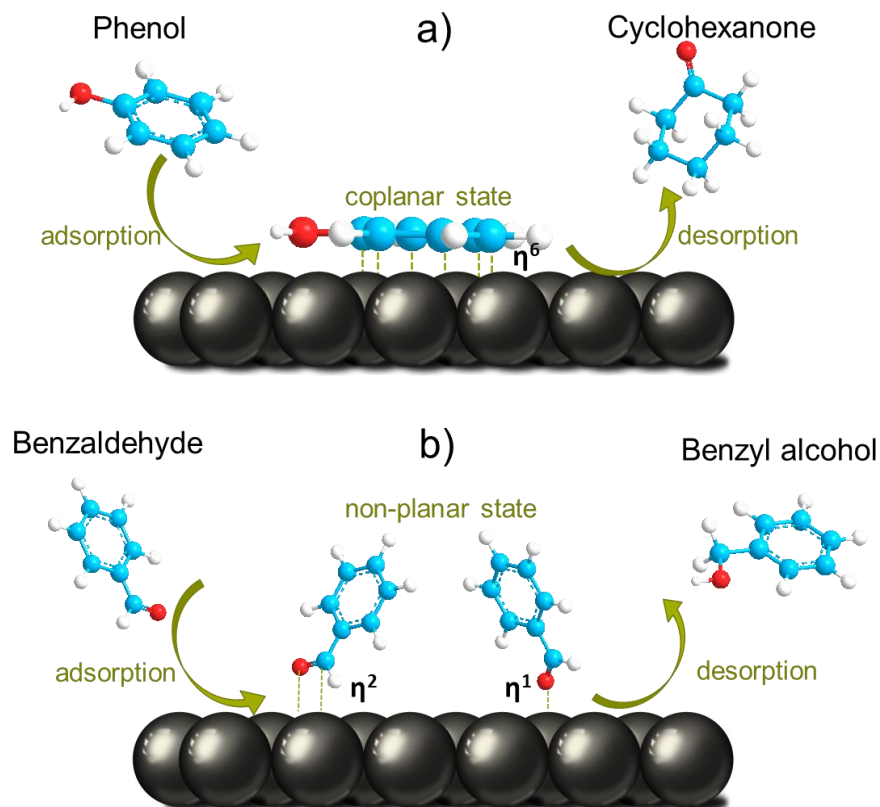
Scheme 4.3. Representations of the proposed adsorption modes of phenol (a) and benzaldehyde (b) that lead to the primary products of the corresponding hydrogenations.

4.3.4. Electrocatalytic hydrogenation of benzaldehyde on C-supported noble metals

The conversion of benzaldehyde on Rh/C followed first order kinetics (Figure A2) in the explored potential range. The intrinsic conversion rates (TOF) of benzaldehyde increased from 511 h^{-1} at -0.5 V to 2267 h^{-1} at -0.9 V vs Ag/AgCl (Figure 4.3). The faradaic efficiency, on the other hand, remained constant at around 65 %.
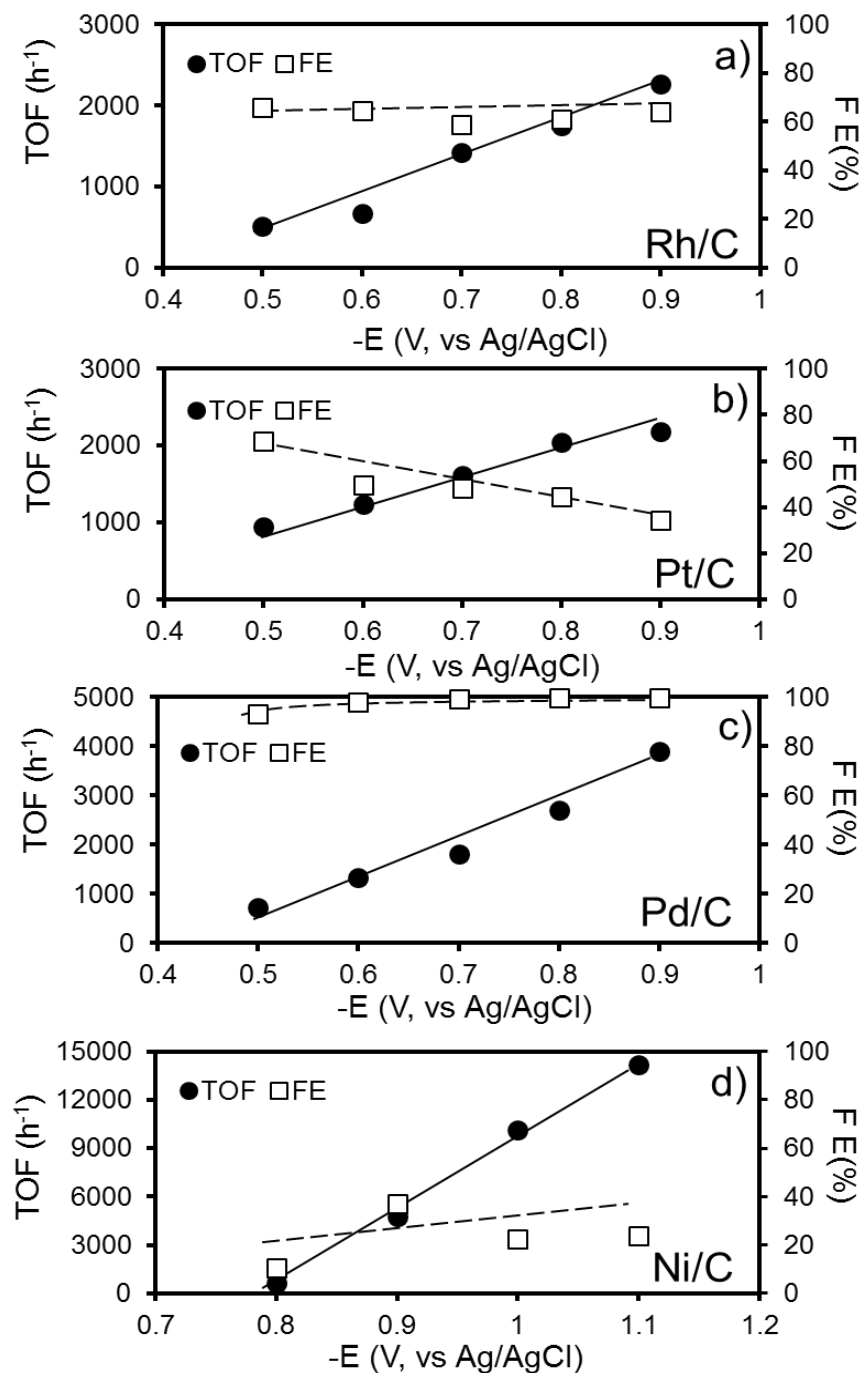
Figure 4.3. Variation of turnover frequency (TOF) and faradaic efficiency (FE) with cathodic potential on a). Rh/C, b). Pt/C, c). Pd/C, and d). Ni/C. ECH reactions are performed at room temperature, with potential range from -0.5 V to -0.9 V (vs Ag/AgCl) on Pt/C, Rh/C and Pd/C, and -0.8 V to -1.1 V on Ni/C, with a stirring speed of 500 rpm.

The conversion of benzaldehyde on Pt/C followed first order kinetics (Figure A2) and TOFs increased from 948 h^{-1} at -0.5 V to 2189 h^{-1} at -0.9 V vs Ag/AgCl (Figure 4.3). In contrast, the faradaic efficiency showed a descending trend with the increase of cathodic potential, i.e., from 68 % at -0.5 V to 39 % at -0.9 V vs Ag/AgCl (Figure 4.3). This indicates that the HER is more favored than ECH with increasingly negative potentials on Pt/C.

In contrast to ECH on Rh/C and Pt/C, the conversion of benzaldehyde on Pd/C followed zero order kinetics (Figure A2). The TOFs increased from 719 h^{-1} at -0.5 V to 3899 h^{-1} at -0.9 V vs Ag/AgCl. The faradaic efficiency on Pd/C was outstandingly high, i.e., from 93 % at -0.5 V to 99 % at -0.7 V vs Ag/AgCl. That is, almost all H produced at the cathode is consumed in ECH instead of HER.

4.3.5. Electrocatalytic hydrogenation of benzaldehyde on Ni/C

In stark contrast with its performance in TCH, Ni/C was active for benzaldehyde conversion in ECH, albeit at higher cathodic potentials than the noble metals. The conversion of benzaldehyde via ECH followed zero order kinetics (Figure A2). The TOF drastically increased from 675 h^{-1} at -0.8 V to 14200 h^{-1} at -1.1 V vs Ag/AgCl (Figure 4.3). However, the faradic efficiency was only 11 % at -0.8 V and increased to 37 % at -1.1 V vs Ag/AgCl (Figure 4.3). Furthermore, hydrobenzoin, the product of benzaldehyde dimerization, was observed with selectivity of up to 3 % (above 80 % benzaldehyde conversion) at -1 V and -1.1 V vs Ag/AgCl.

As Ni can activate H$_2$ at room temperature, the lack of activity of Ni/C in TCH could be due to surface oxidation during reaction in aqueous phase or to high intrinsic hydrogenation barriers of the reaction pathways operating in TCH. We addressed these possibilities by performing transient and coupled TCH and ECH experiments. That is, by switching between 1 bar H$_2$ in the absence of electric potential to 1 bar N$_2$ applying -0.9 V vs Ag/AgCl. The reaction proceeded only in the presence of electric potential as shown in Figure 4.4 a. When H$_2$ was flown in the presence of electric potential the conversion rates of benzaldehyde increased

compared to the rates of ECH alone (in the absence of H_2 flow) as shown in Figure 4.4 b. Thus, we conclude that the inactivity of Ni in TCH is due to its instantaneous oxidation in the solution of acetic acid in the absence of potential. If only electrochemical pathways had existed on Ni/C, the introduction of H_2 would not have affected the ECH rates.
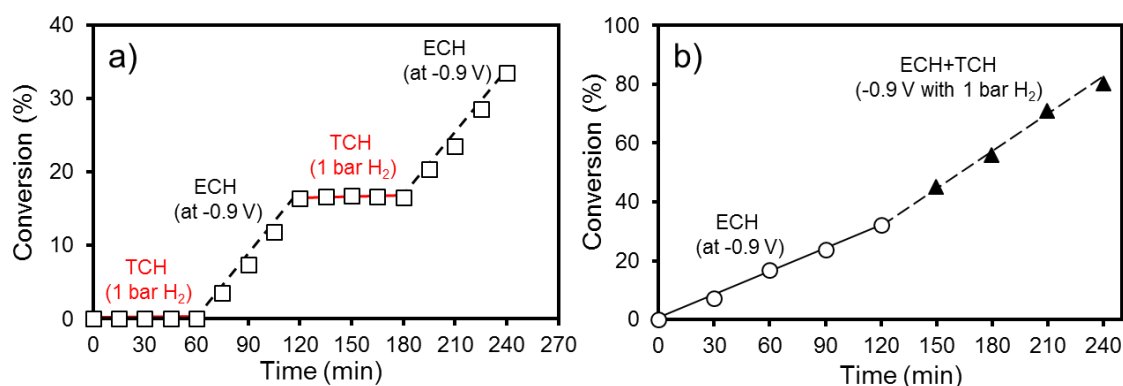
Figure 4.4. a). Conversion of benzaldehyde alternating between 1 bar H_2 in the absence of electric potential and 1 bar N_2 under -0.9 V vs Ag/AgCl. b). Conversion of benzaldehyde between ECH at -0.9 V and ECH coupled with TCH at 1 bar H_2.

4.3.6. On the selectivity to electrocatalytic hydrogenation and H₂ evolution

Overall, the intrinsic activity (TOF) of the catalysts for ECH of benzaldehyde increased as Rh/C < Pt/C < Pd/C < Ni/C (Figure 4.3 and Figure A3). The current density increased as Pd/C < Rh/C < Pt/C < Ni/C, whereas the faradic efficiency increases as Ni/C < Pt/C < Rh/C < Pd/C (Figure A3). Direct comparison of ECH and HER rates (Table A1) shows that ECH is favored over HER by factors of around 1.8 on Rh/C. ECH is also twice as fast as HER on Pt/C at -0.5 V although the HER rates increase faster than ECH rates with cathodic potential. This conducted to lower ECH rates than HER rates at -0.9 V vs Ag/AgCl. Pd/C is a special case because the ECH rates are one or two orders of magnitude higher than HER rates, i.e., HER is suppressed on Pd/C. In contrast, HER is faster than

ECH by factors from 3 to 8 on Ni/C. The high activity of Ni/C, however, overcompensates its low selectivity yielding the faster intrinsic ECH rates among the tested metals.

In order to interrogate the origin of the dissimilar faradaic efficiencies, polarization curves in the absence and the presence of benzaldehyde were recorded at the conditions used for the reaction (Figure 4.5 and Figure A4). Noble metals had identical current onset for H_2 evolution (-0.3 V vs Ag/AgCl), whereas this onset shifted to -0.7 V vs Ag/AgCl on Ni/C.
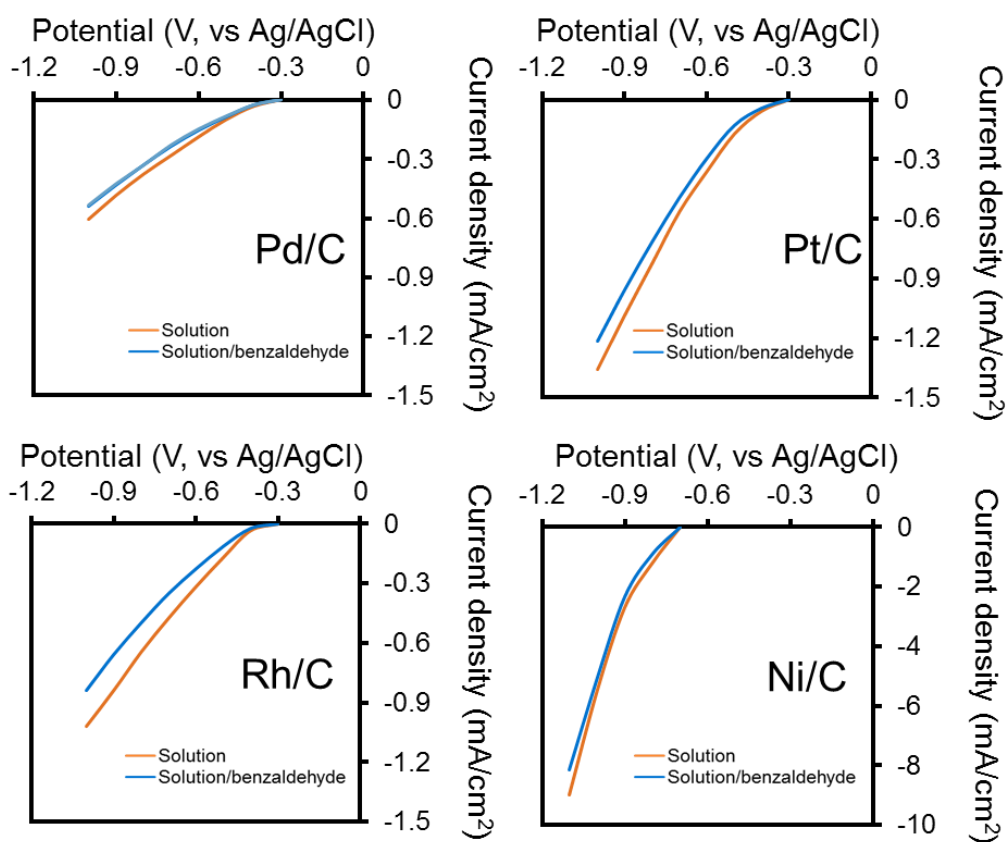
Figure 4.5. Polarization curves (potential vs current density) in the presence of benzaldehyde (BZH) and in its absence (Pure) on Pd/C, Pt/C, Rh/C, and Ni/C. Polarization curves were measured at room temperature with a scan rate of 20 mV·s^{-1}.

In the absence of benzaldehyde, the measured currents correspond only to HER. The corresponding Tafel slopes (calculated from HFR-free potentials according to [24, 29]), were 80 mV·decade^{-1} on Ni/C, 90 mV·decade^{-1} on Pt/C, 98 mV·decade^{-1} on Rh/C, and 145 mV·decade^{-1} on Pd/C (Figure A5 and Table A4). These values indicate that, independent of the corresponding overpotentials for HER, small increases in cathodic potential lead to larger HER rate increases on Ni/C than on the noble metals. Pt/C and Rh/C have similar dependences of current on potential, whereas the largest Tafel slope among the studied catalyst on Rh/C points to the slowest HER rates under the tested conditions. This trend is in agreement with the variations of the faradaic efficiency. Thus, we attribute the different faradaic efficiencies on different catalysts to their intrinsic rates of HER. That is, Ni/C exhibits the fastest HER rates, which leads to the lowest faradaic efficiencies. On the other extreme, Pd/C has the lowest HER rates, which leads to outstanding faradaic efficiencies during ECH. The fundamental implication of this conclusion is that the faradaic efficiency, i.e., the HER/ECH selectivity is governed by kinetics rather than by thermodynamics (H$_2$ evolution overpotential). The presence of benzaldehyde did not affect the onset of current in function of potential but had a detrimental effect on the current density reached at any given potential on all catalysts (Figure 4.5). Accordingly, the Tafel slopes in the presence of benzaldehyde increased compared to those in its absence, i.e., to 100 mV·decade^{-1} on Ni/C, 150 mV·decade^{-1} on Pt/C, 120 mV·decade^{-1} on Rh/C, and 190 mV·decade^{-1} on Pd/C (Table A4). This indicates that benzaldehyde covers a fraction of the reduction sites decreasing the electrocatalytic activity of the catalysts.

4.3.7. Reaction mechanisms for the electrocatalytic hydrogenation of benzaldehyde

The ECH activity trend Rh/C < Pt/C < Pd/C < Ni/C prevailed in the temperature range from 285 K to 310 K (Figure 4.6). The corresponding activation energies

were 21 kJ·mol^{-1} on Rh/C, 25 kJ·mol^{-1} on Pt/C, 14 kJ·mol^{-1} on Pd/C during ECH at -0.7 V (vs Ag/AgCl). These values are lower than in TCH, which we attribute to differences in the reaction mechanisms prevailing in the presence of cathodic potential. The activation energy on Ni/C was 41 kJ·mol^{-1} on Ni at -0.9 V vs Ag/AgCl.
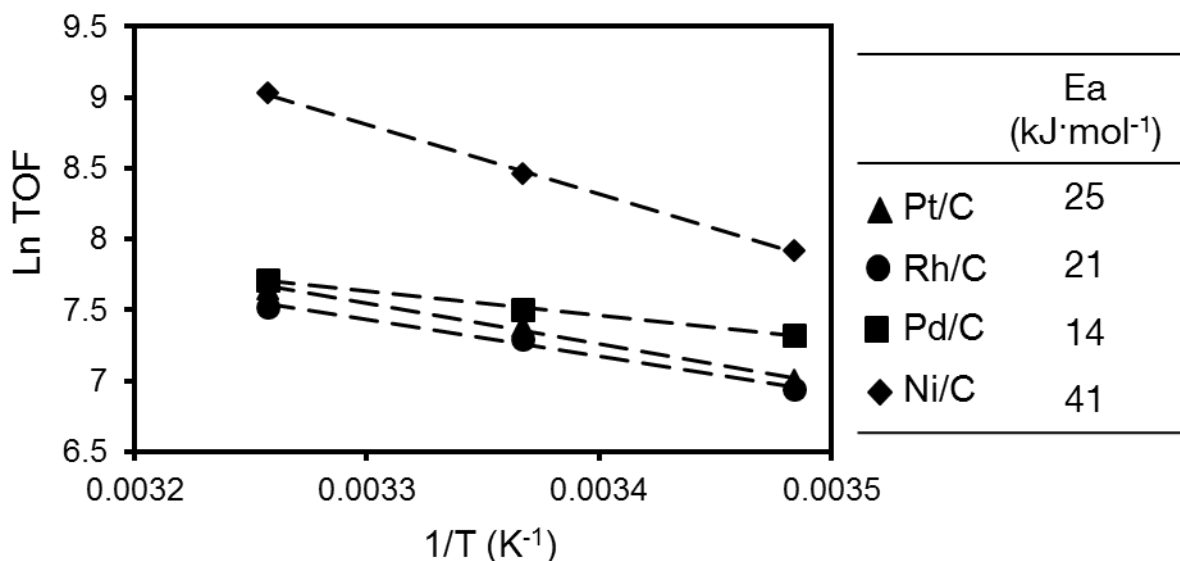
Figure 4.6. Activation energies for benzaldehyde hydrogenation during ECH on Pt/C, Rh/C, RhC, and Ni/C. Reactions are performed with 10 mg catalysts at temperatures of 14 °C to 34 °C, at 1 bar H$_2$ inlet, with 500 rpm stirring speed.

The reaction orders in benzaldehyde of zero on Pd/C and Ni/C and of one on Pt/C and Rh/C observed from the conversion profiles (Figure A2) were confirmed by experiments with varying initial benzaldehyde concentrations (Figure A6). These differences in reaction orders in benzaldehyde cannot be explained by drastic changes in its coverage as the enthalpy of adsorption were dissimilar on e.g., Ni/C and Pd/C (-36 kJ·mol^{-1} and -61 kJ·mol^{-1}, respectively), both exhibiting a reaction order of zero. The presence of potential might affect the energy of adsorption. However, no more than few units within the studied potential range [35, 36].

The H coverages are sustained by electric potential under ECH. Thus, the ECH rates must have positive dependences on hydrogen coverages as all rates increased with increasing cathodic potential. However, the Nernst equation cannot be used to estimate the equivalent H_2 pressure from the applied electric potential because the reactions are performed at conditions far from equilibrium. In a previous work, we found that for the hydrogenation of phenol on Rh/C under identical ECH and TCH conditions, the coverages under 1 bar H_2 and -0.7 V (-0.44 V after IR correction) were similar [9]. On Pt/C, the potential at which the coverages are equivalent to 1 bar H_2 is about -0.7 V given the similar ECH and TCH rates (Figure A7). We infer, therefore, that the H coverages on the catalysts used in this work are of the order of the equivalent to 1 bar H_2.

Electrochemical hydrogenation might proceed through stepwise or concerted addition of protons and electrons. Stepwise addition may also proceed in several sequences, that is, H^+-e^--e^--H^+ (proton addition followed by two reductive steps and a proton addition as final step), e^--H^+-e^--H^+ (alternating electron and proton addition), H^+-e^--H^+-e^- (alternating proton and electron addition), and e^--H^+-H^+-e^- (reduction followed by addition of two protons and reduction as final step). The energy needed to accumulate two charges with the same sign in one molecule would make the e^--e^--H^+-H^+ and H^+-H^+-e^--e^- sequences prohibitive under our reaction conditions. The elementary steps of the most likely sequential electrochemical mechanisms in protic media are shown in Scheme A1 and Scheme A2 of the supporting information as discussed in Refs. [31, 32, 37]. The most likely sequences, in case of stepwise addition are H^+-e^--e^--H^+, H^+-e^--H^+-e^-, e^--H^+-H^+-e^- and e^--H^+-e^--H^+ according polarization curves in function of pH shown in the mentioned Refs.

The discussed steps are shown in Figure 4.7, which also shows the pKa values of the potential intermediate protonated species (conjugated acids of the aldehyde species) and reported cathodic potentials for one-e^- reduction steps [31, 38, 39]. Those thermodynamic parameters do not support stepwise mechanisms. For instance, the pKa of protonated benzaldehyde is around -4, i.e., its concentration at our conditions (pH=5) is negligible. Thus, electrochemical steps involving protonated

intermediates towards hydrogenation of the carbonyl group does not seem likely. On the other hand, the direct reduction of benzaldehyde requires potentials more negative, e.g., -1.9 V vs Ag/AgCl [39] than those accessed in this work (from -0.4 V to -1.1 V vs Ag/AgCl). Therefore, stepwise addition of electrons and protons to the hydrocarbon should have high-energy intermediates.

The absence of radical pathways under our reaction conditions is also suggested by the lack of hydrobenzoin formation (dimer of benzaldehyde), which is expected if radical aldehyde species form in solution. The dimer was detected in small quantities only on Ni/C at 1.1 V vs Ag/AgCl. In contrast, reference ECH experiments performed on the bare carbon felt at constant cathodic current of 50 mV showed the formation of the dimerization product with yields of up to 38% at 65% benzaldehyde conversion (Figure 4.7). This was the result of the high potentials reached at such conditions, i.e., -2.2 V vs Ag/AgCl. Thus, stepwise pathways are indeed enabled when the driven force is enhanced.
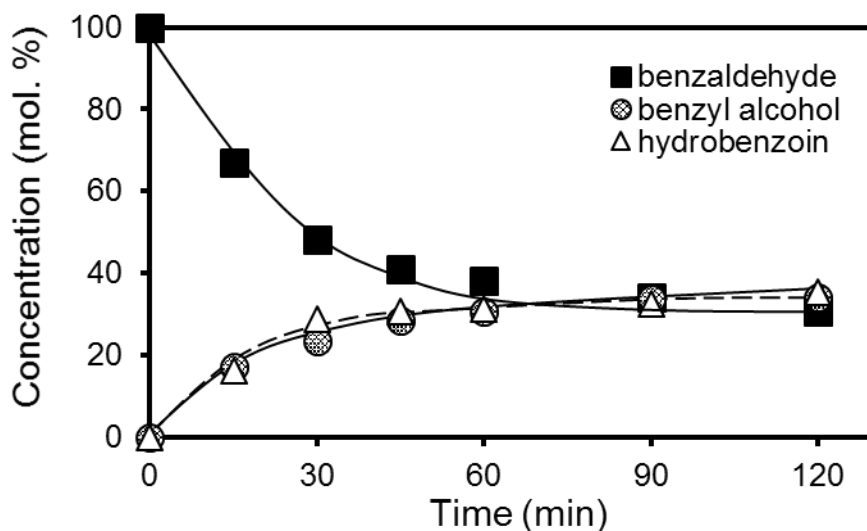
Figure 4.7. Product distribution of benzaldehyde ECH on carbon felt at -2.2 V.

In contrasts to the stepwise electrochemical pathways, the thermal pathways (addition of adsorbed H with radical nature), shown in Fig. 4.8, requires a potential of -0.28 V vs Ag/AgCl (in pH 5 buffer), according to the free Gibbs energy of the overall transformation ($\Delta G° = -34$ kJ·mol^{-1}). Thus, it is spontaneous in the absence of electric potential as shown in the TCH experiments on Pt/C, Pd/C, and Rh/C.

Ni/C is inactive due to surface oxidation as discussed above. The rate determining step in this route is the addition of the second adsorbed H, which proceeds with low barriers, i.e., from 21 kJ·mol^{-1} to 32 kJ·mol^{-1}, on the noble metals (Figure 4.2). Despite of the ease of benzaldehyde reduction with adsorbed H, we consider that it is not the main route under ECH due to the changes in reaction orders, the much higher conversion rates in ECH than in TCH, and the differences in activation energies. That is, lower activation energies for ECH than for TCH by 7 k·mol^{-1}. In previous studies on phenol and di-aryl ether hydrogenation ECH and TCH were concluded to proceed through identical pathways because reaction orders, activation energies and selectivities of both processes were identical [9]. We postulate that the routes that aid benzaldehyde hydrogenation in the presence of electric potential comprise concerted e$^-$/H$^+$ additions. Although such routes are difficult to distinguish from the neutral radical addition postulated in thermal catalysis, concerted e$^-$ and H$^+$ additions allow to avoid high energy intermediates [8, 9]. Figure 4.8 shows that the concerted electrochemical reduction lead to the same intermediates as those in TCH without passing through high energy charged intermediates.
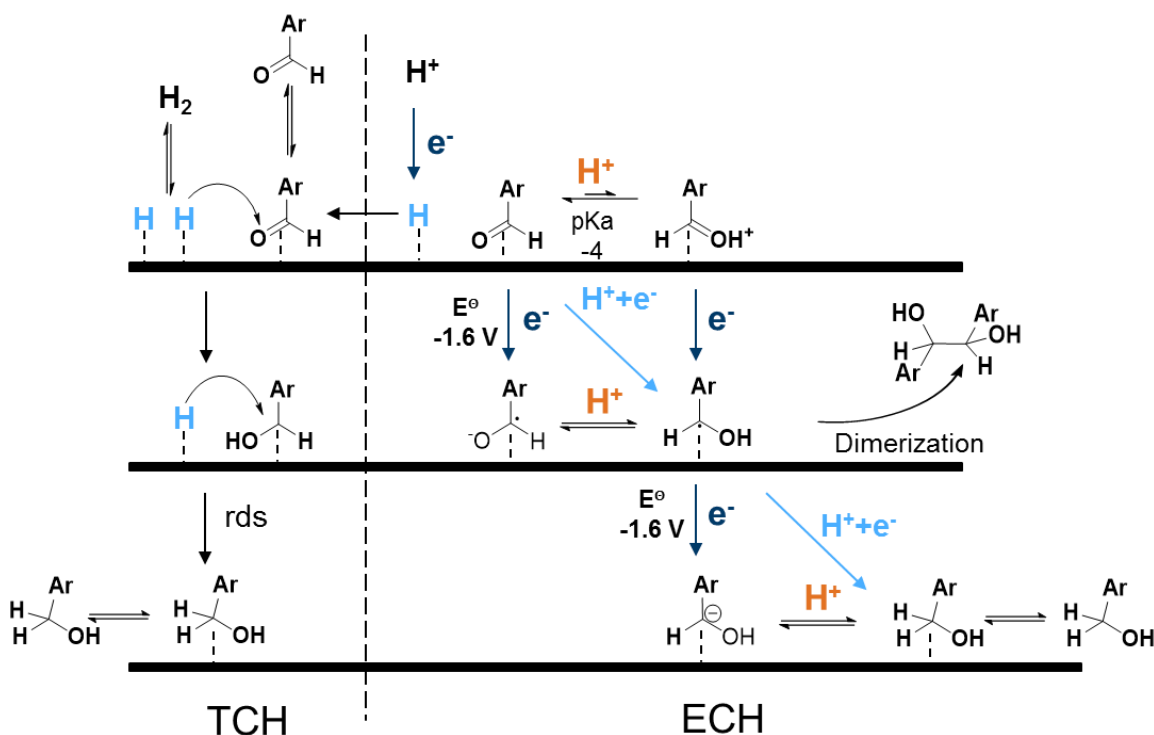
Figure 4.8. Routes for hydrogenation of benzaldehyde via TCH and ECH.

4.4. Conclusions

Thermal catalytic hydrogenation (TCH) and electrocatalytic hydrogenation (ECH) of benzaldehyde were performed at room temperature in aqueous phase on Pt/C, Rh/C, Pd/C, and Ni/C. In TCH the intrinsic activity followed the trend Pd/C > Rh/C > Pt/C (TOFs of 1062 h^{-1}, 964 h^{-1}, and 427 h^{-1}, respectively at 298 K and 1 bar H$_2$), whereas Ni/C was not active. Benzyl alcohol was the only product of the reaction, which is attributed to a preferential η^2 and η^1 adsorption of benzaldehyde and repulsion of the hydroxymethyl group in benzyl alcohol from the surface. Reaction orders of zero in benzaldehyde and 1 in H$_2$ allow proposing that the hydrogenation of benzaldehyde follows a Langmuir-Hinshelwood, where adsorbed H is added stepwise to the adsorbed hydrocarbon. The second H addition is the rate limiting step.

In ECH, the hydrogenation of benzaldehyde proceeds only to benzyl alcohol (as in TCH) but competes with H$_2$ evolution. The hydrogenation rates increase with increasing cathodic potential and the activity trend is Ni/C< Rh/C < Pt/C < Pd/C (e.g., TOFs of 675 h^{-1}, 1753 h^{-1}, 2048 h^{-1} and 2706 h^{-1}, respectively at 298 K and -0.8 V Ag/AgCl). Notably, Ni/C becomes active and turns to be the most active catalyst in ECH under our conditions albeit at higher cathodic potentials than noble metals. The onset of ECH activity coincides with that of HER (more negative than -0.8 V and -0.4 V vs Ag/AgCl for Ni/C and noble metals, respectively). The faradaic efficiency, however, increases as Ni/C < Pt/C < Rh/C << Pd/C (e.g., 11 %, 45 %, 61 %, and 99.6 %, respectively at 298 K and -0.8 V Ag/AgCl). This efficiency is related with the relative HER and ECH rates (kinetic factors), rather than with overpotential of HER (thermodynamic factors).

The marked differences between the performances of the different catalysts in ECH and TCH allow concluding that at least one hydrogenation step in ECH involves the addition of e- and H$^+$ instead of adsorbed hydrogen as in TCH. Moreover, this addition is likely concerted because charged intermediates

(protonated benzaldehyde or one-e⁻ reduced intermediates) are not favored at the reaction conditions and cathodic potentials applied.

4.5. Appendix

4.5.1. Calculations

Conversion, reaction rate, adsorbed hydrogen (H_{ads}) consumption rate, turnover frequency (TOF), and Faradic efficiency (FE) were calculated according to the following equations.

$$\text{Conversion} = \frac{\text{Moles of phenol consumed}}{\text{Initial moles of phenol}} \times 100 \qquad [=] \quad \%$$

$$\text{ECH Reaction rate} = \frac{\text{Moles of reactant consumed via ECH}}{\text{Time} \times \text{Mass of catalyst} \times \text{Metal loading}} \qquad [=] \text{ mol/s·g(metal)}$$

$$\text{TH Reaction rate} = \frac{\text{Moles of reactant consumed via TH}}{\text{Time} \times \text{Mass of catalyst} \times \text{Metal loading}} \qquad [=] \text{ mol/s·g(metal)}$$

$$\text{HER Reaction rate} = \frac{\text{Moles of hydrogen gas produced via HER}}{\text{Time} \times \text{Mass of catalyst} \times \text{Metal loading}} \qquad [=] \text{ mol/s·g(metal)}$$

$$\text{Hads consumption rate of ECH} = \frac{\text{Moles Hads consumed via ECH}}{\text{Time} \times \text{Mass of catalyst} \times \text{Metal loading}} \ [=] \ \text{mol/s·g(metal)}$$

$$\text{Hads consumption rate of HER} = \frac{\text{Moles of Hads consumed via HER}}{\text{Time} \times \text{Mass of catalyst} \times \text{Metal loading}} \ [=] \ \text{mol/s·g(metal)}$$

$$\text{Hads consumption rate of TH} = \frac{\text{Moles of Hads consumed via TH}}{\text{Time} \times \text{Mass of catalyst} \times \text{Metal loading}} \ [=] \ \text{mol/s·g(metal)}$$

$$\text{TOF} = \frac{\text{Moles of phenol consumed}}{\text{Time} \times \text{Dispersion of metal} \times \text{Moles of metal in the catalyst}} \ [=] \ \text{h}^{-1}$$

$$\text{FE} = \frac{\text{Electrons consumed by hydrogenation of organic compounds}}{\text{Total electrons passed}} \times 100 \ [=] \ \%$$

4.5.2. Physicochemical properties of the catalyst

Table A1. Characterization of the catalysts.

	Loading (wt. %)	BET surface area (m^2·g^{-1})	Pore diameter (Å)	metal surface area (m^2·g^{-1})	particle size (nm)[a]	particle size (nm)[b]	dispersion (%)
Pt/C	5	957	45.8	69.2	3.5	3.8	26

Rh/C	5	921	76.6	88	5.1	4.2	20
Pd/C	5	1034	56.5	148	2.9	3	33
Ni/C	5	1272	72.6	3.3	208	200	2.5

Catalysts were measured by N_2 physisorption and hydrogen chemisorption, while the crystal sizes were estimated by TEM measurements.
[a] measured by TEM.
[b] measured by hydrogen chemisorption.

Table A2. Characterization of carbon matrix properties.

	Surface area $(m^2 \cdot g^{-1})$	Particle size (µm)	Purity (%)
Activated carbon	1363	45	99
Carbon felt	-	-	99

4.5.3. Thermal catalytic hydrogenation (TCH) and Electrocatalytic hydrogenation (ECH) of benzaldehyde
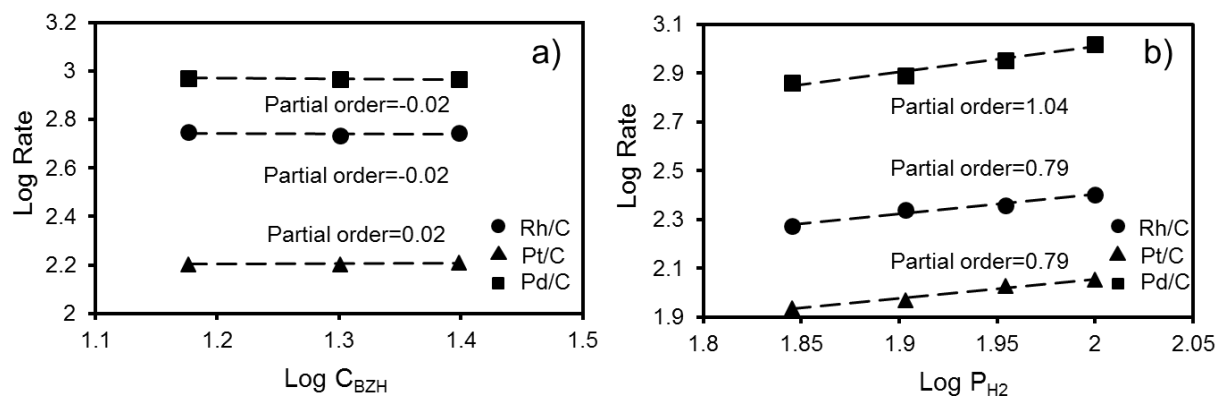
Figure A1. Reaction orders in benzaldehyde (a) and H_2 (b). Reaction orders in benzaldehyde were performed at 1 bar H2 inlet, at room temperature, with benzaldehyde concentration of 15 mmol·L^{-1}, 20 mmol·L^{-1} and 25 mmol·L^{-1}. The reaction orders in H2 partial pressure were measured at 20 mmol·L^{-1} of benzaldehyde, at room temperature, with different H_2: Ar ratio as 1:0, 0.9:0.1, 0.8:0.2, and 0.7:0.3, to give a total pressure of 1 bar.

Table A3. Kinetic profiles of ECH and TCH of benzaldehyde on Rh/C, Pt/C, Pd/C and Ni/C.

Potential (V, vs Ag/AgCl)	I (mA)	Corrected potential (V)[e]	TOF (h^{-1})	FE (%)	ECH H$_{ads}$ rate ($\mu mol \cdot s^{-1} \cdot g_M^{-1}$)	HER H$_{ads}$ rate ($\mu mol \cdot s^{-1} \cdot g_M^{-1}$)
-0.5 [a]	-40	-0.43	511	66	550	280
-0.6 [a]	-70	-0.48	668	64	928	510
-0.7 [a]	-125	-0.49	1419	59	1531	1050
-0.8 [a]	-150	-0.55	1753	61	1890	1020
-0.9 [a]	-185	-0.59	2267	64	2455	1370
TCH [a]	-	-	964	-	-	-
-0.5 [b]	-40	-0.43	948	68	567	260
-0.6 [b]	-82	-0.46	1240	49	840	850
-0.7 [b]	-115	-0.5	1617	48	1144	1219
-0.8 [b]	-160	-0.52	2048	45	1479	1826
-0.9 [b]	-200	-0.55	2189	39	1596	2541
TCH [b]	-	-	427	-	-	-
-0.5 [c]	-55	-0.44	719	93.4	1142	81
-0.6 [c]	-104	-0.49	1330	98	2112	43
-0.7 [c]	-145	-0.54	1820	99.5	2990	15
-0.8 [c]	-200	-0.58	2706	99.7	4298	13
-0.9 [c]	-300	-0.62	3899	99.6	6193	25
TCH [c]	-	-	1062	-	-	-
-0.8 [d]	-15	-0.77	675	11	32	260
-0.9 [d]	-30	-0.85	4730	37	115	370
-1.0 [d]	-80	-0.86	10145	23	374	1268
-1.1 [d]	-130	-0.87	14200	24	636	2018
TCH [d]	-	-	-	-	-	-

[a] Reactions performed on Rh/C.
[b] Reactions performed on Pt/C.
[c] Reactions performed on Pd/C.
[d] Reactions performed on Ni/C.
[e] Corrected potentials were obtained from applied potential with removal of the Ohmic loss (IR affection), R is the resistance caused from the electrolyte measured by high frequency impedance.

	Rate constant	
Pt/C	($\times 10^{-3}$ min^{-1})	
-0.5 V	9.1	
-0.6 V	11.9	
-0.7 V	15.8	
-0.8 V	16.8	
-0.9 V	18.8	
Rh/C	($\times 10^{-3}$ min^{-1})	
-0.5 V	5.6	
-0.6 V	15.1	
-0.7 V	18	
-0.8 V	23.6	
-0.9 V	31.4	
Pd/C	($\times 10^{-5}$ mol·min^{-1})	
-0.5 V	2.1	
-0.6 V	3.6	
-0.7 V	5.4	
-0.8 V	7.7	
-0.9 V	10.5	
Ni/C	($\times 10^{-7}$ mol·min^{-1})	
-0.8 V	4.8	
-0.9 V	34	
-1.0 V	81	
-1.1 V	95	
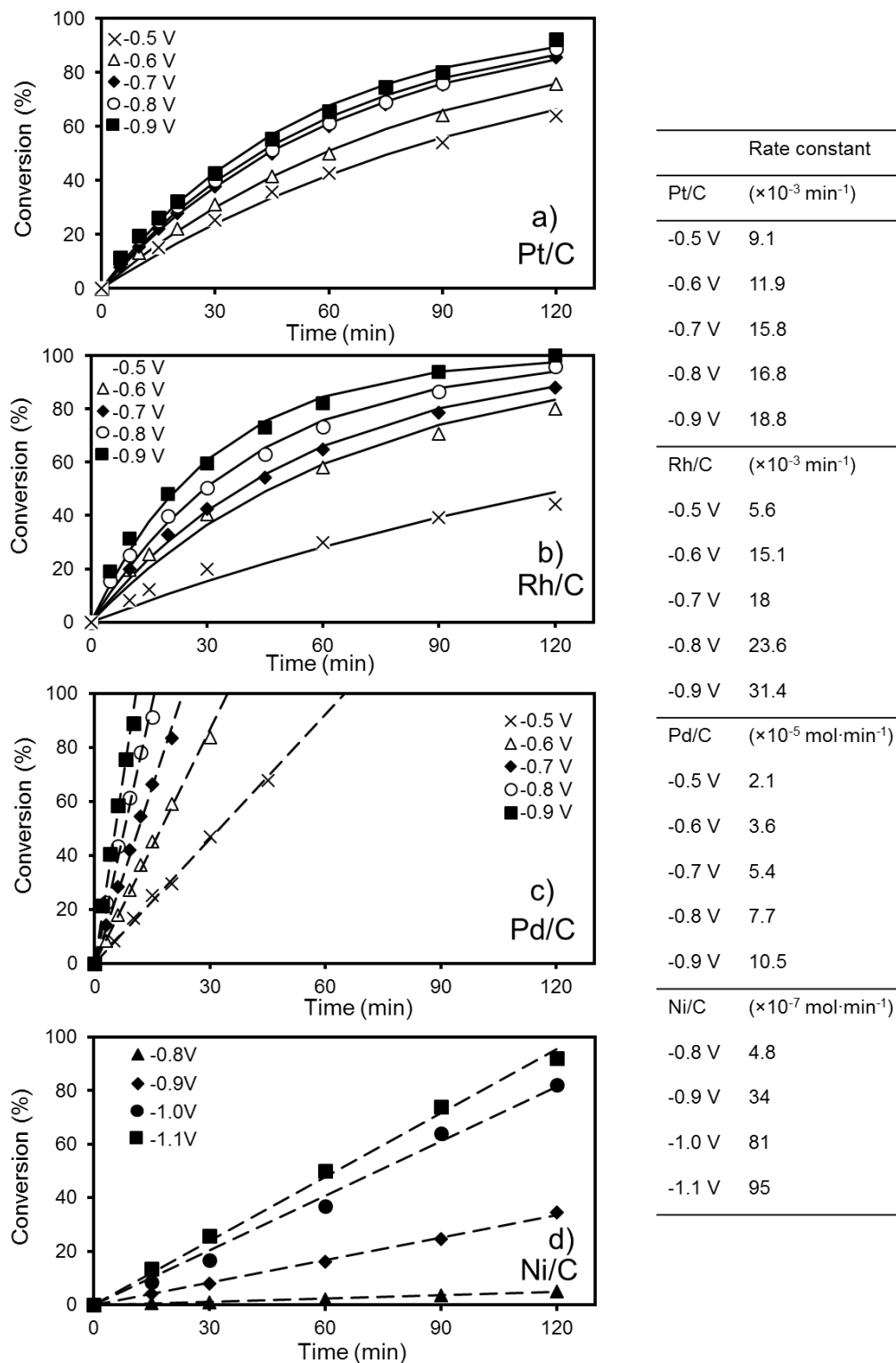
Figure A2. Conversion of benzaldehyde on 10mg of a). Rh/C, b). Pt/C, c). Pd/C, and d). Ni/C at varying potentials. Reactions are performed under room temperature with 500 rpm rotating, the potential range are from -0.5V to -0.9V vs Ag/AgCl on Pt/C, Rh/C and Pd/C, and from -0.8 V to -1.1 V on Ni/C.
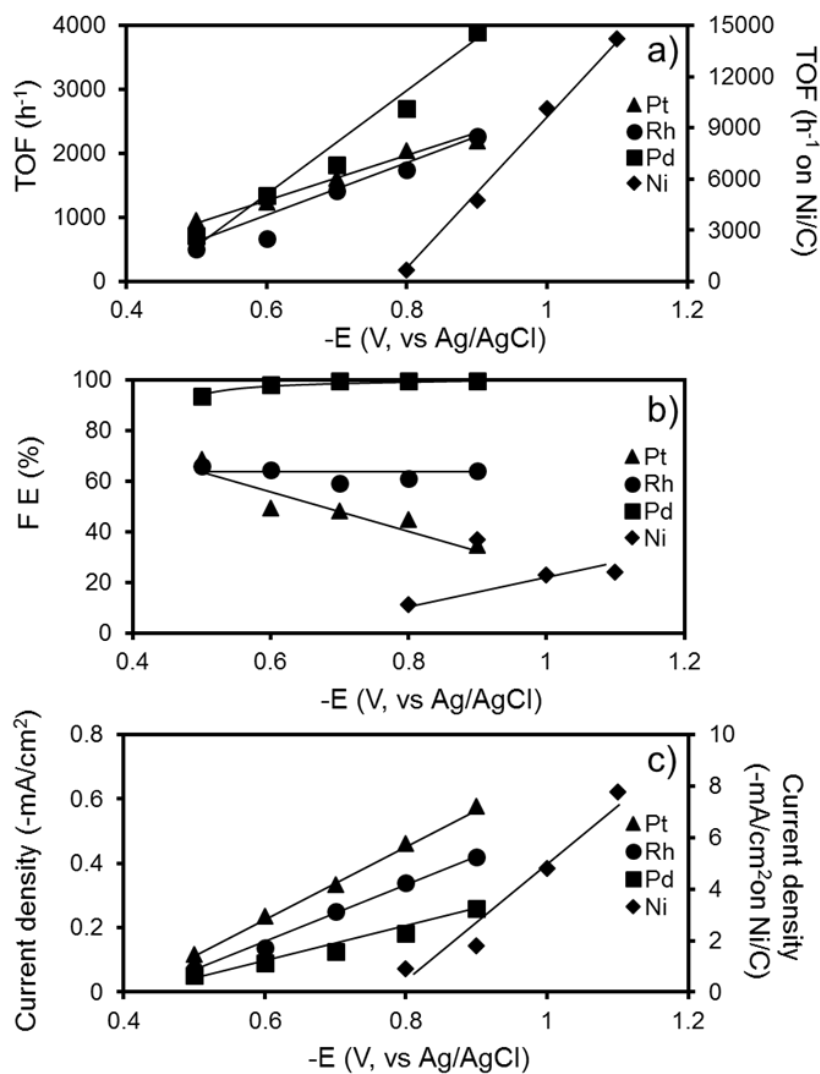
Figure A3. Comparison of a) TOF, b) FE and c) current density on different catalyst via ECH of benzaldehyde.
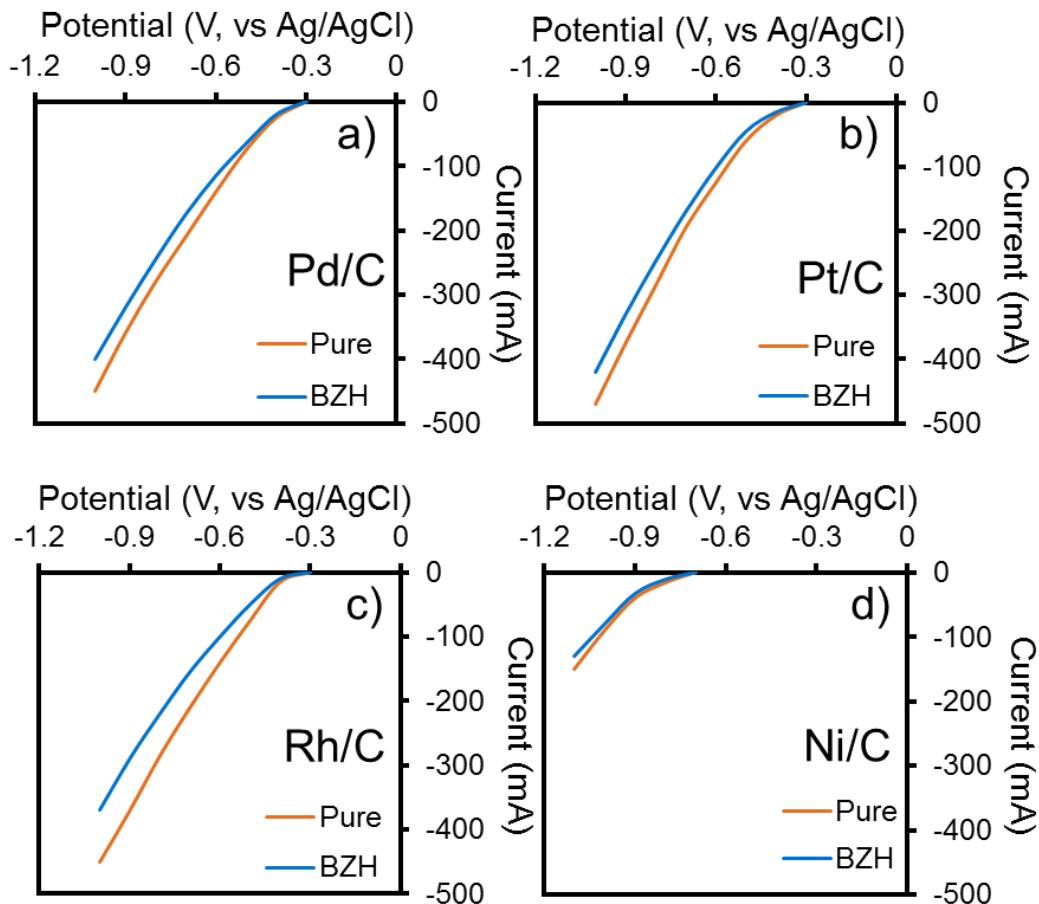
Figure A4. Polarization curves (potential vs current) in the presence and the absence (Pure) of benzaldehyde (BZH) on Pd/C, Pt/C, Rh/C, Ni/C. Polarization curves are performed at room temperature with a scan rate of 20 mV·s^{-1}, from -0.3 V to -1 V vs Ag/AgCl, on Pd/C, Pt/C and Rh/C. and a potential range from -0.7 V to -1.1 V on Ni/C.
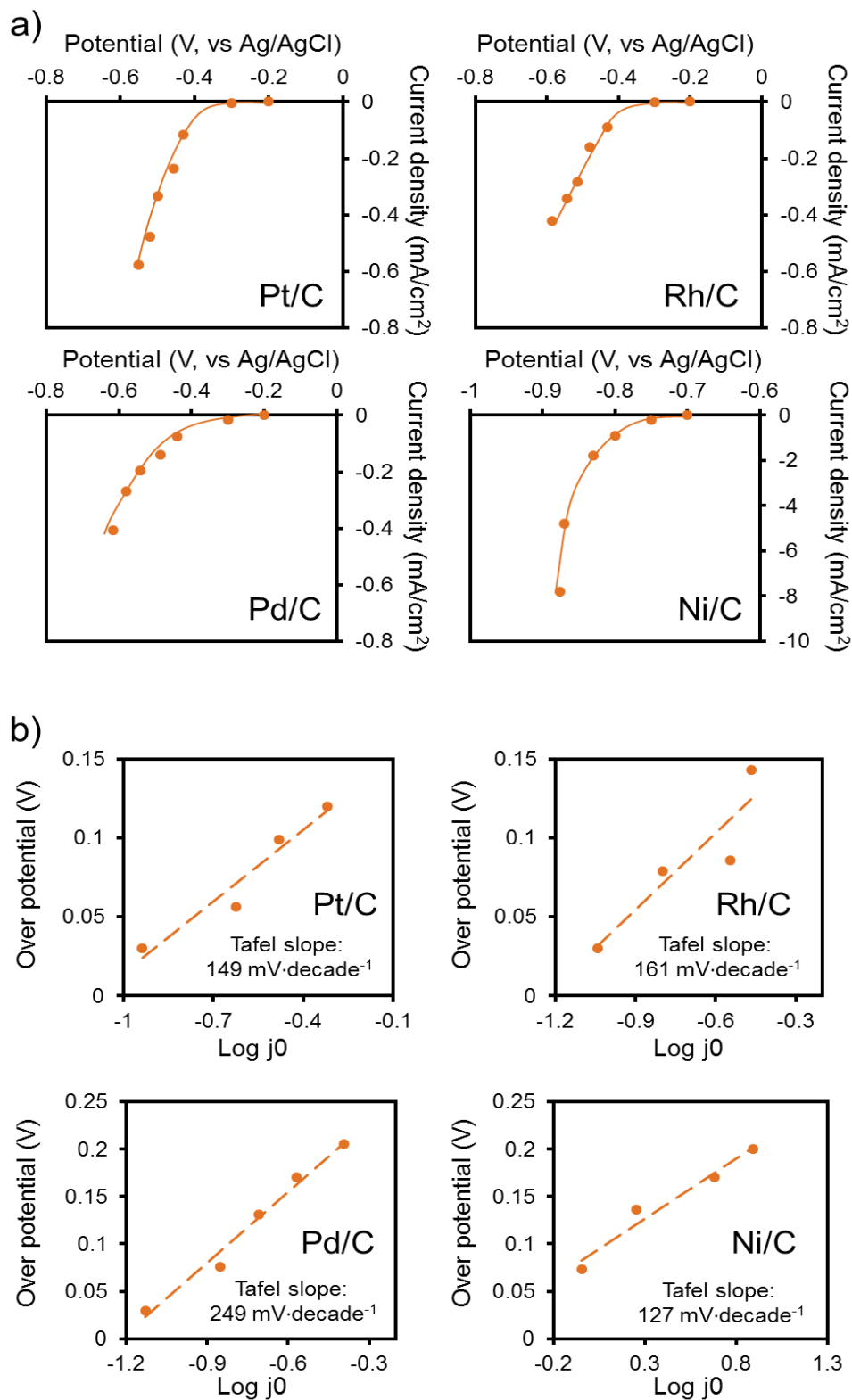
Figure A5. a). Polarization curve of current density in function of iR corrected potential and b) Tafel plots on Pt/C, Rh/C, Pd/C and Ni/C.
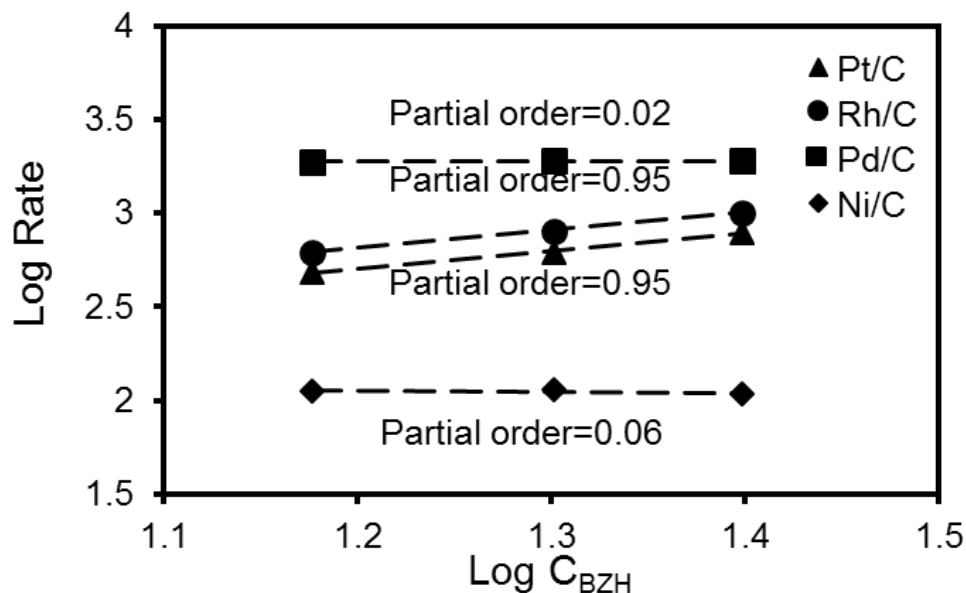
Figure A6. Reaction orders in benzaldehyde for its hydrogenation during ECH on Pt/C, Rh/C, Rh/C, and Ni/C. Reaction orders are measured under room temperature at -0.6 V vs Ag/AgCl on Pt/C, Rh/C and Pd/C, and at -0.9 V on Ni/C. Concentration of BZH is from 15 mmol·L^{-1}, 20 mmol·L^{-1} and 25 mmol·L^{-1}.

$$ArCH=O + H^+ \leftrightarrows ArCH=OH^+ \qquad\qquad (1)$$

$$ArCH=OH^+ + e \rightarrow Ar\dot{C}H\text{-}OH \qquad\qquad (2)$$

$$Ar\dot{C}H\text{-}OH + e \rightarrow ArC^-H\text{-}OH \qquad\qquad (3)$$

$$ArC^-H\text{-}OH + H^+ \leftrightarrows ArCH_2\text{-}OH \qquad\qquad (4)$$
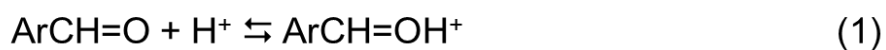
Scheme A1. Elementary steps proposed for the electrochemical hydrogenation of benzaldehyde in acidic media (pH 3, Pt electrode, add more relevant conditions like potential used). The first step is the protonation of benzaldehyde (1), which is

followed by two reduction steps (2), (3). The final step is the addition of a proton to produce benzyl alcohol (4). The rate determining steps are the reduction steps.

$$ArCH=O + e \rightarrow Ar\dot{C}H\text{-}O^- \qquad (5)$$

$$Ar\dot{C}H\text{-}O^- + H^+ \leftrightarrows Ar\dot{C}H\text{-}OH \qquad (6)$$

$$Ar\dot{C}H\text{-}OH + e \rightarrow ArC^-H\text{-}OH \qquad (3)$$

$$ArC^-H\text{-}OH + H^+ \leftrightarrows ArCH_2\text{-}OH \qquad (4)$$
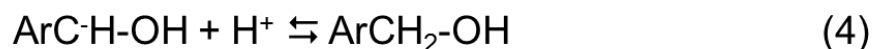
Scheme A2. Elementary steps proposed for the electrochemical hydrogenation of benzaldehyde in neutral media (pH 3, Pt electrode, add more relevant conditions like potential used). The first step is the reduction of benzaldehyde (5), following by the protonation (6), and further follows the reduction and addition of a proton as described in the previous scheme (3) and (4) to produce benzyl alcohol. Reduction steps are the rate determining steps.

Table A4. Heat of adsorption of benzaldehyde and Tafel slope on four catalsyts.

Cataslyt	Rh/C	Pt/C	Pd/C	Ni/C
Heat of adsorption BZH (kJ/mol)	-39	-44	-61	-36
Tafel slope reaction (mV·decade^{-1})	161	149	249	127
Tafel slope CV pure (mV·decade^{-1})	90	98	145	84
Tafel slope CV BZH (mV·decade^{-1})	120	150	190	100
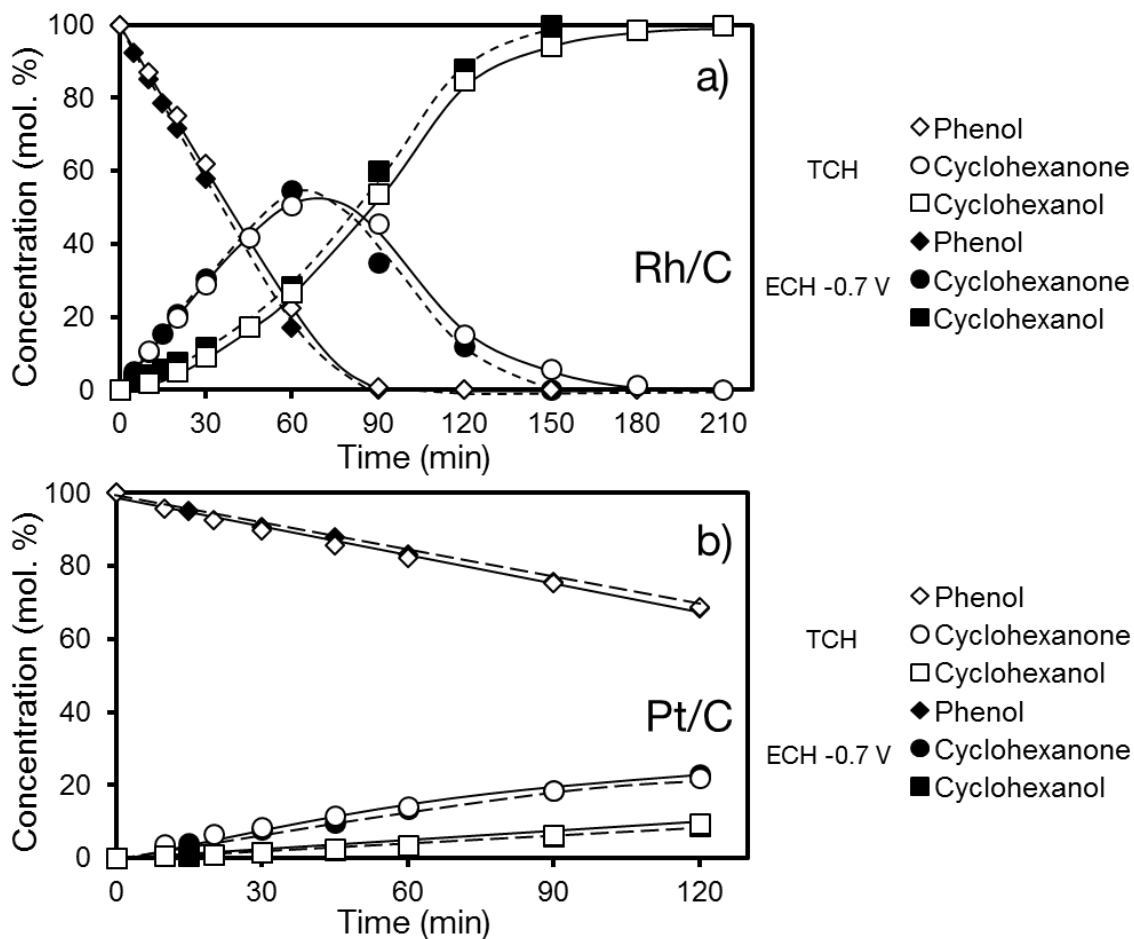
Figure A7. Phenol ECH product distribution curves compared between a) TCH at 1 bar H_2 to ECH at -0.7 V on Rh/C, b) TCH at 1 bar H_2 ECH at -0.75 V on Pt/C. Reactions are performed with 1.06×10^{-6} mol with 10 mg catalyst, at room temperature.

4.6. References

[1] M. Gilkey, B. Xu, ACS Catal. 6 (2016) 1420-1436.

[2] K. Carrol, T. Burger, L. Langenegger, S. Chavez, S. Hunt, Y. Leshkov, F. Brushett, ChemSusChem. 9 (2016) 1-8.

[3] Y. Kwon, Y. Birdja, S. Raoufmoghaddam, M. Koper, ChemSusChem. 8 (2015) 1745-1751.

[4] M. Chatterjee, T. Ishizaka, A. Suzuki, H. Kawanimi, Chem. Commun. 49 (2013) 4567-4569.

[5] A. Corma, S. Iborra, A. Velty, Chem. Rev. 107 (2007) 2411-2502.

[6] M. Chatterjee, A. Chatterjee, T. Ishizaka, H. Kawanami, Catal. Sci. Technol. 5 (2015) 1532-1539.

[7] C. M. Cirtiu, A. Brisach-Wittmeyer, H. Ménard, Catal. Commun. 8 (2007) 751-754.

[8] Y. Song, O. Gutiérrez, J. Herranz, J. A. Lercher, Appl. Catal. B. 182 (2016) 236-246.

[9] Y. Song, S. Chia, U. Sanyal, O. Gutiérrez, J. A. Lercher, J. Catal. 344 (2016) 263-272.

[10] K. Junghans, Chem. Ber. 107 (1974) 3191-3198.

[11] L. Xin, Z. Zhang, J. Qi, D. Chadderdon, Y. Qiu, K. Warsko, W. Li, ChemSusChem. 6 (2013) 674-686.

[12] L. Zhu, H. Sun, H. Fu, J. Zheng, N. Zhang, Y. Li, B. Chen, Appl. Catal. A. 499 (2015) 124-132.

[13] D. Santana, G. Melo, M. Lima, J. Daniel, M. Areias, M. Navarro, J. Electroanal. Chem. 569 (2004) 71-78.

[14] A. Chiltz, P. Jeanson, A. Martel, L. Brossard, J. Lessard, H. Ménard, Can. J. Chem, 78 (2000) 307-315.

[15] X. Wang, R. Rinaldi, Energy. Enivron. Sci. 5 (2012) 8244-8260.

[16] J. Chumpoo, P. Prasassarakich, Energy Fuels. 24 (2010) 2071-2077.

[17] S. Karagöz, T. Bhaskar, A. Muto, Y. Sakata, Fuel. 24 (2005) 875-884.

[18] Z. Tang, F. Jiang, L. Yu, X. Cui, L. Gong, A. Mi, Y. Jiang, Y. Wu, J. Am. Chem. Soc. 125 (2003) 5262-5263.

[19] M. Vannice, D. Poodndi, J. Catal. 169 (1997) 166-175.

[20] F. Pinna, F. Menegazzo, M. Signoretto, P. Canton, G. Fagherazzi, N. Pernicone, Appl. Catal. A. 219 (2001) 195-200.

[21] A. Polcaro, S. Palmas, S. Dernini, Ind. Eng. Chem. Res. 32 (1993) 1315-1322.

[22] A. Sergeev, J. Webb, J. Hartwig, J. Am. Chem. Soc. 134 (2012) 20226-20229.

[23] M. Besson, P. Gallezot, Catal. Today. 81 (2003) 547-559.

[24] Y. Li, H. Wang, L. Xie, Y. Liang, G. Hong, H. Dai, J. Am. Chem. Soc, 133 (2011) 7296-7299.

[25] J. Bhanushali, I. Kainthla, R. Keri, B. Nagaraja, Chemistry Select 1 (2016), 3839-3853.

[26] M. Vannice, D. Poondi, J. Catal. 178 (1998) 386-390.

[27] F. Pinna, F. Menegazzo, M. Signoretto, P. Canton, G. Fagherazzi, N. Pernicone, Appl. Catal. A. 219 (2001) 195-200.

[28] N. Singh, Y. Song, O. Gutiérrez, D. Camaioni, C. Campbell, J. Lercher, ACS. Catal. 6 (2016) 7466-7470.

[29] W. Chen, K. Sasaki, C. Ma, A. Frenkel, N. Marinkovic, J. Muckerman, Y. Zhu, R. Adzic, Angew. Chem. Int. Ed. 51 (2012) 6131-6135.

[30] H. Raus, D. Schuhmann, E. Peyroz, P. Vanel, J. Electroanal. Chem. 137 (1982) 393-396.

[31] P. Zuman, Elelctroanalysis. 18 (2006) 131-140.

[32] A. Kejharová, P. Zuman, J. Electroanal. Chem. 21 (1969) 197-219.

[33] H. Lin, C. Yen, C. Tan, Grenn. Chem. 14 (2012) 682-687.

[34] H. Takagi, T. Isoda, K. Kusakabe, S. Morooka, Energy. & Fuels.13 (1999) 1191-1196.

[35] M. Foresti, M. Moncelli, G. Aloisi, M. Carlá, J. Electroanal. Chem. 255 (1988) 267-280.

[36] M. Carlá, G. Aloisi, M. Foresti, R. Guidelli, J. Electroanal. Chem. 197 (1986) 123-141.

[35] I. Lee, C. Kim, I. Lee, C. Kim, J. Phys. Chem. A. 104 (2000) 6332-6337.

[36] P. Zuman, Czechoslovak Chem. Commun. 74 (2010) 1777-1789.

[37] A. Doherty, C. Brooks, Electrochim. Acta. 49 (2004) 3821-3826.

4.7. Associated Content

Contributions

Oliver Y. Gutiérrez supervised the Hydrogenation of benzaldehyde via electrocatalysis and thermal catalysis on carbon-supported metal catalysts. Yang Song contributed with the design of the experiments, operation of setups, experimental activities, data analysis, and draft writing. Udishnu Sanyal, Dhananjai Pangotra and Guanhua Cheng assisted in experimental activities and discussions, Johannes A. Lercher was responsible for data discussion, supervising and manuscript preparation. Oliver Y. Gutiérrez and Johannes A. Lercher are the principal investigators of this work.

Chapter 5

Summary and Conclusions

The aim of this thesis was to explore the hydrogenation of oxygen-containing hydrocarbons derived from bio-oil. The conversion was performed under very mild operating conditions, i.e., room temperature and ambient pressure in aqueous phase. The focus was put on the in-situ production of reduction equivalents via electrocatalysis. This work initialized with the design of experimental setups, went through the screening of catalysts and reaction conditions to the completion of detail kinetic studies that allowed proposing reaction mechanisms. The kinetic studies included determination of reaction rates, turnover frequencies (TOFs), faradic efficiency (FE) and energy of activation (Ea). Kinetics of catalytic thermal hydrogenation (TCH) and electrocatalytic hydrogenation (ECH) were compared in order to shed insight into the metal-catalyzed hydrogenation of hydrocarbons in aqueous phase.

Phenol was chosen as main model compound because it is a simple but representative compound of lignin-derived bio-oil. In the initial screening, it was found that Rh is more active than Pt and Pd in phenol conversion via ECH. Accordingly, the Ea was 23 kJ·mol^{-1} on Rh/C and 29 on Pt/C. Pd/C showed very low activity as phenol was hardly converted by using it as catalyst. Reaction media has an important impact on phenol electrocatalytic conversion as well. Sulfuric acid, phosphoric acid and acetic acid at pH=5 were used for the ECH of phenol. TOF of phenol conversion reached 33.7 h^{-1} on Rh/C and 28.8 h^{-1} on Pt/C in acetic acid. In sulfuric acid, the TOF dropped to 30.2 h^{-1} and 6.7 h^{-1} on Rh/C and Pt/C, respectively. Thus, acetic acid was chosen as a suitable electrolyte for ECH. The

pH of the solution also plays a very important role in rates of ECH. Generally, phenol conversion is favored at neutral or acidic conditions owning to the pKa of phenol (9.95). In acetic acid the conversion rate increases from 1.3×10^{-5} mol/s·g_{metal} at pH 3 to 1.5×10^{-5} mol/s·g_{metal} at pH 5 on Pt/C and from 1.6×10^{-5} mol/s·g_{metal} at pH 3 to 1.8×10^{-5} mol/s·g_{metal} at pH 5 on Rh/C. Current has effects on the reaction as well. With the increase of the current from -20 mA to - 60 mA, faradic efficiency increases from 9.6 % to 45 % on Pt/C and from 13 % to 77 % on Rh/C. Increase of current results in the increase of potential. Compared to ECH of phenol under the same conditions, much higher activity was observed in TCH, giving TOF of 118.8 h^{-1} on Pt/C and 380.7 h^{-1} on Rh/C. Similar reaction mechanisms are inferred in ECH and TCH due to their similar Ea (33 kJ/mol via TCH and 29 kJ/mol via ECH). Higher reaction rates via TCH could come from relatively higher hydrogen coverage on the catalyst from the external supply of H_2 than from adsorbed hydrogen formed in-situ via ECH. In the reaction network, phenol is converted via two consecutive hydrogenation steps, producing cyclohexanone as intermediate, which is further hydrogenated to cyclohexanol via ECH and TCH. No C-O bond cleavage was observed during the reaction, which is attributed to the low temperature and high activation energy of such step.

In the second step of the project, a new electrocatalysis (two-compartment) reactor allowed shortening the distance between cathode and anode to reduce the resistance in between. With this cell, the impact of potential on the ECH of phenol on Rh/C was thoroughly studied at room temperature in acetic acid at pH 5 (the optimum conditions found in the previous stage). Within the potential range from -0.4 V to -0.9 V vs Ag/AgCl, TOF increased from 15 h^{-1} to 629 h^{-1} with the increase of the potential (absolute values). The faradic efficiency showed two steps in function of potential, increasing from 20 % to 68 % in the range of -0.4 V to -0.6 V, and then remaining constant at around 68% between -0.6V to -0.9V. This indicated that ECH of phenol is favored in this range of potential over the competing reaction, hydrogen evolution reaction (HER). Rates of ECH of phenol are higher than those of TCH when the potential was more negative than -0.7 V. This is an important sign that ECH can be a competitive way to convert biomass under mild conditions.

The concentration profiles observed in ECH at -0.7 V are equivalent to those of TCH, which shows that potential affects the ECH activity by changing the coverage of hydrogen on the catalyst.

After studying the influence of potential on the hydrogenation of phenol, more model reactants with an increasing complexity were studied. The selected compounds were substituted phenolic compounds such as cresols and methyl phenols, symmetric diaryl ethers (diphenyl ether, p-tolyl ether) and asymmetric diaryl ether like benzyl phenyl ether. With the increase of the molecular complexity ECH rates showed a descending trend as the TOF decreased in the sequence 296 h^{-1} > 151 h^{-1} > 138 h^{-1} > 88 h^{-1} > 60 h^{-1} > 43 h^{-1}, for phenol, 4-methylphenol, 4-methoxyphenol, benzyl phenyl ether (BPE), diphenyl ether (DPE), p-tolyl ether (PTE) (ECH of phenolic compounds are performed at -0.6 V and diaryl ethers are at -0.9V), respectively. Rates in TCH showed the same trend. This is attributed to the steric hindrance of the functional groups, which affects the adsorption of the reactant on the surface of the catalyst. Much more negative potential is required to convert diaryl ethers than phenolic reactants because the former were converted in the presence of iso-propanol (diaryl ethers have a low solubility in aqueous phase), which may compete with reactant for adsorbing on the catalyst or may decrease the conductivity.

More products were observed with the increase of the complexity of the reactant. Phenol and 4-methylphenol conversion proceeded only via two consecutive hydrogenation steps, while 4-methoxyphenol converts via hydrogenation or hydrogenolysis with selectivity of 90% and 10%, respectively in ECH and TCH. Diphenyl ether and p-tolyl ether converted in more diverse pathways, including hydrogenation, hydrolysis and hydrogenolysis, with selectivity of 69-73%, 16-23% and 8-12%, respectively. Oxygen-free hydrocarbons, (benzene and cyclohexane from diphenyl ether, toluene and methyl cyclohexane from p-tolyl ether) were produced via hydrogenolysis and further hydrogenation. Benzyl phenyl, as an asymmetric diaryl ether, showed an even more complex product distribution although the same three pathways as the other two diaryl

ethers were concluded. However, hydrogenolysis became the dominant pathway with selectivity of 59-63% instead of hydrogenation (36-39%) and hydrolysis (1-2%). Such high selectivity to hydrogenolysis led to selectivity of 25% to O-free hydrocarbons. The C-O cleavage in di-aryl ethers is attributed to the much lower C-O bond energy in benzyl phenol ether, which is converted much faster than the other two ethers mainly via hydrogenolysis ($4.7 \cdot 10^{-5}$ mol$\cdot$s$^{-1}\cdot$g$_{Rh}^{-1}$ in TCH and $2.1 \cdot 10^{-5}$ mol$\cdot$s$^{-1}\cdot$g$_{Rh}^{-1}$ in ECH). That is, from 4 to 8 times faster than the hydrogenolysis of DPE ($6 \cdot 10^{-6}$ mol$\cdot$s$^{-1}\cdot$g$_{Rh}^{-1}$ in TCH and $5 \cdot 10^{-6}$ mol$\cdot$s$^{-1}\cdot$g$_{Rh}^{-1}$ in ECH) and from 5 to 19 times faster than the hydrogenolysis of PTE ($2.5 \cdot 10^{-6}$ mol$\cdot$s$^{-1}\cdot$g$_{Rh}^{-1}$ in TCH and $4 \cdot 10^{-6}$ mol$\cdot$s$^{-1}\cdot$g$_{Rh}^{-1}$ in ECH). The C-O cleavage via hydrolysis appears to be the same to that in hydrogenolysis, whereas the difference is related to the probability of H$\cdot$ or OH$\cdot$ being added to the adsorbed hydrocarbon moiety.

ECH reactions were performed in a closed system with increase of H$_2$ pressure due to the HER to study whether the concentration of adsorbed hydrogen could be increased. Under normal ECH conditions, the conversion of phenol increased linearly, which reflects the constant TOF along the whole reaction time. In contrast, with increasing H$_2$ pressure, the conversion increases with time because the TOF increases as the coverage of H increases. On the other hand, the conversion of PTE in normal ECH conditions decreased with time due to deactivation and the TOF rapidly decreased as well (especially when ethanol is chosen as the solvent). With increasing H$_2$ pressure, however, deactivation was counteracted and the increases in rate exhibited a reaction order of 1.5 on H$_2$ pressure. This indicates that increasing the coverage of hydrogen at the surface compensates the effect of low hydrocarbon coverages for the hydrogenation rates.

TCH and ECH of benzaldehyde were performed at room temperature in aqueous phase on Pt/C, Rh/C, Pd/C, and Ni/C. In TCH the intrinsic activity followed the trend Pd/C > Rh/C > Pt/C (TOFs of 1062 h^{-1}, 964 h^{-1}, and 427 h^{-1}, respectively at 298 K and 1 bar H$_2$), whereas Ni/C was not active. Benzyl alcohol was the only product of the reaction, which is attributed to a preferential η^2 and η^1 adsorption of benzaldehyde and repulsion of the hydroxymethyl group in benzyl alcohol from the surface. Reaction orders of zero in benzaldehyde and 1 in H$_2$ allow proposing that

the hydrogenation of benzaldehyde follows a Langmuir-Hinshelwood, where adsorbed H is added stepwise to the adsorbed hydrocarbon. The second H addition is the rate limiting step.

In ECH, the hydrogenation of benzaldehyde proceeds only to benzyl alcohol (as in TCH) but competes with H_2 evolution. The hydrogenation rates increase with increasing cathodic potential and the activity trend is Ni/C< Rh/C < Pt/C < Pd/C (e.g., TOFs of 2048 h^{-1}, 1753 h^{-1}, 2706 h^{-1}, and 14200 h^{-1}, respectively at 298 K and -0.8 V Ag/AgCl). Notably, Ni/C becomes active and turns to be the most active catalyst in ECH under our conditions albeit at higher cathodic potentials than noble metals. That is, the onset of ECH activity coincides with that of HER (more negative than -0.8 V and -0.4 V vs Ag/AgCl for Ni/C and noble metals, respectively). The faradaic efficiency, however, increases as Ni/C < Pt/C < Rh/C << Pd/C (e.g., 11 %, 45 %, 61 %, and 99.6 %, respectively at 298 K and -0.8 V Ag/AgCl). This efficiency is related with the relative HER and ECH rates (kinetic factors), rather than with overpotential of HER (thermodynamic factors). Pd/C has outstanding efficiencies (> 98 %) for ECH.

The marked differences between the performances of the different catalysts in ECH and TH allow concluding that at least one hydrogenation step in ECH is electrochemical, i.e., it involves the addition of e- and H^+ instead of adsorbed hydrogen in stark contrast with TCH. However, the concentration of protonated benzaldehyde (pKa of -4 to -5) is very low under our conditions, whereas the reduction potential of benzaldehyde is more negative than those accessed in this study. Thus, stepwise addition of charge carriers is not likely due to the high-energy intermediates expected. We conclude, therefore, that the rate determining step in ECH is a concerted e^-/H^+ addition enabled in the presence of electric potential.

Curriculum Vitae

Yang Song was born in February 8th 1987 in Shanghai, China. After finishing his studies in Shanghai Qibao Senior High School in 2006, he joined the Department of Chemistry in Jilin University, Changchun, Jilin Province in China, majoring in Chemical Engineering and technology. Till in July 2010, he obtained his Bachelor titles in Engineering Chemistry and Advanced Business English (Double Bachelor Degree). In the same year, he was admitted into the Alan G. MacDiarmid Institute for his master studies in polymer chemistry and physics, majoring the research on preparation and application of novel special engineering polymers. He led and collaborated in several projects including the PEEK modification and synthesis of SPI membrane for fuel cell PEMs. During his stay, he published 8 SCI journals (4 as first author), and obtained several rewards including 3-year full covered scholarships. He obtained his Master degree in Polymer chemistry and physic in 2013. The same year, he was granted the doctor candidate position by Prof. Dr. Johannes A. Lercher from Technical Chemistry II, Technische Universität München and the scholarship from Chinese Scholarship Council. Since then, he did his PhD study under Prof. Lercher's supervision on "biomass conversion via electrocatalysis". His research interests are exploring optimum conditions for electrocatalytic biomass conversion under mild conditions in condense phases, from the view of the operating parameters, the property of different catalysts, to different reactant structures.

List of Publications

Journals

1. <u>Yang Song</u>, Shaohua Chia, Udishnu Sanyal, Oliver Y. Gutiérrez* and Johannes A. Lercher*, *"Intergrated catalytic and electrocatalytic conversion of substituted phenols and diaryl ethers",* J. Catal. 2016, 344, 263-272.

2. <u>Yang Song</u>, Oliver Y. Gutiérrez*, Juan Herranz, Johannes A. Lercher* *"Aqueous phase electrocatalysis and thermal catalysis for the hydrogenation of phenol at mild conditions",* Appl. Catal. B: Environ. 2016, 182, 236-246.

3. Nirala Singh, <u>Yang Song</u>, Oliver Y. Gutiérrez, Donald M. Camaioni, Charles T. Campbell and Johannes A. Lercher* *"Electrocatalytic Hydrogenation of Phenol over Platinum and Rhodium: Unexpected Temperature Effects Resolved",* ACS. Catal. 2016, 6, 7466-7470.

4. <u>Yang Song</u>, Udishnu Sanyal, Dhananjai Pangotra, Guanhua Cheng, Philipp Rheinländer, Oliver Y. Gutiérrez* and Johannes A. Lercher* *"Hydrogenation of benzaldehyde via electrocatalysis and thermal catalysis on carbon-supported metal catalysts",* to be submitted soon.

5. Udishnu Sanyal[#], <u>Yang Song</u>[#], Dhananjai Pangotra, Oliver Y. Gutiérrez* and Johannes A. Lercher* ([#]contributed equally) *"Aqueous phase electrocatalytic hydrogenation of biomass surrogates over Pt/C catalysts: Elucidation of Pt particle size on reation kinetics",* to be submitted soon.

Oral Presentations

1. **"Aqueous-phase phenol hydrogenation over platinum and rhodium: electrocatalysis versus thermal catalysis"**

   Nirala Singh, <u>Yang Song</u>, Oliver Y. Gutiérrez, John L. Fulton, Donald M. Camaioni, Charles T. Campbell, Johannes A. Lercher.
   Oral presentation at the "2016 AIChE Annual Meeting", San Francisco, USA, November, 2016.

2. **"Biomass conversion at room temperature via thermal and electrochemical catalysis"**

   Oliver Y. Gutiérrez, <u>Yang Song</u>, Johannes A. Lercher.
   Oral presentation at the "3rd International Symposium on Catalysis for Clean Energy and Sustainable Chemistry", Madrid, Spain, September, 2016.

3. **"Towards Fuel Production from Biomass via Electrocatalysis and Catalytic Hydrogenation at Ambient Conditions"**

   Oliver Y. Gutiérrez, <u>Yang Song</u>, Johannes A. Lercher.
   Oral presentation at the MSE (Munich School of Engineering) Colloquium, Garching, Germany, July 2016.

4. **"Manipulation of reaction pathways in the electrocatalytic hydrogenation of phenol"**

   Udishnu Sanyal, <u>Yang Song</u>, Oliver Y. Gutiérrez, Johannes A. Lercher.
   Oral presentation at the "TUM Catalysis Research Center Graduate Academy 2016", Raitenhaslach, Germany, June 2016.

5. **"Biomass conversion at mild condtions via thermal catalysis and electrocatalysis"**

   <u>Yang Song</u>, Oliver Y. Gutiérrez, Johannes A. Lercher.
   Oral presentation at 28th GCCCD Annual Conference, Munich, Germany, October, 2016.